UNIVERSITÀ DEGLI STUDI DI ROMA "TOR VERGATA"

FACOLTA' DI INGEGNERIA

DOTTORATO DI RICERCA IN

INGEGNERIA DEI SISTEMI SENSORIALI E DI APPRENDIMENTO

XXI CICLO DEL CORSO DI DOTTORATO

Study and Optimization of Polariton LASERs

Eleonora Petrolati

A.A. 2007/2008

Tutor: Prof. Aldo Di Carlo - Dr. Andrea Reale

Coordinatore: Prof. Corrado Di Natale

Trust I seek and I find in you

Every day for us something new

Open mind for a different view

And nothing else matters

Index

Index ……………………………………………………………………… i

Abstract ……………………………………………………………………… iv

Chapter 1 – Background and motivation ……………………………… 1

1.1 Scientific background ……………………………………………… 4

1.1.1 Microcavities and Polaritons ……………………………………… 4

1.1.2 Microcavities as OPAs ……………………………………………… 9

1.1.3 The need for wide band gap materials ………………………… 9

1.1.4 Simulation softwares ……………………………………………… 11

References ……………………………………………………………… 13

Chapter 2 – Device simulation ……………………………………… 15

2.1 TiberCad ……………………………………………………………… 15

2.1.1 The Exciton Model in TiberCad ………………………………… 18

2.2 The simulation tool Dessis ………………………………………… 23

2.2.1 Upgrading of Dessis material parameter file ………………… 26

References ……………………………………………………………… 28

Chapter 3 - Design and optimization of GaN based LED and Polariton Laser / VCSEL 30

3.1 Influence of mesa contact dimension on the GaN/InGaN LED properties 30

3.2 Design of current confinement layer 36

3.3 The influence of mobility unbalance 40

3.4 Enhancement of carrier focusing 45

3.5 Discussion on the inverted structure 50

3.6 Electrically injected bulk polariton laser 56

References 60

Chapter 4 - Design of a new electrical injection polariton laser 62

4.1 Why a new structure 62

4.2 The patented design 61

References 66

Chapter 5 - Results of the StimScat Project (October 2008) 67

5.1 Microcavity properties and design 68

5.2 Observation of Polariton lasing at room temperature: optical injection 72

5.3 Electrical injection structures 74

References …………………………………………………………………………… **77**

Appendix A ………………………………………………………… **79**

Appendix B ………………………………………………………… **82**

Appendix C - List of publications and activities ………………………… **104**

Acknowledgements …………………………………………………… **109**

Abstract

A polariton laser is a new concept of device based on the Bose Einstein condensation of cavity exciton-polaritons. It offers intrinsically high modulation speeds, low thresholds, long lifetime and low power consumption. Polariton lasing has been demonstrated at low and room temperature in optically pumped structures. Electrical injection of excitons and polaritons states have been reported for GaAs structures, while the realization of an electrically driven polariton laser is still missing.

The aim of the work presented in this thesis has been the modelling, design and optimization of GaN based devices, with regard to the aspects involved in the realization of the electrical injected polariton laser. To achieve these goals, a new simulation software has been developed to study the exciton transport in semiconductors and used together with conventional tools. Several simulations have been performed to understand the behaviour of GaN based light emitting diodes (LED), Vertical Cavity Vertical-cavity surface-emitting laser (VCSEL) and Polariton laser (PLASER) structures and new designs of GaN based devices have been proposed in order to optimize the electrical injection in GaN-based VCSELs/PLASERs and to achieve the polariton lasing in these structures. The strong interplay between carrier mobility, focussing efficiency and electrical injection has been carried for the first time.

The results of this work have received dissemination through 4 publications in international journals, presentations and posters at international conferences, and a patent concerning a new design for electrical injection in GaN based VCSELs/PLASERs. This work has been developed within the European Project StimScat (STIMulated SCATtering) started the 1st of September 2005 and ended the 1st of September 2008. The aim of the project was the realization of two new forms of opto-electronic device, namely the polariton laser and polariton-based micron-size optical parametric amplifier, both operating at room temperature.

Abstract

Il laser a polaritoni rappresenta una nuova classe di dispositivi basati sulla condensazione di Bose-Einstein di eccitoni-polaritoni in microcavità. Questo dispositivo prevede tra le caratteristiche principali un basso consumo di potenza, lunghi tempi di vita e basse tensioni di soglia. L'effetto laser dei polaritoni è stato dimostrato sia a basse temperature che a temperatura ambiente in strutture a pompaggio ottico. Inoltre, mentre l'iniezione elettrica di eccitoni e polaritoni è già stata dimostrata per strutture basate su GaAs, la realizzazione di un laser a polaritoni ad iniezione elettrica realizzato con GaN rimane ancora una sfida.

Lo scopo del lavoro di questa tesi è stato proprio progettare ed ottimizzare dispositivi basati su GaN, con particolare interesse agli aspetti coinvolti nella realizzazione del primo laser a polaritoni ad iniezione elettrica. Per raggiungere questo obiettivo, è stato sviluppato prima di tutto un nuovo simulatore in grado di studiare il trasporto di eccitoni nei semiconduttori. Sono state realizzate quindi diverse simulazioni per analizzare il comportamento di diodi ad emissione di luce (LED), laser a cavità verticale (VCSEL) e strutture per laser a polaritoni (PLASER) realizzati con GaN. Inoltre sono stati progettati nuovi design di dispositivi con lo scopo di ottimizzare l'iniezione elettrica nei VCSELs ed ottenere l'effetto laser dovuto ai polaritoni. Per la prima volta, è stata dimostrata la stretta interazione tra mobilità di portatori, efficienza di focusing e iniezione elettrica.

I risultati di questo lavoro sono stati pubblicati in riviste internazionali e presentati a diverse conferenze. Inoltre è stato realizzato un brevetto riguardante una nuova struttura per realizzare l'iniezione elettrica nei VCSEL e nei PLASER realizzati con GaN. Questo lavoro è stato sviluppato all'interno del progetto europeo StimScat (STIMulated SCATtering), che ha avuto inizio il primo Settembre 2005 ed è terminato il primo Settembre 2008. Lo scopo di questo progetto è stato la realizzazione di due nuovi dispositivi optoelettronici: il laser a polaritoni e il micro-amplificatore ottico parametrico a polaritoni, entrambi operanti a temperatura ambiente.

Chapter 1

Background and motivation

The semiconductor lasers have a wide range of use and represent an huge and evolving market. This development is linked with the advanced technology that allows the production of new types of lasers for new applications. Examples include the development of blue lasers, which opened the new market of Blue-ray DVD.

From a technical point of view, one of the main challenges imposed by the semiconductor lasers has been and is still to reduce their operating threshold. This threshold determines the energy consumption, but also the emission of heat which is fundamental for the integration of the components and their lifetimes.

The first semiconductor laser produced fifty years ago had an extremely high current threshold, and for this reason they were unusable. Several revolutions based on the use of double heterostructures, quantum wells, vertical-emitting lasers (VCSEL) and quantum dots helped to reduce of several orders of magnitude the current threshold. Fig. 1.1 shows the evolution over time of the current threshold as it was presented by Z. Alferov (a double heterostructures developer and a Nobel Prize winner in 2000).

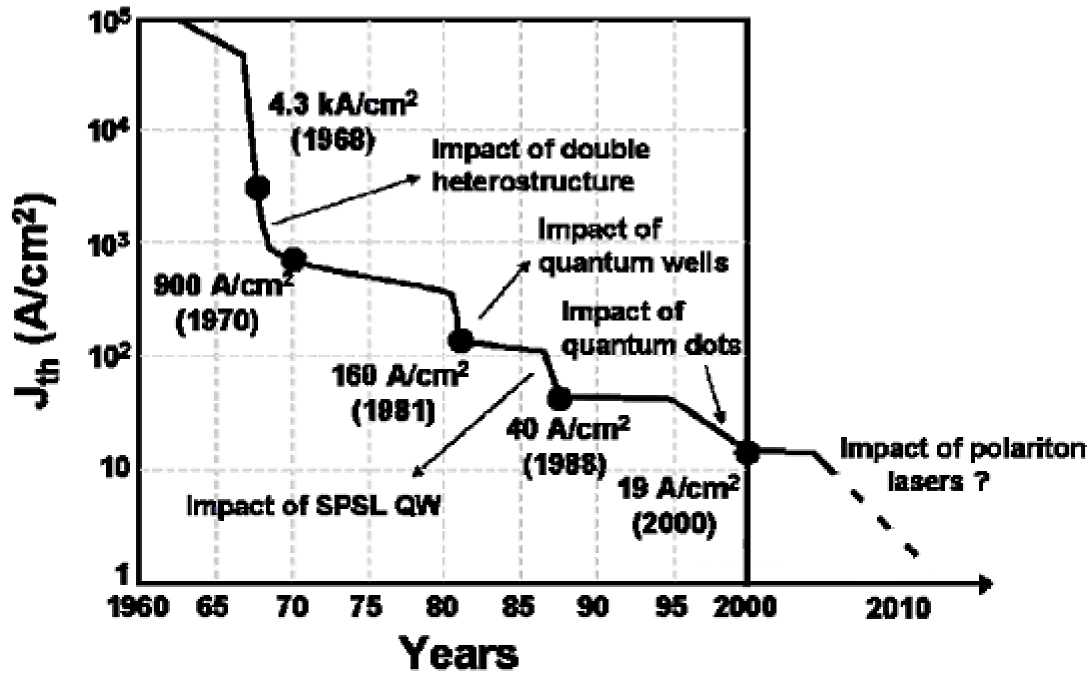

Fig. 1.1 - Chronological evolution of the current threshold in semiconductor lasers shown by Alferov during his presentation for Nobel prize in 2000.

Recently a new kind of laser has been introduced based on Bose-Condensation of Polaritons, i.e the quasiparticle arising from the interaction between excitons and photons. Polaritons have a number of novel properties including scattering stimulated by final state occupancy, very light mass and new dispersions. Many new fundamental and applied opportunities arise from these properties. The high exciton binding energy and large oscillator strength of GaN provide the materials properties to achieve the realization of the Polariton laser even at rom temperature. At the same time GaN microcavity (MC) technology, required to correctly couple exciton and photons, is in its infancy and poses a number of challenges.

Although GaN devices are efficient light emitters, they have high thresholds for inversion due to the high carrier densities of states. MCs in the strong coupling regime overcome this intrinsic limitation, with up to 4 orders of magnitude lower density of states. Stimulation is thus much easier

to attain, with the promise of low thresholds for coherent emission, an order of magnitude lower than present blue or ultra-violet semiconductor lasers.

The aim of the work presented in this thesis was the modeling, design and optimization of GaN based devices, with regard to the aspect involved in the realization of the first polariton laser. This work has been developed within the European Project StimScat (STIMulated SCATtering) started the 1st of September 2005 and ended the 1st of September 2008. The aim was to realize two new forms of opto-electronic device, namely the polariton laser and polariton-based micron-size optical parametric amplifier, both operating at room temperature.

While polariton lasing has been demonstrated by using all optical technique, the realization of an electrically driven polariton laser is still missing. There are several issues which have to be addressed for electrical injection such as efficient current injection, efficient exciton formation, contacting technologies, separate electron and hole injection etc.

The project assembled a collaboration from leading laboratories around Europe, with the necessary expertise:

- The University of Sheffield (USFD)
- Centre de Rechereche sur l'Hétéro-Epitaxie et ses Applications (CRHEA)
- University of Strathclyde (U-Strath)
- Ecole Polytechnique Fédérale de Lausanne (EPFL)
- University of Southampton (USTN)
- LASMEA, University Clermont-Ferrand II (LASMEA)
- Sharp Laboratories of Europe (SLE)
- University of Rome “Tor Vergata” (Rome)

Stimscat focus on Gallium Nitride (GaN) based semiconductor microcavities (MCs) in which excitons and photons are strongly coupled together to form exciton-polariton coupled modes, to fabricate new forms of coherent light emitters and compact optical parametric amplifiers, with

major potential advantages over present-day technologies. These radically new device concepts have major potential advantages over present day technologies, in terms of low threshold, short wavelength coherent emission and low power operation.

The specific overall objectives of StimScat were:

- The design, fabrication and testing of the first polariton laser at room temperature. The demonstration of this new form of coherent light source would represent a major breakthrough on the international scale with implications for both pure and applied science. It also corresponds to the achievement of Bose condensation in a solid state material, an equally significant fundamental advance. The research focus on both optical and electrical injection. The research on electrical injection structures have additional wide relevance to the development of GaN-based resonant cavity LEDs and VCSEL structures.
- In similar structures demonstrate ultrafast optical parametric amplifier (OPA) operation at room temperature and above in compact micron size devices, as opposed to the mm-cm scale in standard OPAs.

The field of polariton physics and of stimulated scattering in semiconductors is one which has been pioneered by European scientists.

1.1 Scientific background

1.1.1 Microcavities and Polaritons

The novel properties of polaritons in semiconductor microcavities (MCs) provided the scientific underpinning for the advances of polariton science and technology. [1-3] MCs permit

unprecedented control of the interactions of light with matter in solid state systems. They allow separate control of the properties of both correlated electron-hole pairs (excitons) and photons and of their interactions with one another to form polaritons. The polaritons have a number of novel properties including bosonic character and scattering stimulated by final state occupancy, [4-7] very light mass and dispersions of totally new forms which permit novel scattering processes.[2] A large variety of opportunities for both fundamental and applied advances arise from these properties.

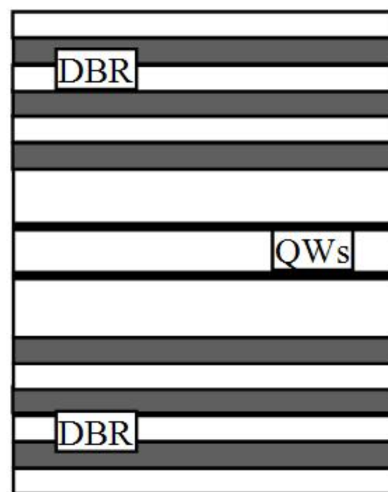

Fig. 1.2- Schematic diagram of a semiconductor microcavity, showing quantum wells in the cavity region surrounded by high reflectivity (>99%) distributed Bragg reflector (DBR) mirrors.

A typical inorganic semiconductor based microcavity (MC) is shown in Fig 1.2. The MC is composed of a planar Fabry-Perot cavity in which the high reflectivity mirrors are formed from ~10-20 repeats of distributed Bragg reflector quarter wavelength $\lambda/4$ layers. Quantum wells (QWs) are embedded within the cavity at the antinodes of the optical field to achieve maximum interaction between the QW excitons and the confined photon field. Both the exciton and photon states are confined, with the dispersion relations shown by the dashed lines in Fig 1.3.

The excitons and photons couple together to form new quasi-particles, cavity-polaritons which are part exciton, part photon. The existence of these new particles forms the basis of the new

phenomena and device structures. This is the regime of strong-coupling, and arises so long as the splitting between the two polariton branches is greater than the linewidths of the uncoupled modes. The splitting between the two polariton branches is given by the vacuum Rabi splitting, ΔVRS, and is determined by the exciton-photon interaction strength. The excitation oscillates back and forth between the two modes until the polariton decays by photon leakage through the Bragg mirrors and is converted to an external photon.

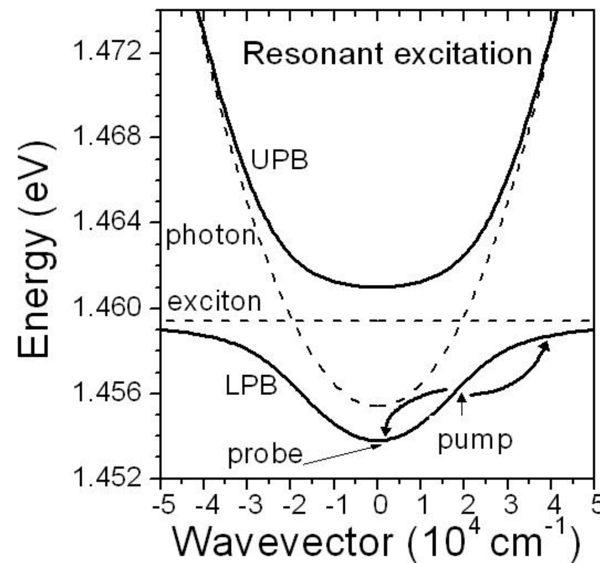

Fig. 1.3 - Dispersion of microcavity in strong coupling regime. Dashed – uncoupled exciton, cavity. Full - polariton coupled mode dispersion. LPB, UPB lower, upper polariton branches. Resonant excitation at the point of inflection leading to E and k-conserving pair scattering is indicated. The probe beam stimulates scattering to k=0, and forms the basis of OPA operation.

The polaritons have very small mass of order $10^{-4}m_e$ as a result of the strong photon dispersion in the cavity (Fig. 1.3). This results in a density of states ~10^4 times smaller than that for excitons, a very important property which facilitates the achievement of state occupancies greater than one, the basis of the polariton laser.

The shape of the lower polariton dispersion curve is noteworthy (Fig. 1.3), with a point of inflection between k=0 and the uncoupled exciton energy. This permits new pair scattering processes (Fig 3) from the pump into signal and idler beams, in which energy and momentum are conserved ($2E_{laser}=E_{signal}+E_{idler}$, $2k_{laser}=k_{signal}+k_{idler}$). Such pair processes are not achievable for the quadratic dispersions of either excitons or photons alone. Furthermore, the polaritons are directly accessible in reflectivity and emission, a key point for all the applications.

Polariton distributions can be probed directly along the dispersion curve by varying the external angle of the excitation beam, and populations can be injected at precise points in k-space, all features which do not arise in either bulk semiconductors or QWs.

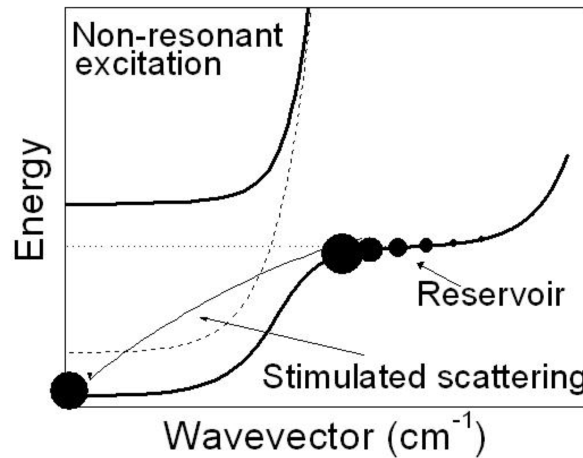

Fig.1. 4 - Polariton dispersion over large range of k (log scale), showing the exciton reservoir formed under non-resonant excitation conditions. The curved line indicates scattering out of the reservoir to k=0, stimulated by final state population leading to the polariton laser and Bose condensation.

The dispersion curves of Fig. 1.3 and Fig. 1.4 are controllable by design, by varying the number of quantum wells, the length of the cavity and the energy separation between the uncoupled modes (the detuning). This allows control of the depth of the 'trap' formed by the lower polariton branch (Fig. 1.3), and of the separation of the bottom of the trap from its 'environment' (the exciton reservoir), hence allowing loss processes to be minimised.

Both the exciton and photon components of polaritons are bosons, and hence the polaritons themselves have bosonic character. As a result they exhibit specific bosonic properties such as stimulated scattering and macroscopic state occupation (for fermions by contrast the state occupancy is restricted to one by the Pauli principle). The probability for a transition is proportional to (1+Nfinal), and since for bosons Nfinal may be >1, stimulation of transitions may occur. This is the origin of stimulated emission in conventional lasers, and stimulation of scattering between initial and final states depicted in Fig. 1.3 and Fig. 1.4.

Stimulation of scattering from k_{laser} to k=0 in Fig. 1.3 or from the reservoir to k=0 in the polariton laser, leads to macroscopic occupation of the k=0 state.[8,9] The polaritons at k=0 convert to external photons by leakage through the Bragg mirrors and lead to the new form of coherent emission embodied in the polariton laser (Fig. 1.4).

Such a process is distinct from the stimulation in a photon laser since it is the polariton scattering process which is stimulated, as opposed to the photon emission in a laser. This separation of stimulation and emission leads to coherent emission without the requirement for population inversion, as in a photon laser, and hence to the prospect of very low threshold coherent emission.

In an equivalent description, the stimulation of scattering to k=0 leads to condensation of the polaritons to a state with macroscopic occupation from an incoherent exciton distribution. The achievement of polariton lasing is of major significance from the point of view of fundamental physics: a dynamical Bose condensate is formed in a process where symmetry is spontaneously broken from the incoherent reservoir to the coherent condensed state. Relative to Bose-condensates of atoms, the polariton condensate is composed of strongly interacting quasi-particles, has approximately 100 times higher density, is strongly coupled to the environment and importantly has a critical temperature greater than 300K, due to the very small polariton mass.

1.1.2 Microcavities as OPAs

In addition to the polariton laser application involving non-resonant carrier injection and stimulated scattering to the light emitting k = 0 state, the same or similar microcavities have considerable potential as very low threshold, micron size optical parametric amplifiers (OPAs). The principles of the OPA operation can be understood by reference to Fig. 1.3. In the presence of a pump beam at the point of inflection of the lower polariton dispersion, scattering of the pump polaritons to k=0 can be stimulated by a weak probe injected at $k = 0.5 \times 10^4$ $cm^{-}1$. Due to the very strong polariton interactions and the automatic phase matching between pump, signal and idler enabled by the unusual shape of the dispersion curve, very high ultrafast gains of the probe beam can be realised. Gains up to 10000 have been reported [5], with maximum temperature of operation of 200K in CdTe-based microcavities, the high temperature limit being determined by the relatively small exciton binding energy (20meV) in the CdTe quantum wells.

Compared to standard OPAs, the MC-based structures have micron size (as compared to mm-cm in conventional OPAs), gains up to $10^7 cm^{-1}$ and orders of magnitude lower threshold (up to 106 times) due to the triple resonance condition evident on Fig. 1.3, and the large nonlinear coefficients of resonant semiconductor media. Such OPAs are inherently ultrafast because no energy is stored within the medium. They also have high potential as ultrafast switches. Since all the pump energy is split into signal and idler, they are very efficient in their redistribution of power in different directions.

1.1.3 The need for wide band gap materials

Many of the underpinning advances in polariton physics have been achieved in GaAs/AlGaAs based structures, and more recently in CdTe-based systems. In these materials due to the small

exciton binding energies (E_x) and small exciton oscillator strengths (f) the stimulated scattering phenomena are restricted to low temperatures (<50K) and to relatively low exciton densities. For example it was shown in [11] that in GaAs-based structures, due to the small exciton binding energies and oscillator strengths, exciton screening, loss of strong coupling and of the essential bosonic character occurs before the onset of polariton lasing.

For these reasons, one need to focus on GaN wide band gap materials where the large E_x and f provide the necessary electronic properties to enable polariton laser operation at both low and elevated temperatures and to achieve polariton-based optical parametric amplifier operation at 300K and above. The high oscillator strength enables large splittings between the polariton modes, and thus resistance to broadening effects which occur due to population of the exciton reservoir. The high exciton binding energy is also essential since the excitons in the quantum well will be stable at room temperature and highly resistant to screening. These two conditions provide the essential requirement to achieve polariton lasing, namely that the strong coupling between excitons and photons is retained under excitation conditions sufficient to achieve state occupancies greater than one and thus stimulated scattering to k=0 states.

As well as the obvious technological drive to achieve 300K operation, further advantages for polariton lasing arise from operation at higher temperature: at high temperatures the probability of energy and momentum conserving pair scattering from the reservoir into the trap increases strongly as a result of the wide spread in energy of the excitons, thus increasing strongly the probability of achieving condensation to k=0.

Wide band gap semiconductor materials, although efficient light emitters, have high thresholds for population inversion and lasing. Although GaN blue lasers are commercially available, they suffer from high threshold current (in the kA/cm^2 range). This high J_{th} is to a large degree an intrinsic limitation due to the high carrier densities of states resulting from the high masses in wide band gap materials. The polariton laser offers a means to overcome this limitation: the polariton mass, and hence the density of states in the light emitting region, is 10^4 times smaller than that for

excitons, thus offering the prospect of very low threshold current, at least an order of magnitude less than in conventional “photon” lasers. Furthermore, the processes of stimulation and emission are separated in the polariton laser, as opposed to the situation in conventional VCSEL or edge emitting lasers, again leading to the prospect of very low threshold.

As well as promising low threshold coherent emission, the polariton laser is a generically new form of coherent light emitting device. It also offers intrinsically high modulation speeds and because of the low thresholds long lifetime and low power consumption. Such high performance green/blue/UV devices have potential to have a wide variety of applications in e.g. DVD writers/readers, projection tv, high definition printers.

1.1.4 Simulation software

The device simulators that are mostly used at present emerged during the ’80 (Silvaco [15]) and ‘90 (DESSIS of ISE-TCAD, acquired by Synopsis and now called Sentaurus Device [16]) and are based on a continuous media simulation approach. In particular, DESSIS is a multi-dimensional simulator for simulation of one, two and three-dimensional semiconductor devices and has mixed-mode capabilities for circuit simulation. Depending on the device which is simulated and on the accuracy which is needed different transport models can be used, which are drift-diffusion, self-heating, hydrodynamic, or Monte-Carlo. [17]

However all the available device simulators did not include models to describe exciton or polariton transport. Moreover, they needed improvements to handle GaN based device simulations, due to the particular properties of GaN wide band gap materials. Even the new device designs proposed on this work outlined the need of new simulation approaches or new refinements for the existing simulators.

For all these reasons, the work has been focused also on the developing of a new device simulator, called TiberCad, and on the improvement of Dessis to perform the optimization of the design of devices for the realization of polariton laser.

References

[1] M S Skolnick, T A Fisher and D M Whittaker, Semiconductor Science and Technology 13, 645, 1998

[2] M S Skolnick, A I Tartakovskii, R Butté, D M Whittaker and R M Stevenson, IEEE J Sel Top QE 8, 1060, 2002

[3] Special issue of Semiconductor Science and Technology, editors L Vina and J J Baumberg

[4] F Tassoné, C Piermarocchi, V Savona, A Quattropani and P Schwendimann, Phys Rev B56, 7554, 1997, Phys Rev B59, 10830, 1999

[5] P G Savvidis, J J Baumberg, R M Stevenson, M S Skolnick, D M Whittaker, Phys Rev Lett 84, 1547, 2000

[6] R M Stevenson, V N Astratov, M S Skolnick, M Emam-Ismail, P G Savvidis, J J Baumberg, Phys Rev Lett 85, 3680, 2000

[7] R Houdré, C Weisbuch, R P Stanley, U Oesterle and M Ilegems, Phys Rev Lett 85, 2793, 2000

[8] A Imamoglu and R J Ram, Phys Lett, A214, 193, 1996

[9] Le Si Dang, D Heger, R André, F Boeuf and R Romestain, Phys Rev Lett 81, 3920, 1998

[10] M Saba, C Ciuti, J Bloch, V Thierry-Mieg, R André, Le Si Dang, S. Kundermann, A. Mura, G. Bongiovanni, J. L. Staehli, B. Deveaud, Nature 414, 731, 2001

[11] R Butté, G Delalleau, A I Tartakovskii, M S Skolnick, V N Astratov, J J Baumberg, G Malpuech, A Di Carlo, A V Kavokin, J S Roberts Phys Rev B65, 205310, 2002

[12] G Malpuech, A di Carlo, A V Kavokin, J J Baumberg, A Zamfirescu and P Lugli, Appl Phys Lett 81, 412, 2002

[13] G Malpuech, A V Kavokin, A Di Carlo and J J Baumberg, Phys Rev B65, 153310, 2002

[14] P G Lagoudakis, M D Martin, J J Baumberg, A Qarry, E Cohen, and L N Pfeiffer, Phys Rev Lett 90, 206401 (2003)

[15] Silvaco TCAD Solutions, http://www.silvaco.com.

[16] Synopsis Inc., http://www.synopsis.com.

[17] M.Auf Der Maur, A Multiscale Simulation Environment for Electronic and Optoelectronic Devices, PhD Thesis, Università di Roma Tor Vergata.

Chapter 2

Device simulation

The first part of the work has concerned the implementation of the exciton transport equations in TiberCad, the multiscale device simulator developed by the Optoelectronic Group at the Electronic Engineering Department of the University of Rome "Tor Vergata".

At the same time, the improvement of the material parameter file of Dessis, a device simulation tool from Ise-TCad simulation software, has been carried out to create the requirement for the GaN based device simulation and to have a comparison from a commercial simulator and the in-house simulator TiberCad.

2.1 TiberCad

TiberCAD is a multiscale tool for the simulation of modern nanoelectronic and optoelectronic devices. Applications range goes from nanoelectronic to laser technologies including molecular electronics and bio-devices.

The TiberCAD project is aimed at the implementation of a device simulator which captures the most important physical concepts encountered in present and future electronic and optoelectronic devices. On the one hand the down-scaling of device dimensions requires the inclusion of more advanced quantum mechanical concepts which go beyond classical transport theories. On the other hand new devices are emerging whose functionality is based on properties not only related to electrons and holes but also to other quasi-particles in the system such as excitons, polaritons etc.

Often the active part of a device which needs a more elaborate and careful quantum-mechanical treatment is small compared to the overall simulation domain. The computational cost of the more accurate model, however, forbids its application to the whole domain. Moreover, in many systems, mechanical strain due to lattice mismatch or processing plays a crucial role for device performance and therefore needs an accurate description. Usually mechanical properties depend on a length scale that is much larger than the electrically active part of the device. This raises the need for a multiscale simulation environment capable of simulating different regions of a device using different physical models and coupling these simulations in a consistent way.

The models describing the different physical aspects encountered in modern devices are separated in TiberCAD into three families.

The first one contains the classical or semi-classical transport models for the quasi-particles in the system. These are based on drift-diffusion or hydrodynamical models, possibly with quantum corrections [1]. The drift-diffusion equations are written in terms of an adequate electro-chemical potential as shown for electrons in Eq. (2.1):

$$\nabla\left(\mu_n n \nabla \phi_n\right) = R - G - \frac{\partial n}{\partial t} \qquad (2.1)$$

where Φ_n, μ_n, R and G are the electro-chemical potential, the mobility, the recombination and the generation rate, respectively.

The second one comprises models for the description of mechanical strain induced by lattice mismatch or external forces. The current implementation is based on continuous elasticity theory, assuming crystallographically perfect heterointerfaces [2]. In this framework one solves a system of partial differential equations as given in Eq. (2.2):

$$\frac{\partial}{\partial x_i} C_{ijkl}\left(\varepsilon_{kl}^{0} + \frac{1}{2}\left(\frac{\partial u_l}{\partial x_k} + \frac{\partial u_k}{\partial x_l}\right)\right) = 0 \qquad (2.2)$$

where C_{ijkl}, ε^{0}_{kl} and u_l are the elasticity moduli tensor, the lattice-matching abrupt strain induced by lattice mismatch and the deformation vector field, respectively. External mechanical forces can be applied by implying adequate boundary conditions, which allows the simulation of piezoelectric effects. The inclusion of atomistic models like valence force field is foreseen for the future.

The third class contains quantum-mechanical models for the calculation of electronic and optical properties of bulk materials and heterostructures. In this case a Schrödinger type equation has to be solved which leads to an eigenvalue problem. The hamiltonian for these models is calculated based on tight-binding and **k·p** theories, including strain corrections in the usual ways [3]. An extension to account for quantum transport theories like non-equilibrium Green's functions is under development.

The three sets of models are completed with the Poisson equation and with the models for material properties as e.g. mobility, recombination and generation processes or dependence of band gap on strain and doping. The different models are in general not independent from each other. Mechanical strain for example is an input for the quantum-mechanical calculation of the band properties of the materials, which in turn are needed for drift-diffusion simulations. A general iteration scheme for self-consistent coupling of different models will be implemented based on underrelaxation or predictor–corrector schemes [4]. Special care is needed if a model is not applied to the whole simulation domain. In this case the simulation results in the different regions have to be consistent on the common boundaries.

The partial differential equations occurring in the different models are discretized in the framework of the finite element method (FEM) and the box integration method.

All models are implemented for one, two and three space dimensions. This allows especially the simulation of 2D and 3D structures including realistic strain patterns, which is important for small structures.

TiberCAD is implemented in C++ using heavily the object-orientated features of the language. It is organized in a highly modularized way which allows for easy addition of new physical models and solvers. Every physical model is encapsulated in its own software module. The modules have a common interface so they can be handled in a model independent way by the control module of the simulator. Material parameters are stored in a database which is accessible to the different modules. The control module is responsible for the creation and setup of all the data structures and models and the flow control of the simulation.

TiberCAD relies on freely available software libraries which provide data structures and routines for the mesh handling for use with FEM [5] and environments for the numerical solution of the resulting (usually sparse) matrices [6] and [7].

2.1.1 The Exciton model in TiberCad

A model for exciton formation, dissociation and transport is proposed in the following for the simulation of electrically pumped polariton laser with a geometry similar to that of a VCSEL and resonant cavity LEDs. How the strain effects and the geometry of the device influence the exciton distribution for a GaN/InGaN laser structure have been demonstrated.

As already said, polariton laser offers intrinsically high modulation speeds, low thresholds, long lifetime and low power consumption. Gallium nitride is a material of choice for polariton lasers and room temperature operation is expected for laser structures based on this material [8].

In order to perform realistic simulations the 2D/3D TiberCAD software [9] has been used, extending it to include exciton formation and transport. Four equations are solved simultaneously, namely the Poisson equation, hole and electron transport at Drift-Diffusion level and the exciton transport equations. Exciton dynamics can be described by a simple Drift-Diffusion model [10,11]:

$$\frac{\partial x(\mathbf{r},t)}{\partial t} = G - R - \nabla \mathbf{J}_x \qquad (2.3)$$

$$\mathbf{j}_{drift}(\mathbf{r},t) = -\mu_x x(\mathbf{r},t) \nabla E_g(\mathbf{r}) \qquad (2.4)$$

$$\mathbf{j}_{diff}(\mathbf{r},t) = D_x \nabla x(\mathbf{r},\mathbf{t}) \qquad (2.5)$$

where x is the exciton concentration, G is the generation term, R the recombination term, E_g is the band gap profile, D_x the exciton diffusion coefficient, μ_x the exciton mobility and J_x is the exciton current density. In our approximation, the generation term reads:

$$G = \gamma\left(np - n_i^2\right) \qquad (2.6)$$

and the recombination term can be described as:

$$R = \frac{x}{1/\tau_{rad} + 1/\tau_{non-rad}} \qquad (2.7)$$

where n and p are the electron and the hole concentrations, γ is the generation rate parameter, τ_{rad} and τ_{non-}rad are the radiative and nonradiative recombination time constants.

The exciton system is treated in the model as the classical Boltzmann gas. Therefore, the exciton density is described as:

$$x = N_x \exp(-\psi_x / kT) \qquad (2.8)$$

with the density of states:

$$N_x = 3\left(\frac{2\pi m_x kT}{h^2}\right)^{3/2} \qquad (2.9)$$

(m_x is the exciton effective mass) and the chemical potential:

$$\psi = \phi_x - E_x \qquad (2.10)$$

where ϕ_x is the effective exciton potential, which is analogous to the electro-chemical potential of electrons and holes, and E_x is the exciton energy, described as:

$$E_x = E_g - B \qquad (2.11)$$

where B is the exciton binding energy.

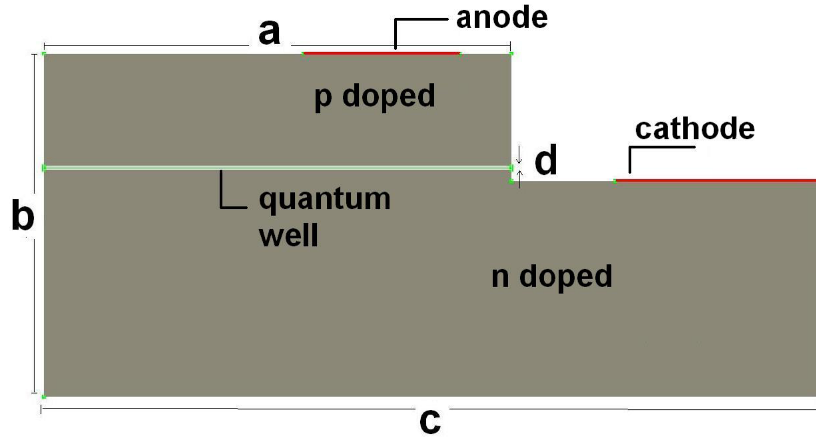

Fig. 2.1- Simulated structure: a = 3 μm, b = 0.723 μm, c = 2 μm, d = 3 nm.

The exciton generation, recombination and dissociation time constants are obtained by Monte Carlo simulations which account for all the electron/hole/exciton scatterings in GaN [12]. In order to study the stationary case, the continuity equation for the effective exciton potential can be written as:

$$\nabla \cdot J_x = -\nabla(\mu_x x \nabla \psi_x) = G - R \qquad (2.12)$$

The Eq. (2.12) is solved together with the stationary Drift-Diffusion equations for electrons and holes, using the Finite Element Method with proper boundary conditions, thus providing a self-consistently calculated potential profile.

A GaN based diode structure with an embedded $In_{0.14}Ga_{0.86}N$ quantum well as shown in Fig. 2.1 has been simulated. In Fig.2.2 the variation of the energy gap inside the quantum well and the ε_{xx} component of the strain are shown.

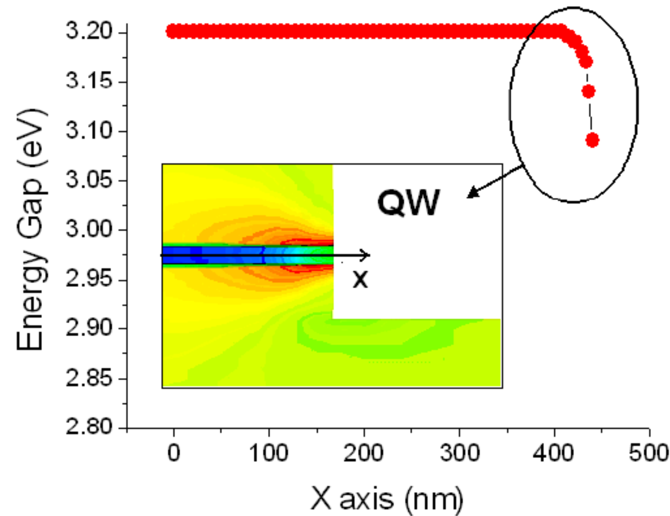

Fig. 2.2- Energy gap profile inside the quantum well (along x -direction). The strain (ε_{xx} component) is shown in the inset.

Results demonstrate a stronger lattice constant variation near the surface due to the strain relaxation at the free surface. The strain becomes less compressive moving toward the surface and this induce a decrease of the energy gap close to the surface. From the Eq. (2.3), one expects that the exciton current flow increases near the surface. In Fig. 2.3, it has been demonstrated that due to the inhomogeneous strain effects near the surface, the excitons are generated and also confined there. Generation of exciton in this region is also related to the electron/hole current which, for this device layout, is large near the laser diode surface. Finally in Fig. 2.4 the carrier densities are shown along the y-direction. As expected, the excitons are strongly confined inside the quantum well. For this polarization, the exciton density is about 10^{12} cm^{-3}. From these simulations the conclusion is that an optimized device layout is required to focus the excitons to the cavity region which is typically at the center of the structure.

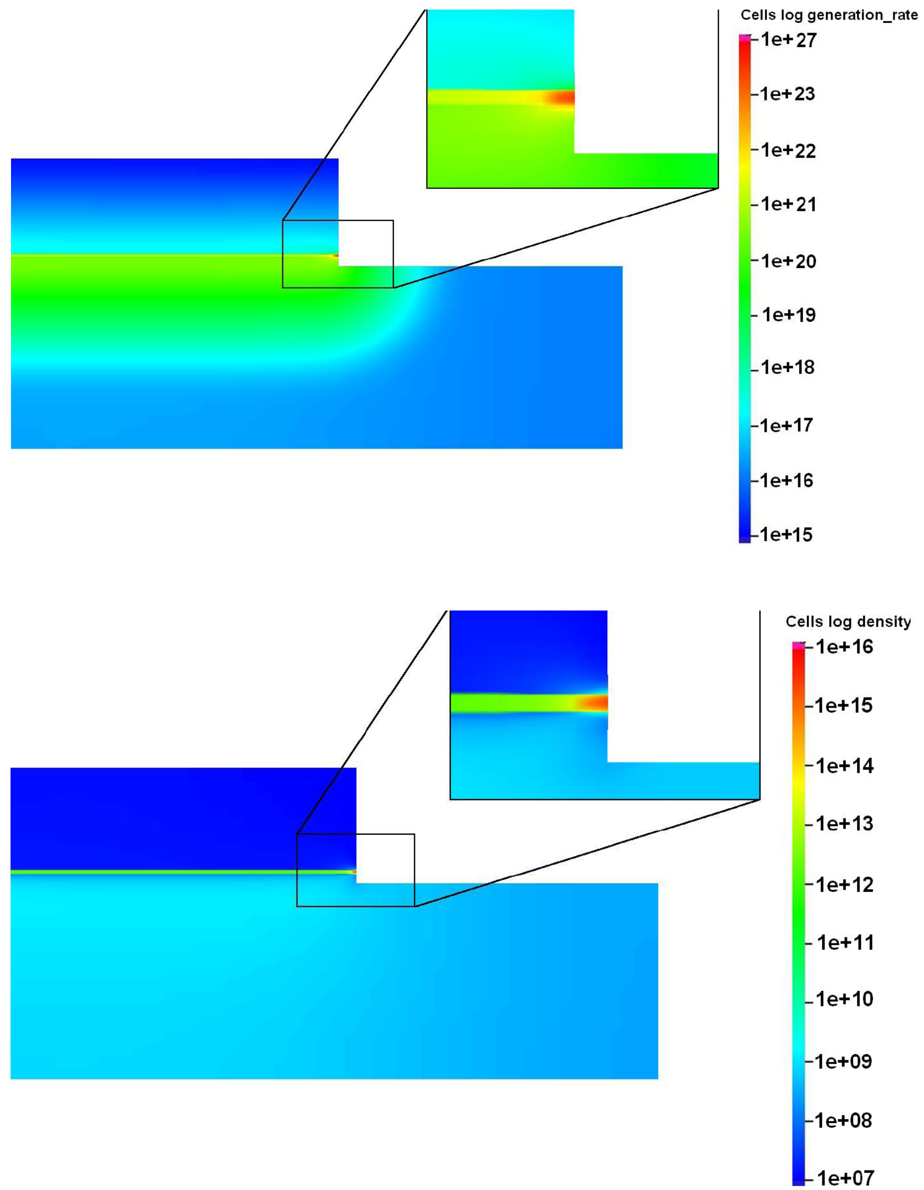

Fig. 2.3- Excitons generation (up) and density (down) maps at 4V applied.

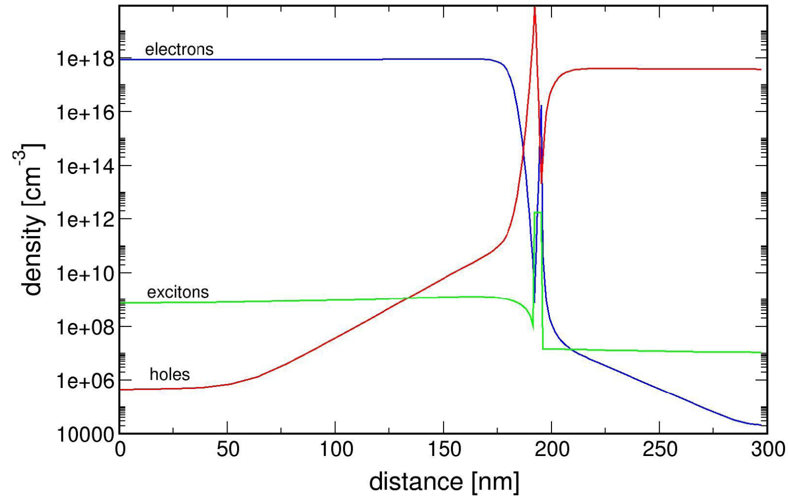

Fig. 2.4- Electron, hole, and exciton density profile along a vertical section of the device.

2.2 The simulation tool Dessis

Dessis is a multidimensional, electrothermal, mixed-mode device and circuit simulator for one-, two-, and three-dimensional semiconductor devices. It incorporates advanced physical models and robust numeric methods for the simulation of most types of semiconductor device ranging from very deep submicron Si MOSFETs to large bipolar power structures [13].

Dessis simulates numerically the electrical behavior of a single semiconductor device in isolation or several physical devices combined in a circuit. Terminal currents [A], voltages [V], and charges [C] are computed based on a set of physical device equations that describes the carrier distribution and conduction mechanisms.

Physical phenomena in semiconductor devices are very complicated and, depending on applications, are described by partial differential equations of different level of complexity.

Coefficients and boundary conditions of equations (such as mobility, generation–recombination rate, material-dependent parameters, interface and contact boundary conditions) can be very complicated and can depend on microscopic physics, the structure of the device, and the applied bias.

Dessis allows for arbitrary combinations of transport equations and physical models, which allows for the possibility to simulate all spectrums of semiconductor devices, from power devices to deep submicron devices and sophisticated heterostructures.

A real semiconductor device, such as a transistor, is represented in the simulator as a 'virtual' device whose physical properties are discretized onto a non-uniform 'grid' (or 'mesh') of nodes.

Therefore, a virtual device is an approximation of a real device. Continuous properties such as doping profiles are represented on a sparse mesh and, therefore, are only defined at a finite number of discrete points in space.

The doping at any point between nodes (or any physical quantity calculated by Dessis) can be obtained by interpolation. Each virtual device structure is described in the ISE TCAD tool suite by two files:

- The grid (or geometry) file contains a description of the various regions of the device, that is, boundaries, material types, and the locations of any electrical contacts. This file also contains the grid (the locations of all the discrete nodes and their connectivity).
- The data (or doping) file contains the properties of the device, such as the doping profiles, in the form of data associated with the discrete nodes. By default, a device simulated in 2D is assumed to have a 'thickness' in the third dimension of 1 μm.

These features can be summarized as:

- An extensive set of models for device physics and effects in semiconductor devices (drift-diffusion, thermodynamic, and hydrodynamic models).

- General support for different device geometries (1D, 2D, 3D, and 2D cylindrical).
- A extensive set of nonlinear solvers.
- A mixed-mode support of electrothermal netlists with mesh-based device models and SPICE circuit models.

Device structures can be created in various ways, including 1D, 2D, or 3D process simulation (DIOS), 3D process emulation (DEVISE), and 2D (MDRAW and DEVISE) or 3D (DIP and DEVISE) structure editors.

Dessis includes optional models for the comprehensive simulation of semiconductor lasers and lightemitting diodes (LEDs). Both edge-emitting lasers and vertical-cavity surface-emitting lasers (VCSELs) are supported. Drift-diffusion or hydrodynamic transport equations for the carriers, the Schrödinger equation for quantum well gain, modal optical rate equations, and the Helmholtz equation are solved self-consistently in the quasistationary and transient modes.

Spontaneous and stimulated optical recombinations are calculated in the active and bulk regions according to Fermi's golden rule. They are added as carrier recombination mechanisms in the continuity equations and as modal gain and spontaneous emission in the photon rate equations. Different line-width broadening models are available for gain broadening.

Both bulk and quantum well (QW) lasers can be simulated. In the case of QW lasers, the optical polarization dependence of the optical matrix element is automatically taken into account. The QW subbands are calculated as the solution of the single-band Schrödinger equation in the effective mass approximation, assuming a box-shaped potential or by a multiple-bands **k·p** method. Strain effects can also be taken into account. The distribution of carriers in the well is determined according to the quantum mechanical wavefunctions and QW density of states.

In the unquantized direction, drift-diffusion transport applies to the carriers. In the quantized direction, two transport models are available. The simple transport model assumes thermionic

emission at the heterointerfaces, which form the quantum well. The advanced transport model separates the QW carrier distributions into a bound and continuum distribution. The fraction of bound and continuum carriers is then self-consistently computed by additional scattering equations, mainly contributed by carrier-carrier and carrier-optical phonon scatterings.

2.2.1 Upgrading of Dessis material parameter file

Gallium nitride and related nitrides are quite new for simulation tools. Even thought several real application have been already achieved with GaN [14], identification of correct material parameters is still under debate. For this reason, the material parameter file of Dessis was improved by direct comparison with available experimental data. This part of the work was made in the collaboration of the group from EPFL of Lausanne. The information used for the upgrading of the file come from Refs. [15-17]. Here, the parameters for nitrogen-containing semiconductors have been studied and described (Fig. 2.5). In Appendix A and B, a complete description of the new material parameter file is reported.

Parameters	GaN	AlN	InN
a_{lc} (Å) at $T=300$ K	3.189	3.112	3.545
c_{lc} (Å) at $T=300$ K	5.185	4.982	5.703
E_g (eV)	3.510	6.25	0.78
α (meV/K)	0.909	1.799	0.245
β (K)	830	1462	624
Δ_{cr} (eV)	0.010	-0.169	0.040
Δ_{so} (eV)	0.017	0.019	0.005
$m_e^{\parallel}$	0.20	0.32	0.07
$m_e^{\perp}$	0.20	0.30	0.07
A_1	-7.21	-3.86	-8.21
A_2	-0.44	-0.25	-0.68
A_3	6.68	3.58	7.57
A_4	-3.46	-1.32	-5.23
A_5	-3.40	-1.47	-5.11
A_6	-4.90	-1.64	-5.96
A_7 (eV Å)	0.0937	0	0
a_1 (eV)	-4.9	-3.4	-3.5
a_2 (eV)	-11.3	-11.8	-3.5
D_1 (eV)	-3.7	-17.1	-3.7
D_2 (eV)	4.5	7.9	4.5
D_3 (eV)	8.2	8.8	8.2
D_4 (eV)	-4.1	-3.9	-4.1
D_5 (eV)	-4.0	-3.4	-4.0
D_6 (eV)	-5.5	-3.4	-5.5
c_{11} (GPa)	390	396	223
c_{12} (GPa)	145	137	115
c_{13} (GPa)	106	108	92
c_{33} (GPa)	398	373	224
c_{44} (GPa)	105	116	48
d_{13} (pm/V)	-1.6	-2.1	-3.5
d_{33} (pm/V)	3.1	5.4	7.6
d_{15} (pm/V)	3.1	3.6	5.5
P_{sp}(C/m^2)	-0.034	-0.090	-0.042

Fig. 2.5Recommended band structure parameters for wurtzite nitride binaries.

References

[1] M.G. Ancona and G.J. Iafrate, Quantum correction to the equation of state of an electron gas in a semiconductor, Phys. Rev. B. Condens. Matter 39 (1989), p. 9536

[2] M. Povolotskyi and A.D. Carlo, Elasticity theory of pseudomorphic heterostructures grown on substrates of arbitrary thickness, J. Appl. Phys. 100 (2006), p. 063514

[3] S.L. Chuang and C. Chang, View the MathML source method for strained wurtzite semiconductors, Phys. Rev. B 54 (1996), p. 2491.

[4] A. Trellakis, A.T. Galick, A. Pancelli and U. Ravaioli, Iteration scheme for the solution of the two-dimensional Schrödinger–Poisson equations in quantum structures, J. Appl. Phys. 81 (1997), p. 7880

[5] B.S. Kirk, J.W. Peterson, libMesh library, http://libmesh.sourceforge.org.

[6] S. Balay, K. Buschelmann, W.D. Gropp, D. Kaushik, M.G. Knepley, L.C. McInnes, B.F. Smith, H. Zhang, PETSc Web page. http://www.mcs.anl.gov/petsc, 2001.

[7] V. Hernandez, J.E. Roman, V. Vidal, SLEPc Web page. http://www.grycap.upv.es/slepc.

[8] G. Malpuech et al. App. Phys. Lett. 81,412 (2002).

[9] www.tibercad.org

[10] Tamor M.A. and Wolfe J.P. 1980, Phys.Rev.Lett44 1703;

[11] V Emiliani, et al. J. Phys.: Condens. Matter 11 (1999) 58895900.

[12] G. Kokolakis et al. Phys. Stat. Sol. (a) 195, 618 (2003)

[13] Dessis Manual, ISE Integrated Systems Engineering, Release 9.5

[14] Merfeld D. W. et al., Influence of GaN Material Characteristics on Device Performance for Blue and Ultraviolet Light-Emitting Diodes, Journal of Electronic Materials, Nov 2004

[15] Vurgaftman I. and Meyer J. R., Band parameters for nitrogen-containing semiconductors, J. Appl. Phys., Vol. 94, No. 6, 15 September 2003

[16] Chris G. Van de Walle and Jorg Neugebauer, Small valence-band offsets at GaN/InGaN heterojunctions, Appl. Phys. Lett. 70(19), 12 May 1997

[17] C. Zellweger, Realization of GaN-based light emitting devices, EPFL thesis

Chapter 3

Design and optimization of GaN based LED and Polariton Laser / VCSEL

The second part of the work concerned the study of new structures and devices to optimize the design of the polariton laser.

The first step was to compare experimental data and simulation results of simple LED structures in order to validate the simulation tool performances. Then, several designs of LED structure have been simulated to understand the influence of the geometrical parameters and the material properties on the characteristics of the device. As a consequence, new VCSEL structures have been designed, optimizing the electrical injection.

These results led to publication of papers and a patent, as described in the next chapter.

3.1 Influence of mesa contact dimension on the GaN/InGaN LED properties

As previously shown, the basic geometry of electrically driven polariton lasers is very similar to that of vertical cavity surface emitting lasers (VCSELs) and resonant cavity light-emitting diodes (RCLEDs). For this reason, a simple GaN-based LED geometry has been intentionally adopted in order to better understand the factors affecting the LED characteristics (Fig. 3.1). Using this geometry, devices with several p-contact and mesas diameters have been studied.

Starting from standard LED structures grown in LASPE laboratories of EPFL (Lausanne, Switzerland), experimental studies and simulations of GaN-based LED structures have been done in order to highlight and to confirm the factors influencing the devices performances and to improve the software simulations. Several parameters are used to evaluate the emission characteristics of a LED structure. The quantum efficiency, together with the I-V characteristics, will be used as quality parameters. A simple LED geometry has been intentionally adopted in order to better understand the factors affecting the LED characteristics.

The LED structures studied are grown by MOVPE on 2 inch sapphire substrates. The typical geometry of the device consists of: 2 µm Si doped (3×1018 cm-3) n-GaN layer; 3 x QWs [12 nm Si doped GaN; 1.5 nm $In_{0.14}Ga_{0.86}N$]; 20nm $Al_{0.2}Ga_{0.8}N$ electron-barrier; 120 nm Mg doped (~3×10^{17} cm^{-3}) *p*-GaN layer. For this geometry, the device has been studied with three different MESAs diameters (540 µm, 240 µm, 190 µm) P-type contacts are realized using a Ni/Au metallization on top of the MESA structures with a diameter 140µm smaller than the MESA diameter (Fig. 3.1). For this LED with 3 QWs a central emission wavelength λ = 403 nm is measured. Device with similar structure but different number of quantum well have been also fabricated in order to compare with the 3QW reference structure.

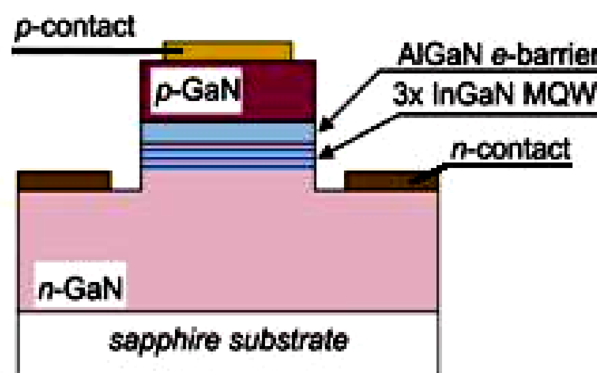

Fig. 3.1 - Schematic cross section of the reference structure.

Devices are simulated using the IseTCad simulation software. Here, Poisson equation, carrier continuity equations for electrons and holes, and transport equations at drift-diffusion level are solved in a self-consistent fashion. Full account of spontaneous and polarization field is considered. Material parameters used in the simulation are tuned according the experimental data previous reported by EPFL [1-3] and described in the previous chapter.

The setup used for the characterization of the device made in LASPE laboratories consists of a probe station, a large area silicon photodiode (Hamamatsu S1337-1010BR) and a HP 4145A semiconductor parameter analyzer used as DC voltage source, current and photocurrent monitor. The devices are in direct contact with the surface of the detector and the emitted light is collected from the backside of the substrate.

The IV characteristics of LED having different contact and MESA size as a function of the injection current is shown in Fig. 3.2 where both experimental and simulation results have been compared.

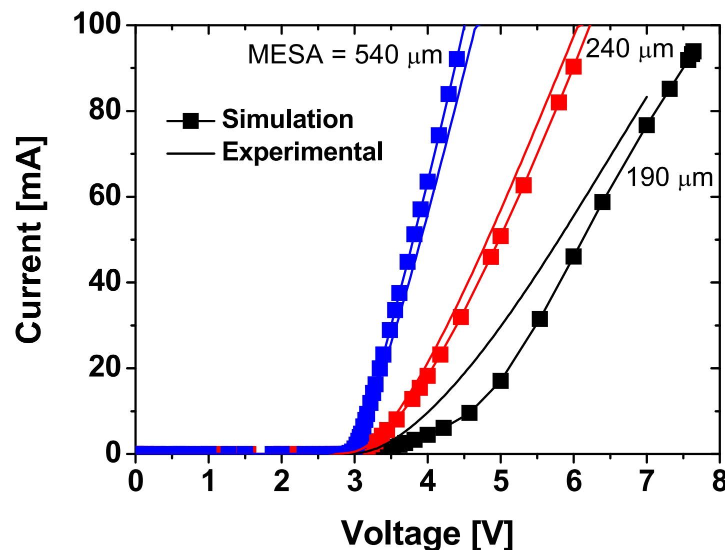

Fig. 3.2 - Current-voltage (IV) characteristics of the fabricated LEDs for several MESA diameters. Comparison between simulation results and experimental data.

A very good comparison between experiment and simulation is achieved (in the simulation nominal parameter are considered). This shows the very good control and reproducibility of material parameters in the fabrication process.

External quantum efficiency (η_{ext}) of InGaN/GaN based LEDs has been shown to increase by increasing the number of QWs in the active region [4]. Samples having one, three and five QWs have been fabricated, characterized and simulated in order to find an upper limit for the number of QWs which optimizes the η_{ext}. Simulations have been performed by varying the numbers of QWs in the 50μm mesa diameter device. The internal quantum efficiency, η_i as the ratio between the radiative recombination rate in the QWs and the total recombination rate have been calculated. η_i is related to the external quantum efficiency η_{ext} by the equation:

$$\eta_{ext} = \gamma_{inj} \cdot \eta_i \cdot \eta_{extract} \qquad (3.1)$$

where γ_i is the injection efficiency and $\eta_{extract}$ is the extraction efficiency. In the following, the simplifying assumption that both γi and ηextract are independent on the number of quantum wells have been done. Fig. 3.3, shows the calculated internal quantum efficiency as well as the measured external quantum efficiency, both normalized to the maximum efficiency value obtained for the device with one quantum well. A qualitative agreement between simulation results and experimental data is achieved. The efficiency increases by using a larger number of quantum wells. This is due to the more strict dependence of radiative recombination rate (RR) on the quantum well number with respect to the sum of RR and the non-radiative recombination rate (RNR). In fact, the contribution to the RR arises from the QWs while the RNR is the sum of the bulk and QW contributions, RNR=RNR(bulk)+RNR(QWs). Saturation of quantum efficiencies for both experimental and simulation results, is achieved for samples where the number of QWs is equal or larger than three. By increasing the number of quantum well, RNR(QWs) becomes much larger that RNR(bulk) which results in a saturation of the efficiency.

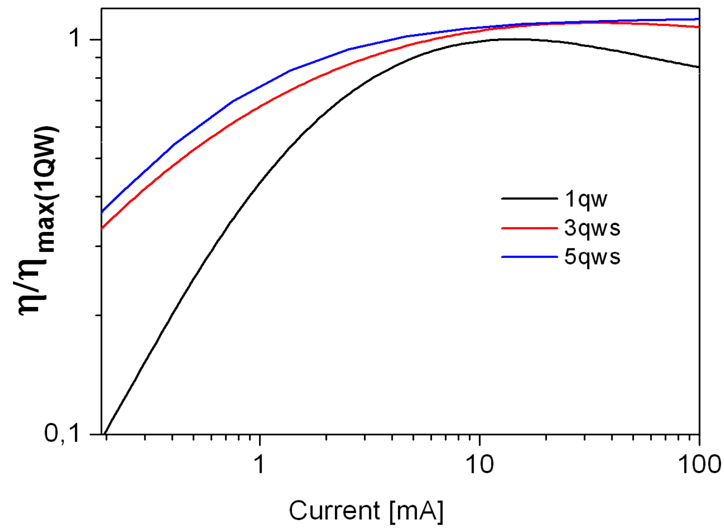

Fig.3.3 - Simulated Internal Quantum Efficiency for devices with a different number of quantum wells.

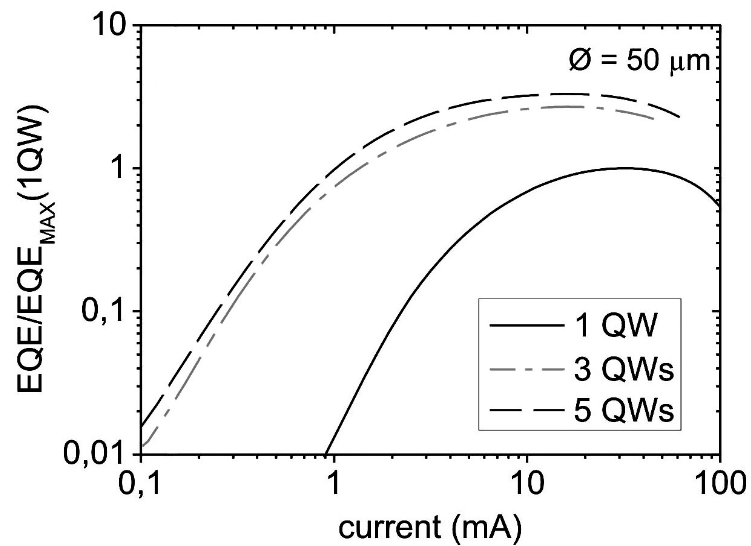

Fig.3.4 - Experimental External Quantum Efficiency (EQE) for devices with a different number of quantum wells.

The difference in η_{ext} is even more dramatic in the low injection range, where η_{ext} for devices with 5 QW is more than 2 orders of magnitude higher than for samples with only 1 QW. In the

realized devices, the presence of non radiative channels (i.e. dislocations, point defects, etc.) bypassing the active region, is responsible for the decreasing of η_{ext} in the low current range. Having a defect free structure would imply a constant η_{ext} independently of the injection current. For this reason, considering a constant superficial defect density, when the device size is decreased (higher current density for the same current value), the η_{ext} curves shift toward lower injection current values as shown in Fig. 3.5. It can be also observed that, as the contact size is decreased, the maximum EQE increases. This value, for devices having a 50 μm contact diameter, is almost two times higher than for devices having a 400 μm contact diameter. This result could be explained by considering an improved light extraction near the MESA edges.

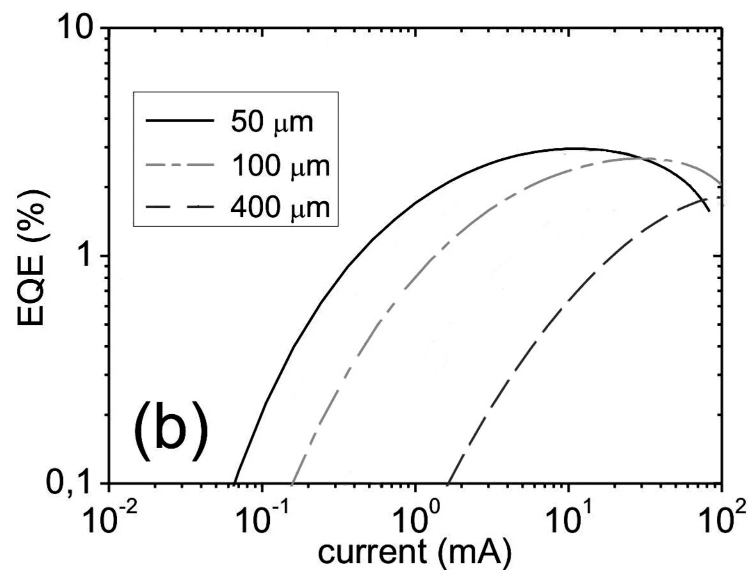

Fig. 3.5 - External quantum efficiency versus driving current for LEDs for different mesa diameter.

In fact, light extracted from LEDs is the sum of the light extracted directly from the substrate and of a small fraction of light extracted from the device sidewalls that reaches the bottom side of the substrate. Other phenomena, like photon re-absorption into the QWs as well as photon recycling, affect the overall efficiency of the devices. Absorption in the n-GaN and p-GaN regions can be neglected for the propagation direction perpendicular to the emitting surface, since the

device thickness (~3 μm) is much smaller than the absorption length at 400 nm (100 to 500 cm^{-1}) [5].

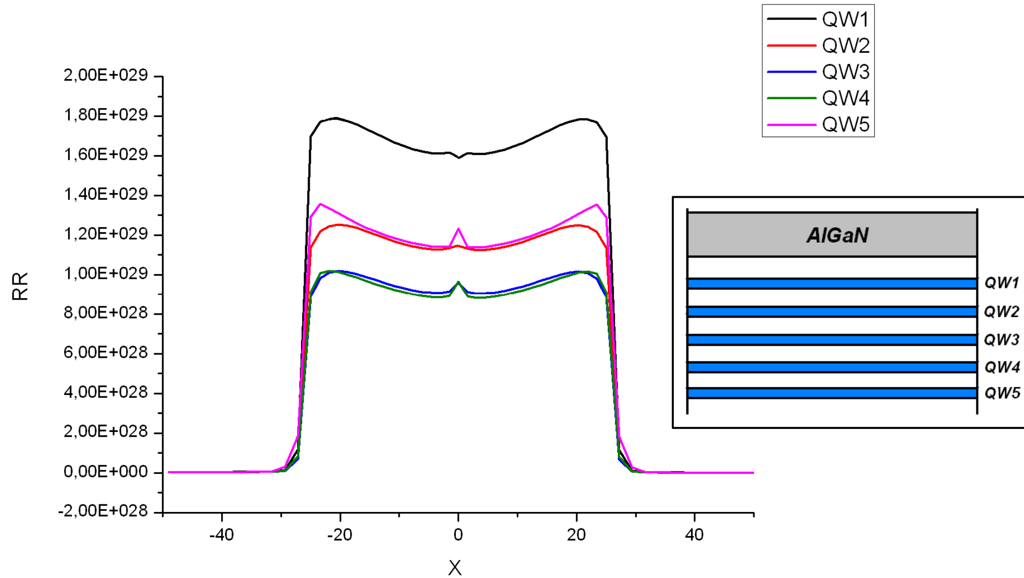

Fig. 3.6 - Radiative recombination rate [$cm^{-3}s^{-1}$] inside the quantum wells (x-direction) at 5V applied.

The simulation results of Fig. 3.6 show that the radiative recombination between holes and electrons mainly occurs into the first QW close to the AlGaN barrier. This is due to low hole mobility (20 $cm^2V^{-1}s^{-1}$) with respect to the electron one (1500 $cm^2V^{-1}s^{-1}$) and to the presence of an AlGaN e-blocking layer.

3.2 Design of current confinement layer

In order to optimize the current confinement in the center part of the device, three different structure have been simulated. As shown in Fig. 3.7, the first design has the AlInN current confinement layer below the active region, with the aim of forcing the carrier transport in the center part of the device (as shown in Ref. [6]); the second design has a double confinement layer; the

third one a single layer above the active region. The Internal Quantum Efficiencies (IQE) (Fig. 3.8), the Focusing Efficiencies (Fig. 3.9) (defined as the ration between the total radiative recombination rate of the QWs in the aperture region and the total recombination rate of the QWs in the whole device) and the IV characteristics (Fig. 3.10) of these three structures have been investigated.

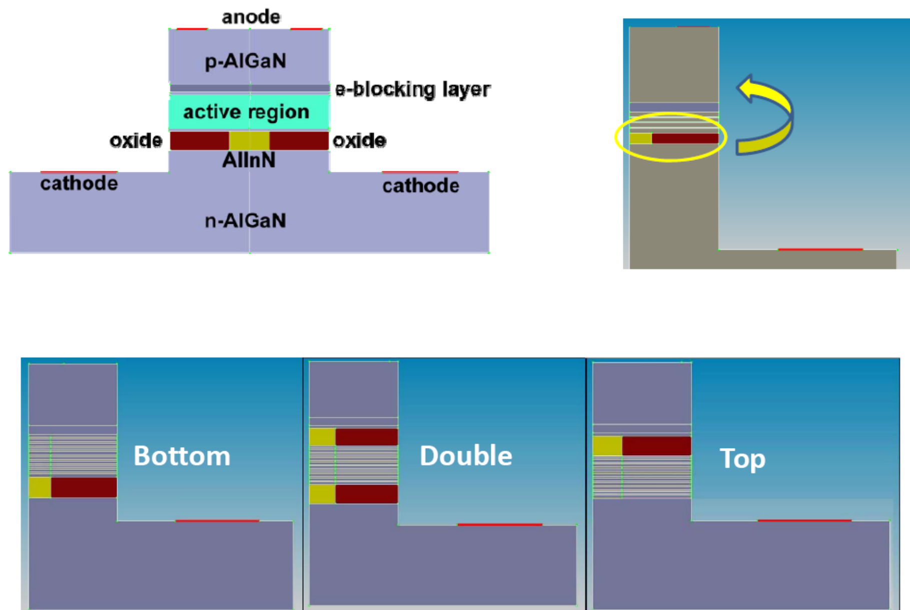

Fig. 3.7 - Three different design for the AlInN current confinement layer

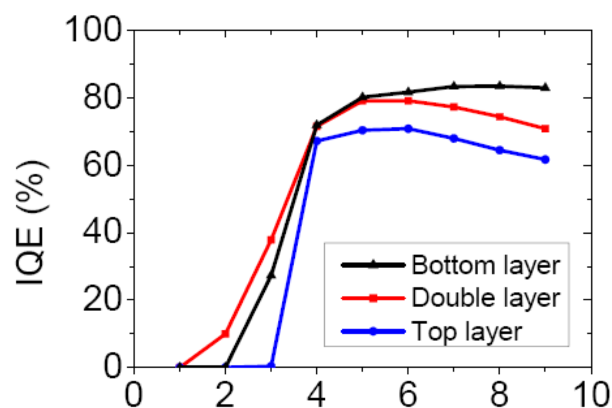

Fig. 3.8 - Internal quantum efficiencies for three different design of the AlInN current confinement layer

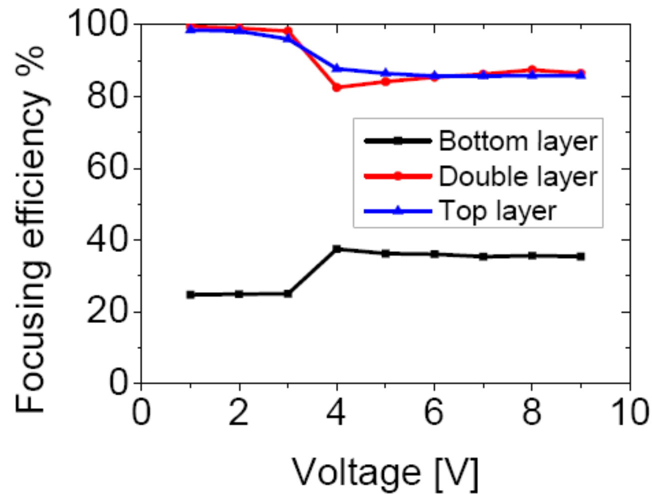

Fig. 3.9 - Focusing efficiencies for three different design of the AlInN current confinement layer.

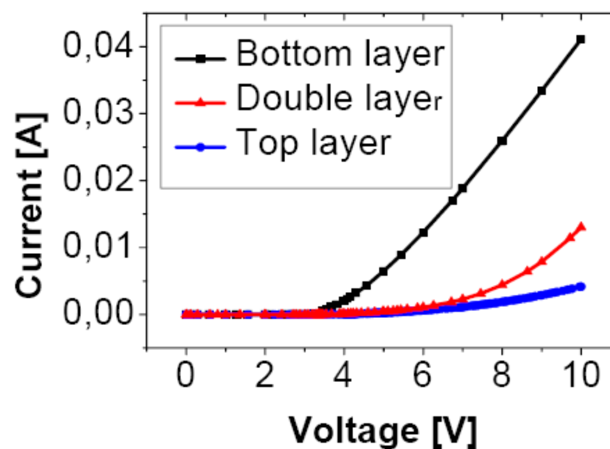

Fig. 3.10 - IV characteristics for three different design of the AlInN current confinement layer

As shown, the focusing efficiency increases by using the top layer and the double layer. But the the current is strongly reduced. For these reasons, the structure with the bottom AlInN layer has been chosen as the best trade off of the characteristics studied in these simulations.

However, the AlInN layer is not enough to confine the current in the center part of the device: when the applied voltage increases, a spread of the current has been observed in the device (fig. 3.11). [18] This behavior has been confirmed also by simulations. As shown in fig. 3.12, the maximum value of the radiative recombination rate is quite focused in the center part of the device

for 3V applied, but when the voltage increases, radiative recombination rate spreads towards the p contact region. This behavior will be better described and explained in the next paragraphs.

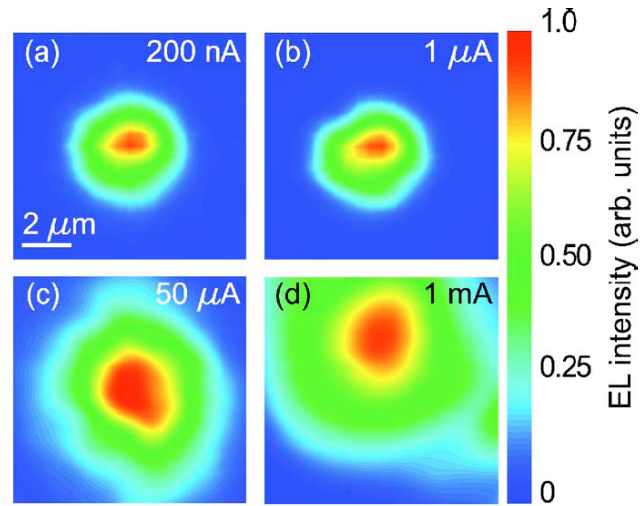

Fig. 3.11 - EL intensity maps of a GaN based LED with AlInN layer confinement realized at EPFL laboratories, at (a) 200 nA, (b) 1 μA, (c) 50 μA, and (d) 1 mA injection currents.

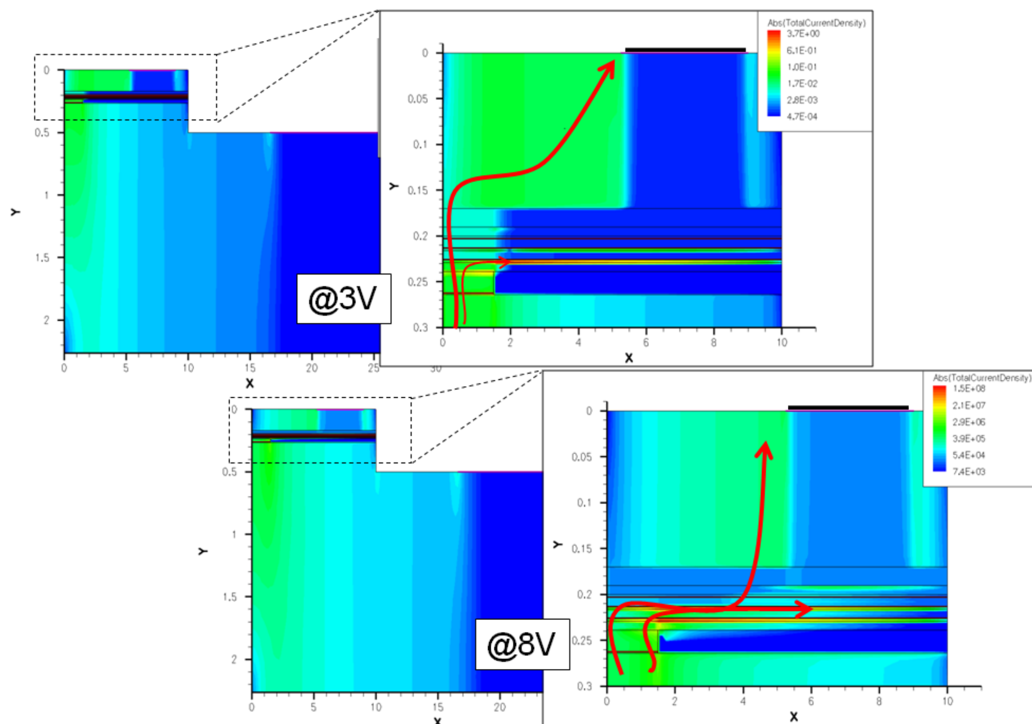

Fig. 3.12 – Radiative recombination rate map in the half part of the device (in x=0 is the symmetry axis for cylindrical symmetry) at 3V and 8V applied.

3.3 The influence of mobility unbalance

Concerning the enhancement of electrical and optical coupling properties of POLARITON laser (PLASER) and VCSEL structures, one of the main problems remains the focusing of the carrier density in the central part of the device where optical mode confinement is present. For this reason the use of an efficient current confinement layer is required even though this has been shown to be limited to low applied voltages.[6] The main effect of the reduce carrier focusing efficiency is the excitation of unwanted higher order modes strongly raising the lasing threshold to an unacceptable level. [7]

So far, the presence of strong polarization field [8] and the large resitivity of the p-layers forming the structure [7, 9] have been advocated to explain the non-uniform charge injection which reduces the carrier focussing efficiency and the consequent failure in the realization of electrically driven VCSEL and PLASER. In fact, as will be showed, this effect is mainly related to the strong unbalance between electron and hole mobilities.

The simulated structure is similar to the one developed in [6]. A schematic layout of simulated device is shown in Fig. 3.13: the mesa diameter is 20 μm, contacts are rings with inner/outer diameters of 10.5/18 μm for the p-contact and 33.25/52.25 μm for the n-contact, the current confinement is achieved by selective oxidation of an $Al_{0.82}InN$ layer of 25 nm high, leaving an horizontal aperture of 5 μm. The structure has the following layer sequence: 85nm p-doped ($3x10^{19}cm^{-3}$) $Al_{0.15}GaN$, 10nm p-doped ($3x10^{19}cm^{-3}$) $Al_{0.20}GaN$ electron barrier layer, 3x $GaN/Al_{0.15}GaN$ (2nm/3nm) QWs forming the active region, 25 nm partially oxidized $Al_{0.82}InN$ layer, 140 nm n-doped ($3x10^{18}cm^{-3}$) $Al_{0.15}GaN$.

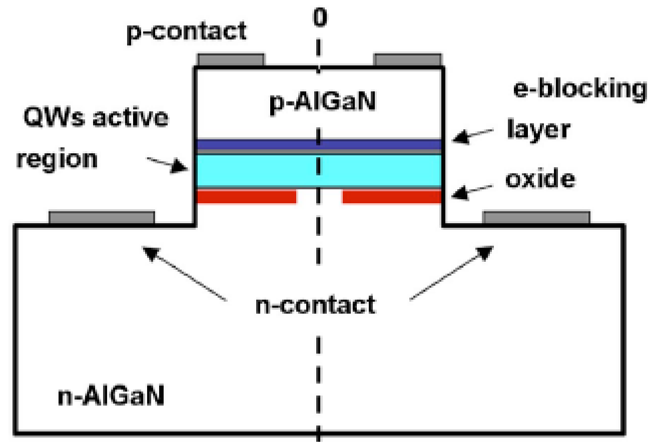

Fig. 3.13 - Schematic section of the simulated device (cylindrical symmetry has been used in simulation)s. The dashed line represent the symmetry axis.

Material parameters used in the simulations have been tuned according the experimental data presented in Refs.[1][2][11]. We have considered a realistic field dependent mobility model [13]:

$$\mu(E) = \frac{\mu_0}{\left[1 + \left(\frac{\mu_0 E}{v_{sat}}\right)^{\beta}\right]^{1/\beta}} \qquad (3.2)$$

where μ_0 denotes the low field mobility, E the driving field, v_{sat} the saturation velocity and β is the Caughey-Thomas parameter [14].

The low field mobilities are equal to μ_{oe}=1100cm^2/Vs for electrons [14] and μ_{oh}=20 cm^2/Vs for holes [15]. In the simulations, the Bragg reflectors have been not considered since the attention has been focused only on charge injection mechanisms.

As clearly shown by the 2D maps of Fig 3.14a, the radiative recombination rate, which is proportional to the local product of electron and hole densities, is not focussed in the central region of the VCSEL where the intensity of the electromagnetic field is high. This characteristic is not related to the choice of the thickness and doping of the different layers forming the structure. In

fact, additional simulations have been performed to equalize the p and n layers resistances [7] but also in this case the radiative recombination rate is not focussed in the central part of the VCSEL.

The main motivation for the lost of carrier injection focussing is the strong unbalance of the electron and hole mobilities. Electrons injected in the QWs experience a larger drift ($v_{drift}=\mu E$) compared to the holes injected by the p-contact and consequently the recombination between electron and hole occurs far apart from the center of the device toward the p-contact region. One should consider that in the active region the electric field along the y-axis reaches values of the order of kV/cm.

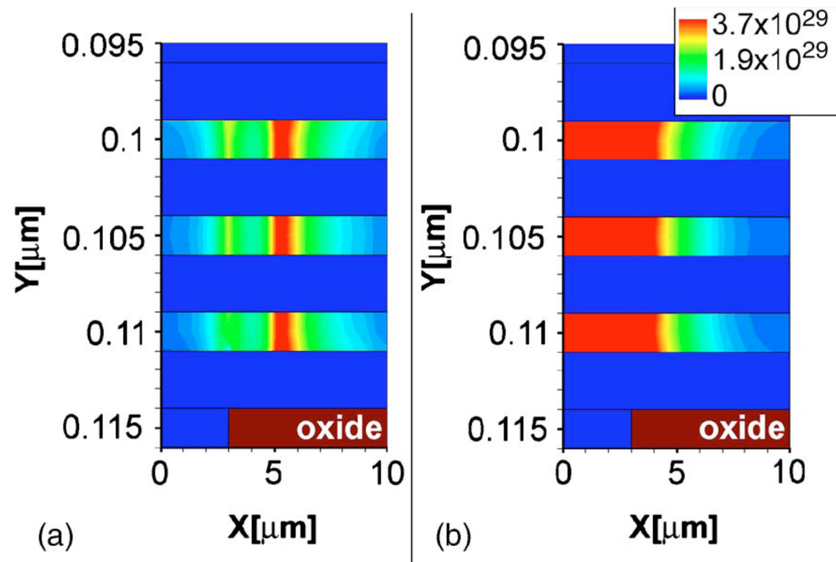

Fig. 3.14 - Recombination maps (cm−3 s−1) for the VCSEL at 7 V around the active region. (a) Simulation result with real mobility values μ_{0e}=1100 cm2 /V s, μ_{0h}=20 cm2 /V s and (b) simulation results with electron mobility=hole mobility=1100 cm2 /V s.

To prove this assertion several simulations have been performed where a perfectly balanced electron and hole mobility, both equal to 1100 cm^2/Vs, is considered. The calculated 2D radiative recombination rate map is shown in Fig. 3.14b. In this case, a stronger focusing of the recombination rate in the central zone of the quantum wells is shown. To be noticed that this conclusion is not related to particular choice of the mobility value but only to the balance between electron and hole mobilitites.

In fig. 3.15 the radiative recombination rate and the absolute value of the current density for both balanced and unbalanced mobility case along the horizontal x-direction for the central quantum well have been reported. The focusing effect induced by the balancing of the mobility is quite evident. However, focusing induced by mobility balance is only related to the radiative recombination and not to the current density. In fact, current density peaks in the region of high velocity (i.e. high electric field) independently of the mobility value. This shows how the optimization procedures for current injection in GaN-VCSEL (or PLASER) should concentrate directly on carrier focusing without pursuing the focusing of the current which is related to both densities and velocities.

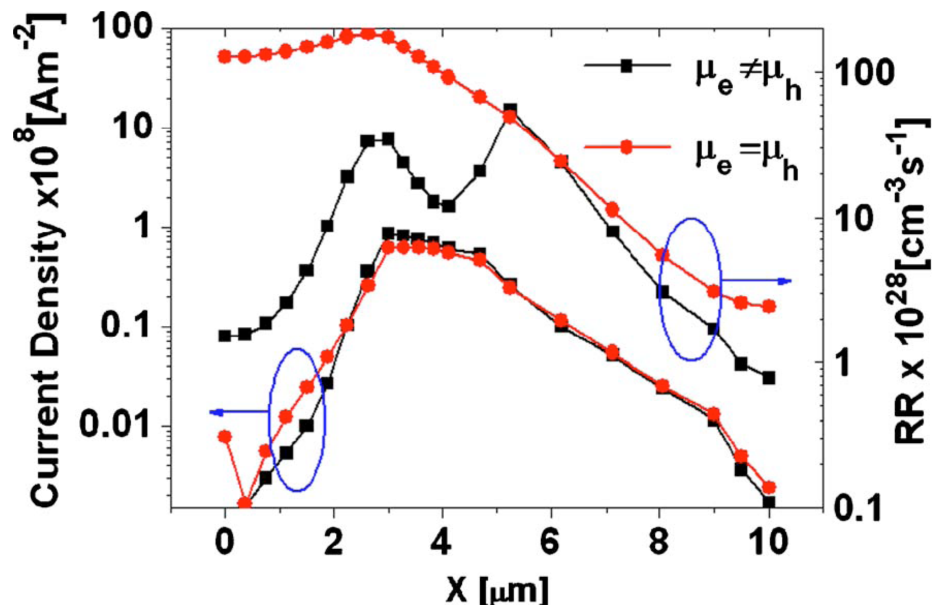

Fig. 3.15 - Radiative recombination rate and absolute value of the current density for both balanced and unbalanced mobility case in the middle quantum well along the horizontal x direction.

In order to describe quantitatively the focussing properties of the structure and the relation with the mobility, the focussing efficiency (FE) has been extracted from the simulation. Moreover, the internal quantum efficiency (IQE) as the ration between the total radiative recombination rate in the QWs and the total recombination rate in the structure (obtained summing the radiative and non-radiative recombination rates) has been calculated.

The calculated FEs for both real unbalanced mobility model and perfectly balanced mobility model as a function of the applied potential are shown in Fig 3.16. Above threshold (V_{th}~3 V) the focussing efficiency is much larger in the balanced mobility simulation than in the real unbalanced mobility condition. Almost the 60% radiative recombination occurs in the aperture region of the QW when electrons and holes have the same mobility. This reduce to 20% when a the realistic unbalanced model for the mobility is considered. As discussed above, these results do not depend on the mobility value used for the mobility balanced simulations and are not related to the presence of heterointerfaces between GaN/AlGaN forming the QWs. In fact, the same conclusion holds for a VCSEL with bulk GaN active region. The internal quantum efficiency, on the other hand, is not influenced by the mobility balance (fig.3.16).

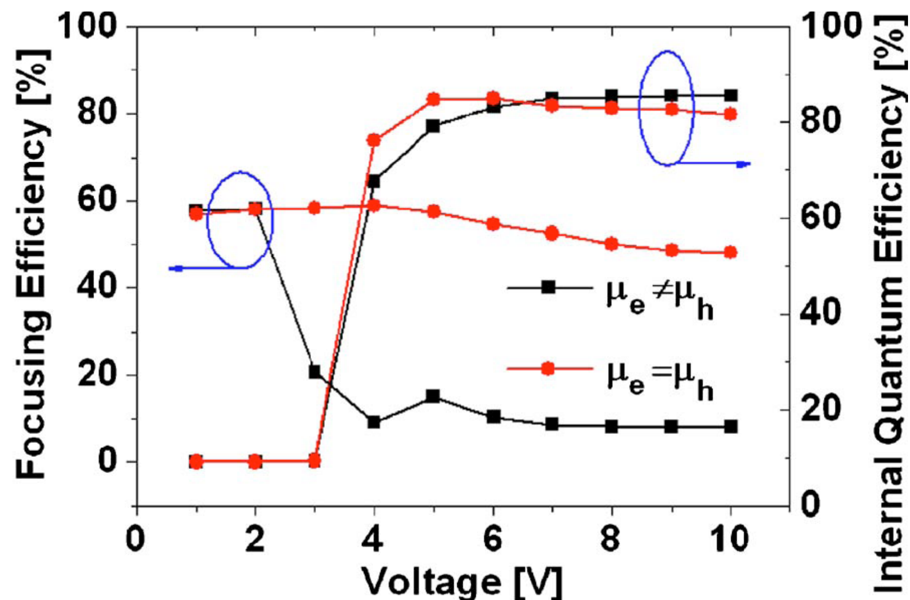

Fig. 3.16 - FE and IQE for the VCSEL. Results are reported for real mobility values and for the case where electron mobility=hole mobility=1100 cm2̃ V s.

Several design strategies could be considered for contrasting the reduce focussing efficiency induced by the electron and hole mobility unbalance, as a proper strain engineering of the layers to improve hole mobility or considering an inverted structure, where the n-doped part of the device is growth on the p-doped layers.

3.4 Enhancement of carrier focusing

The relation between the focusing efficiency and the unbalance between electron and hole mobility have been outlined in the previous section. To overcomes the focusing limitation of conventional GaN based VCSELs and PLASERs a new device structure is proposed where the n-layer is on the top of the p-layer .

The schematic layouts of the simulated structures are shown in Fig.3.17. Here a conventional structure (Fig. 3.17a), similar to the device described before where the p-doped layer is on top of the n-doped layer, and a new "inverted" structure (Fig. 3.17b) where the n-layer is on top of p-layer are proposed. For both structures the mesa diameter is 20 μm, upper contacts are rings with inner/outer diameters of 10.5/18 μm and 33.25/52.25 μm for the other contact, the current confinement is achieved by selective oxidation of an $Al_{0.82}InN$ layer of 25 nm high, leaving an horizontal aperture of 6 μm [16]. The conventional structure (fig. 17.a) has the following layer sequence: 85nm p-doped ($3x10^{19}cm^{-3}$) $Al_{0.15}GaN$, 10nm p-doped ($3x10^{19}cm^{-3}$) $Al_{0.20}GaN$ electron barrier layer, 3x GaN/$Al_{0.15}GaN$ (2nm/3nm) QWs forming the active region, 25 nm partially oxidized $Al_{0.82}InN$ layer, ~140 nm n-doped ($3x10^{18}cm^{-3}$) $Al_{0.15}GaN$.

The "inverted" structure (fig. 17.b) has 71 n-doped ($3x10^{18}cm^{-3}$) $Al_{0.15}GaN$, 25 nm partially oxidized $Al_{0.82}InN$ layer, 3x GaN/$Al_{0.15}GaN$ (2nm/3nm) QWs forming the active region, 10nm p-doped ($3x10^{19}cm^{-3}$) $Al_{0.20}GaN$ electron barrier layer, 125nm p-doped ($3x10^{19}cm^{-3}$) $Al_{0.15}GaN$. Only few realization of such inverted structure [16] have been reported even though the relation with focusing efficiency has never been outlined.

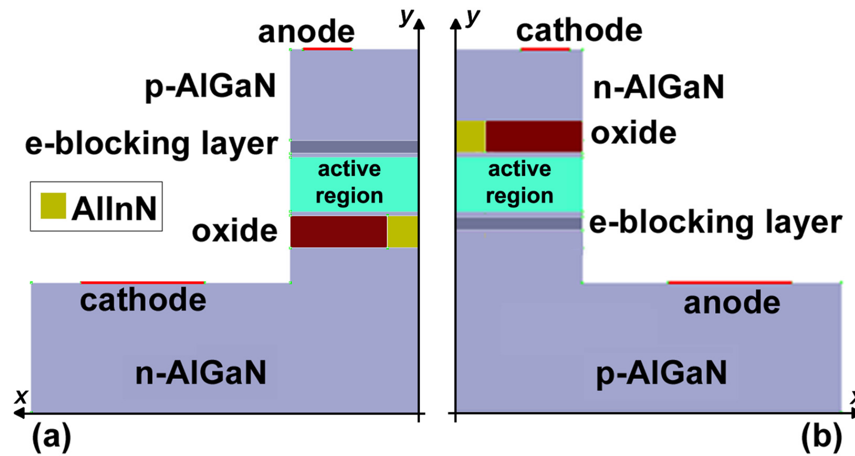

Fig. 3.17 - Schematic structure of the conventional (a) and inverted (b) device.

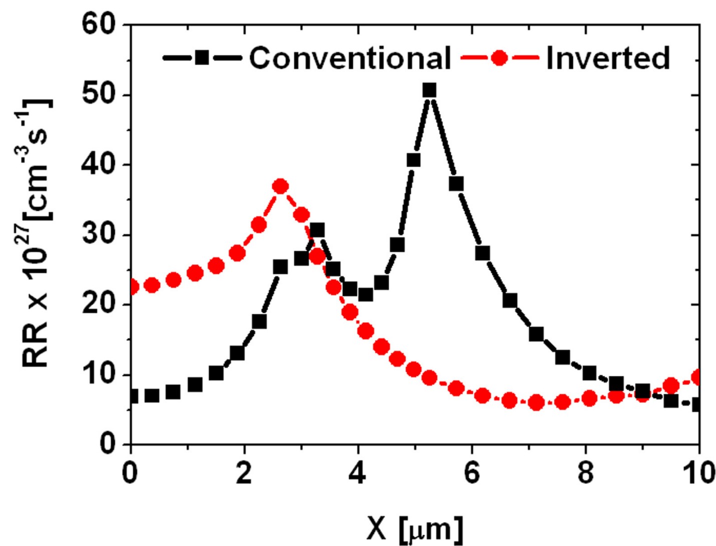

Fig. 3.18 - Radiative recombination rate for the conventional and inverted structure in the middle QW along the horizontal direction. The origin of the X axis is the centre of the device. Results are obtained for an applied potential of 5 V.

Fig. 3.18 shows the radiative recombination rate, which is proportional to the local product of electron and hole densities, in the middle QW along the horizontal direction (here the *x*-axis origin is the centre of the device). One can observe that for the conventional device the radiative

recombination is not focussed in the central region of the VCSEL where the intensity of the electromagnetic field is high.

In order to describe quantitatively the focusing properties of the structure, we extract from the simulation a focusing efficiency (FE). The FE for the conventional structure (Fig. 3.19) is quite low and it is below 20% in typical operative conditions. As said, the main reason for this low FE is the unbalance between electron and hole mobilites, which is quite large in GaN related semiconductors.

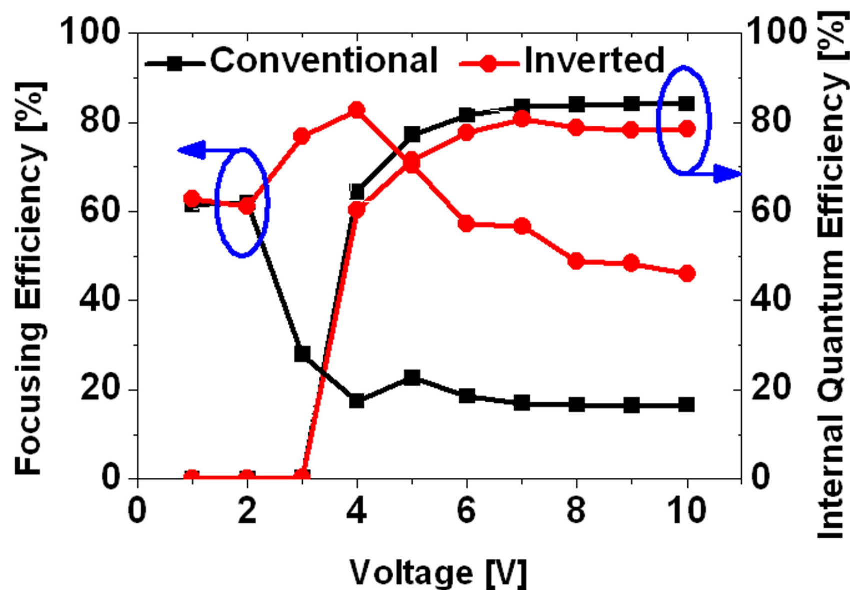

Fig. 3.19 - Focusing efficiency and Internal Quantum efficiency for the conventional and inverted structure as a function of the applied potential.

As shown in the radiative recombination rate of Fig 3.18 and in the focusing efficiency plotted in Fig. 3.19, the inverted structure allows for a better confining of electron and holes in the current aperture region resulting in a strong improvement of the focusing efficiency which reaches an average value of 60% in the operative region with a peak of 80% in the region close to the threshold (the typical operative region for PLASERs). Fig. 3.19 shows also the internal quantum efficiency (IQE).

In order to understand the reasons for the large improvement of the focusing efficiency in Fig. 3.20 hole and electron density maps at 5V for both the conventional and the inverted structure are shown. In the conventional structure, a large potential drop occurs in the active region between the p-side end of the current aperture and the p contact which are quite close each other (~2 μm). The induced field, of the order of few kV/cm, pushes electrons toward the p contact and this explains the shape of the electron density in the active region (Fig. 3.20a). On the other hand, the inverted structures present a larger distance between the p-side end of the current aperture and the p-contact. This reduces the electric field along the y direction in the active region, resulting in a focusing of the electron injected in the active region as shown in Fig. 3.20c.

To point out that, if a conventional structure with a current aperture above the QWs is considered, the FE increases for the same reasons given above for the inverted structure. However, the current flowing in the device will be very reduced due to the high access resistance between the p-layer and the QW region induced by the presence of the oxide. This does not occur in the inverted structure since the resistive effect of the oxide is compensated by the higher electron mobility with respect to that of the holes.

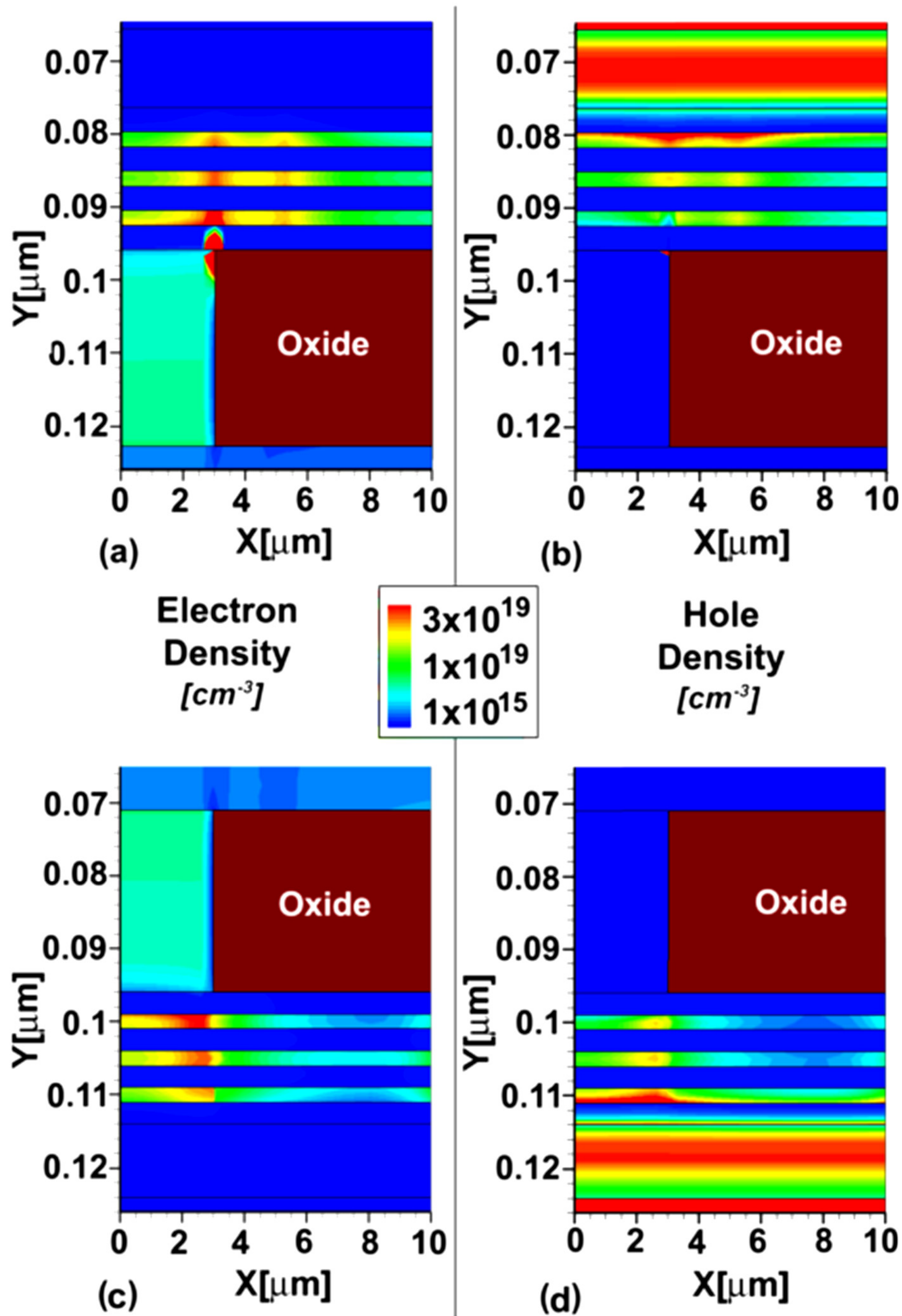

Fig.3.20 - Electron and hole density at 5 V for the conventional (a,b) and inverted (c,d) structure.

3.5 Discussion on the inverted structure

It could be interesting to stress the relation between the confinement effect of the oxidized AlInN layer (current aperture) and the n/p contacts. In fact, while the current aperture has always positive focusing properties, the contacts tends to spread the carriers in the whole active region. This spreading effect is mainly due to the electric field in the active region induced by the contact proximity. Thus to avoid the negative influence of the contacts on the focusing efficiency, one need to separate the active region from the contact region. Clearly, this is much more critical for the top contact being closer to the active region with respect to the bottom contact.

As shown, the negative influence of the contacts can be avoided by placing the active region below the current aperture. In principle this could be made for both conventional (p-on-top) and inverted (n-on-top) structure, but, as yet discussed, the large difference between hole and electron mobilities makes the internal quantum efficiency quite low for conventional structure with respect to the inverted one. This phenomena is clearly shown in Fig. 3.21 where we plot the x-component of Electric Field as a function of the x-coordinate along the central quantum well.

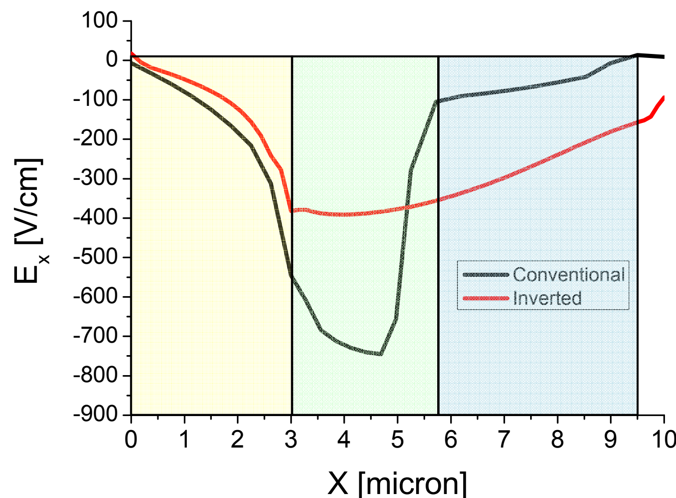

Fig. 3.21: x-component of the Electric field along the middle QW. Current aperture extend from 0 to 3 micron (yellow region), top-contact region extend from 5,75 to 9 micron (blue region).

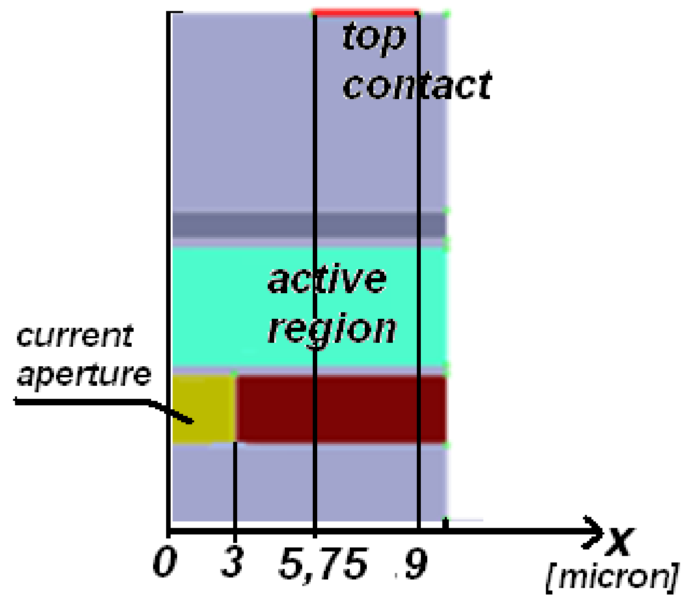

Fig.3.22 - Half section of the device showing the different regions along x-direction (from 0 to 3 micron: aperture region; from 5,75 to ~ 10 micron: top-contact region)

For the conventional structure Ex reaches -750 V/cm in the region just after the current aperture while this reduces to -450 V/cm for the inverted structure. This large field difference is responsible for the larger spreading in the Conventional structure with respect to the inverted one.

At small voltage the potential drop induced by the contact is quite low, consequently the induced electric field is low and the current aperture dominates the focusing properties of the device which is similar for both conventional and inverted geometries. However, holes are less confined in the current aperture being the electric field low (Electric Field, being negative, tend to to push holes toward the current aperture). For this reason the FE is only 60%. One should also notice that below 3V the structure is off and any value of the FE does not have a practical meaning. By increasing the applied potential the electric field in the contact region tend to increase and, as discussed above, this has negative consequences on FE in the structure where the active region is more close to the contact region (that is in the conventional structure).

The inverted structure has a maximum FE around 4 V. At larger potential the electric field out of the current aperture tend to increase pushing electron in that region (that is, reducing the FE).

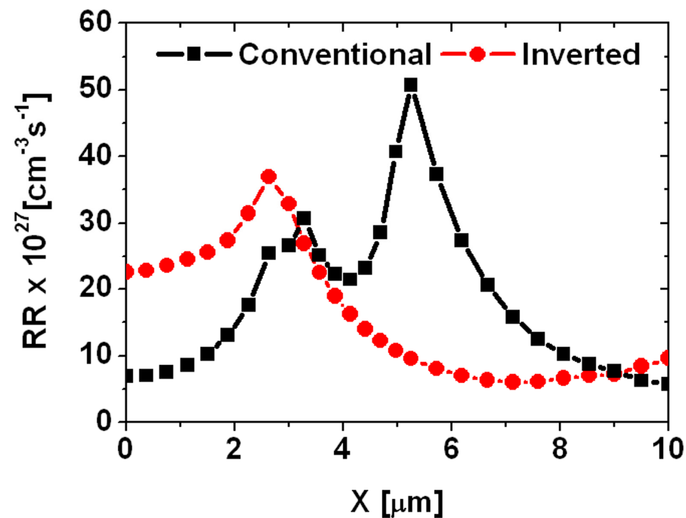

Fig. 3.23 - Radiative Recombination for both conventional and inverted structure along the middle QW

Moreover and as already shown, for the conventional structure two peaks in the radiative recombination (Fig. 3.23) (as well as in the carrier density as shown in Fig 3.24a and 3.24b) are observed. The first peak is related to the edge of the current aperture while the second peak is related to the edge of the top contact. In the region between these two edges the density tend to reduce because the velocity increases due to the high electric field (Fig. 3.21).

Under the top contact or in the current aperture the density reduces for real space transfer of the carriers (a further justification of this phenomena can be done observing fig 5 where the vectorial current density inside the half section of the device is shown) . On the other hand, in the inverted structure one observes only one peak related to the edge of current aperture (Fig 3.22). As discussed above, the influence of the top contact is screened by the oxide and this is can be observed also for the carrier densities inside the active region (Fig. 3.24a and Fig. 3.24b) as well as in the current density map (Fig. 3.25) where one can see a better focalization of the current.

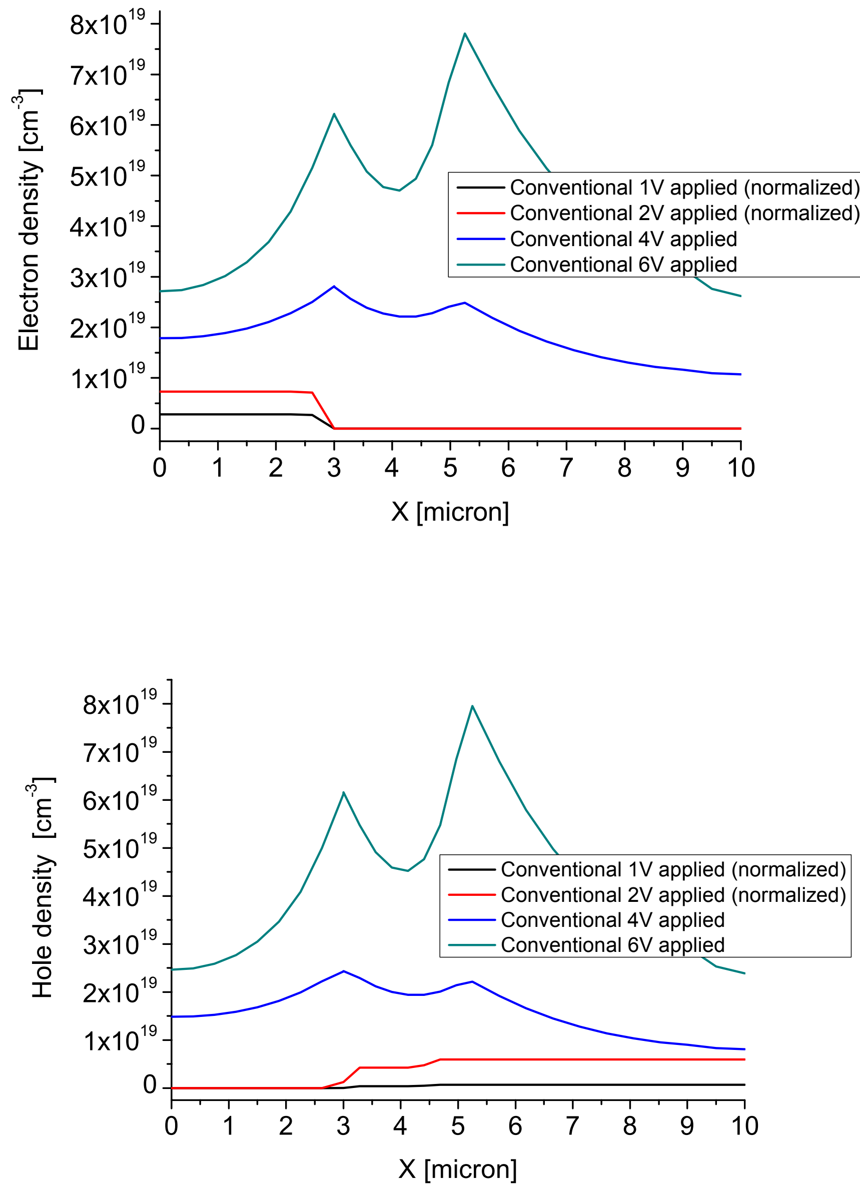

Fig. 3.24 - Electron densities(a) and hole densities (b) for different applied voltages along the x-direction of the active region for the conventional structure.

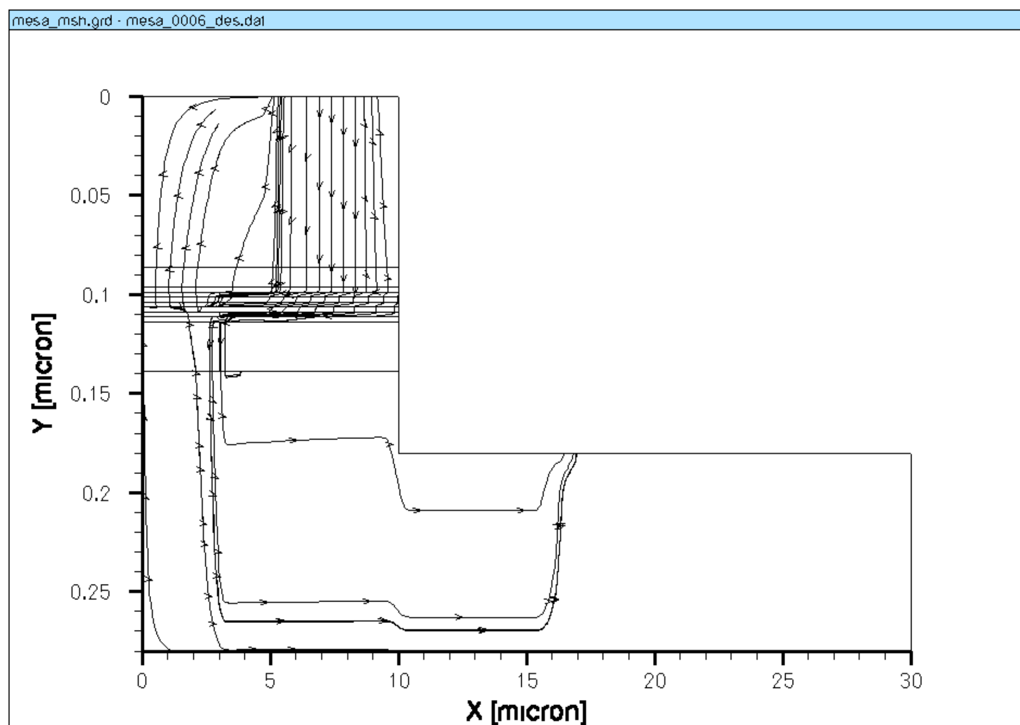

Fig. 3.25: Vectorial current density inside the conventional structure at 4 V applied.

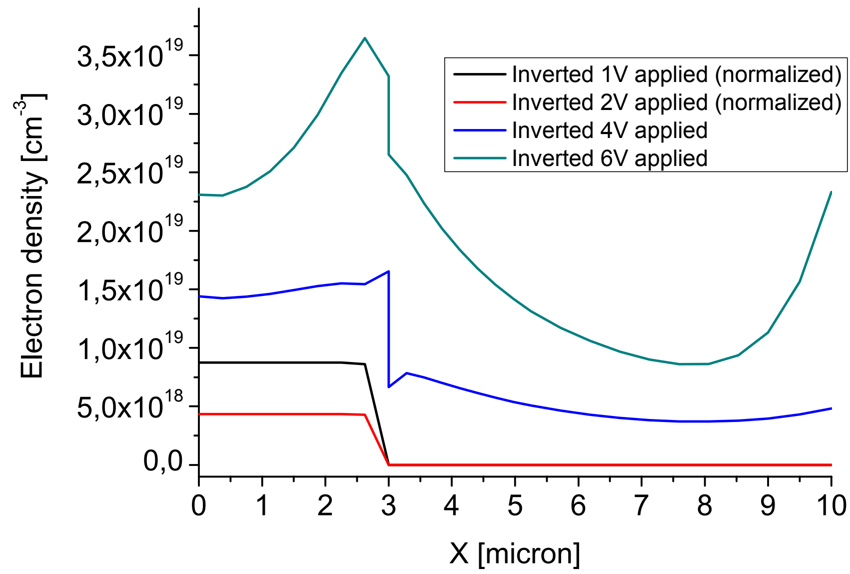

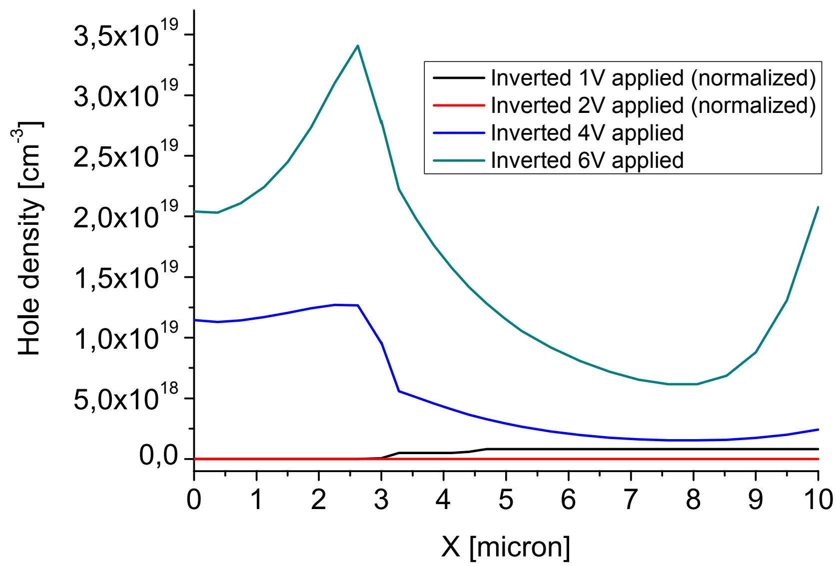

Fig. 3.26: Electron densities(a) and hole densities (b) for different applied voltages along the x-direction of the active region for the inverted structure.

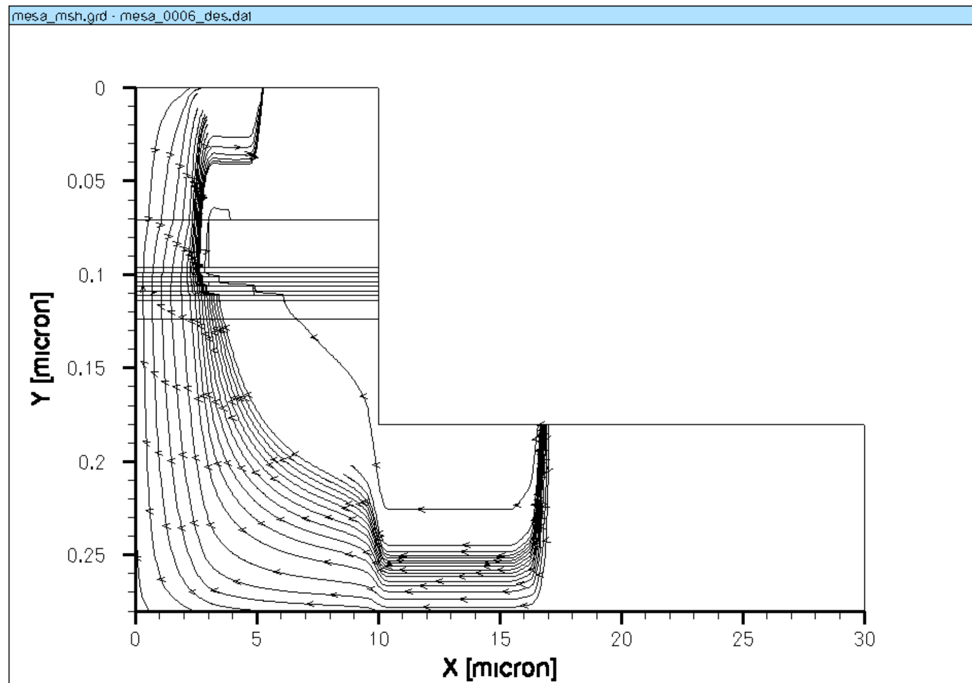

Fig. 3.27: Current density inside the conventional structure at 4 V applied.

3.6 Electrically injected bulk polariton laser

A bulk 5λ/2 (350 nm) GaN cavity grown on *c*-plane sapphire with 35-period $Al_{0.85}In_{0.15}N/Al_{0.2}Ga_{0.8}N$ lattice-matched distributed Bragg reflector in the bottom and 10-period dielectric SiO_2 / Si_3N_4 DBR on top has been considered, similar to the one where the polariton lasing has been observed [17] but with a current injection scheme similar to the one recently developed for the realization [18] of nitride VCSELs.

The full device scheme is shown in Fig. 3.28 together with carrier densities. Inside the cavity one can see four layers: 80 nm of *n*-doped AlGaN, 25 nm of AlInN current aperture, 220 nm of bulk GaN (active region), and 80 nm of *p*-doped AlGaN. The doped regions provide carrier injection into the active region, and the aperture reduces the current spreading in order to focus the

density in the active region. A Rabi splitting of 50 meV and a local quality factor of 2800 has been considered, which have been measured experimentally for such cavity parameters.[17]

A very important parameter is the nonradiative lifetime which determines the density-current dependence in the absence of polariton lasing. Various values are given in the literature.[19] Simulations show that for a very short lifetime of 3 ps measured in low quality structures grown on silicon substrates [20] the threshold current exceeds 5 kA/cm2. It drops to 50 A/cm2 for a reasonable lifetime estimate of 50 ps (which we use for the figures shown below) and even to 35 A/cm2 for a lifetime of 150 ps (not yet achieved experimentally).

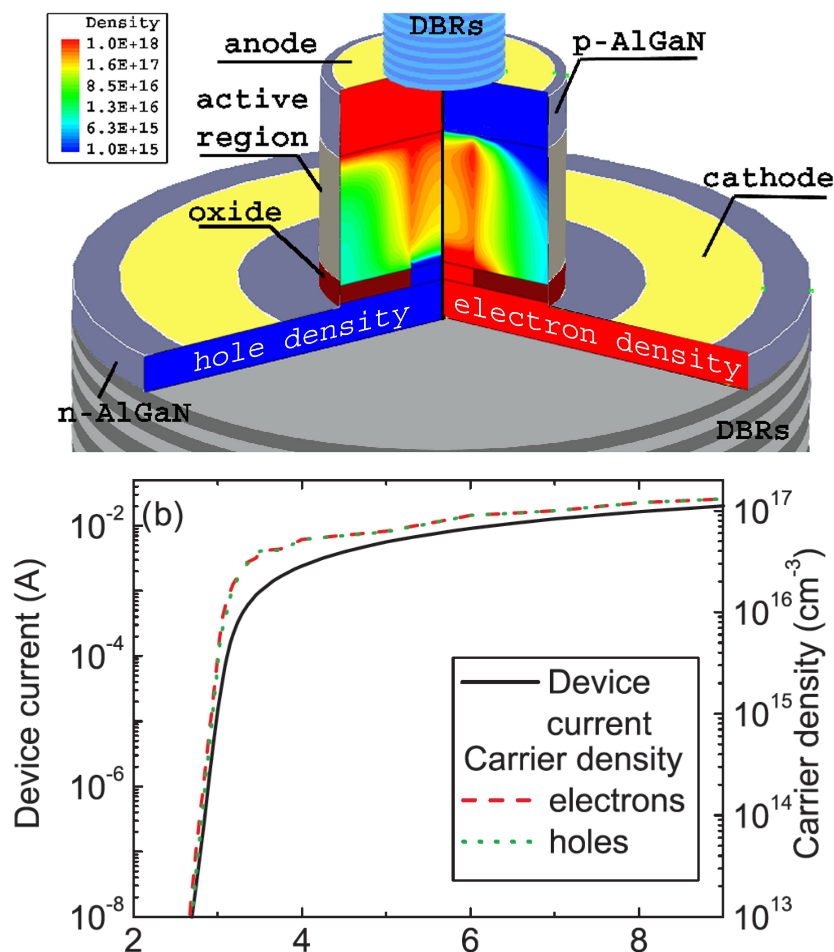

Fig. 3.28: (up) Device structure showing electron and hole density maps (cm−3) for the electrically injected bulk polariton laser at threshold. (down) I-V characteristic of the polariton laser (solid line) and corresponding carrier densities (dashed, dotted lines).

The simulator consists of two parts connected selfconsistently: electrical injection and exciton-polariton formation and relaxation. Electrical injection simulations are performed by using a two-dimensional simulator with cylindrical symmetry.[21] The simulation is performed by solving hydrodynamical transport equations in order to find carrier densities and their effective temperature. These simulations show that the effective carrier temperatures in bulk active region and in the polariton lasing regime are very close to the lattice temperature (room temperature). Fig. 3.28 shows electron and hole densities in different regions of the device at 3.35 V, when the polariton lasing starts to take place. One can see the effect of the current confinement aperture, which increases the carrier densities in the region between the dielectric mirrors. In this region the distribution is quite homogeneous, with similar values of density for the carriers of both types, required for the efficient exciton formation.

Fig. 3.28 shows also the *I* -*V* characteristic of the device and the average carrier densities. Because of the short nonradiative lifetime, the values of carrier density in the active region at any voltage do not exceed 1.4x10^{17} cm^{-3}, far below the transparency condition (10^{19} cm^{-3}) which determines the normal lasing threshold. This result means that the properties of GaN make extremely hard, if not impossible, the realization of a normal laser based on this material. On the other hand, such carrier density value is high enough to allow for polariton lasing to take place.

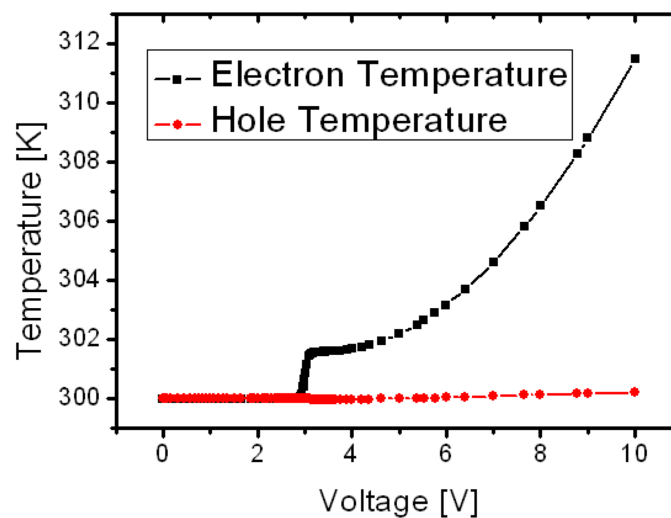

Fig. 3.29:Carrier temperatures for different applied voltages.

Exciton formation and dissociation in a self-consistent manner using the carrier density and distribution function given by the first component of the simulator have been calculated. In fig. 3.29 the carrier temperatures are shown for different applied voltages. The important peculiarity of the electrically pumped polariton laser is that the excitons are formed close to the ground state, contrary to the case of optical pumping, when their initial effective temperature is higher than that of the lattice.

Fig. 3.30 shows the result of the complete simulation of the electrically injected polariton laser: emission intensity and carrier density as functions of injection current. The emission intensity is directly proportional to the ground state population, obtained by the polariton relaxation simulations. It depends strongly on the carrier density in the active region, which increases smoothly versus the injection current. One can see a clear nonlinear emission threshold indicating the onset of polariton lasing at approximately 50 A/cm2, which corresponds to a voltage of 3.35 V. This is not a record-breaking value in general, but a bulk laser operating at room temperature in UV can already be useful with such injection current. The threshold could be further decreased by producing samples with longer nonradiative lifetime or by fabricating QW-based GaN polariton lasers. Above threshold the emission increases exponentially with current until it saturates. The maximal emission power is expected to be about 10 mW.

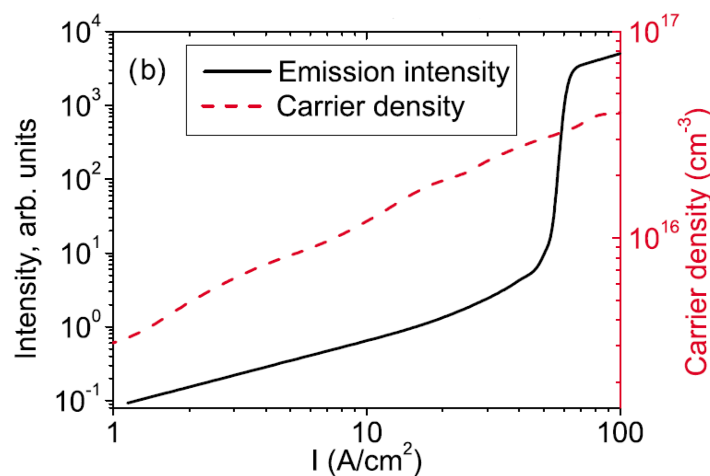

Fig. 3.30: Intensity of emission and average carrier density as functions of injection current.

References

[1] Vurgaftman I. and Meyer J. R., Band parameters for nitrogen-containing semiconductors, J. Appl. Phys., Vol. 94, No. 6, 15 September 2003

[2] Chris G. Van de Walle and Jorg Neugebauer, Small valence-band offsets at GaN/InGaN heterojunctions, Appl. Phys. Lett. 70 (19), 12 May 1997

[3] C. Zellweger, Realization of GaN-based light emitting devices, EPFL thesis

[4] S. J. Chang, W.C. Lai, Y. K. Su, J.F. Chen, C. H. Liu, U. H. Liaw, IEEE Journal on Selected Topics in Quantum Electronics 8, 278 (2002).

[5] O. Ambacher, W. Rieger, P. Ansmann, H. Angerer, T. D. Moustakas and M. Stutzmann, Sol. State Commun. 97, 365 (1996).

[6] J. Dorsaz, H.-J. Bühlmann, J.-F. Carlin, N. Grandjean, and M. Ilegems, Appl. Phys. Lett. 87, 072102 (2005);

[7] P Mackowiak, R. P. Sarzała and W Nakwaski, Semiconductor Science and Technology 16, 598 (2001)

[8] B. Lahiri, R. Datta, and S. Kundu, Physica E-Low-Dimensional Systems & Nanostructures 25, 449-455 (2005).

[9] P Mackowiak, T. Czyszanowski, R. P. Sarzała, M. Wasiak, and W Nakwaski, Opto-electronics Review 11, 119 (2003)

[10] ISE-TCAD User's Manual, ISE Integrated Sys. Eng. AG, Zurich, Switzerland

[11] Petr G. Eliseev, Marek Osin'ski, and Hua Li, Irina V. Akimova, Appl. Phys. Lett. 75, 3838 (1999)

[12] Alexey Dmitriev and Alexander Oruzheinikov, J. Appl. Phys., Vol. 86, 3241 (1999)

[13] C. Canali, G. Majni, R. Minder, and G. Ottaviani, *IEEE Trans. on Electron Devices*, vol. ED-22, pp. 1045 (1975)

[14] U. V. Bhapkar and M. S. Shur, J. Appl. Phys., vol. 82, no. 4, pp. 1649-1655, (1997)

[15] M. S. Shur and M. Asif Khan, MRS. Bull. 22, 44 (1997)

[16] R Butté et al, Current status of AlInN layers lattice-matched to GaN for photonics and electronics, J. Phys. D: Appl. Phys. 40 6328-6344 (2007)

[17] S. Christopoulos, G. Baldassari, A. J. D. Grundy, P. Lagoudakis, A. V. Kavokin, J. J. Baumberg, G. Christmann, R. Butte, E. Feltin, J.-F. Carlin, and N. Grandjean, Phys. Rev. Lett. 98, 126405 (2007) and references therein.

[18] A. Castiglia, D. Simeonov, H. J. Bluehlmann, J.-F. Carlin, E. Feltin, J. Dorsaz, R. Butte, and N. Grandjean, Appl. Phys. Lett. 90, 033514 (2007).

[19] K. P. Korona, Phys. Rev. B 65, 235312 (2002).

[20] F. Stokker-Cheregi, A. Vinattieri, F. Semond, M. Leroux, I. R. Sellers, J. Massies, D. Solnyshkov, G. Malpuech, M. Colocci, and M. Gurioli, Appl. Phys. Lett. 92, 042119 (2008).

[21] DESSIS ISE-TCAD User's Manual, ISE Integrated Systems Engineering AG, Zurich, Switzerland; for proof of reliability; see M. Streiff, A. Witzig, M. Pfeiffer, P. Royo, and W. Fichtner, IEEE J. Sel. Top. Quantum Electron. 9, 879 (2003).

Chapter 4

Design of a new electrical injection polariton laser

4.1 Why a new structure

Due to the progress of StimScat project, a microcavity with an active layer made by GaN has been carried out and allowed to observe the effect of polariton laser under optical pumping at room temperature [1]. The measured current threshold was extremely low and consistent with theoretical expectations [2, 3], as shown before. In 2007, a structure with a quantum wells active layer has been realized, demonstrating also the polariton laser effect at room temperature under optical pumping with a current threshold reduced by a factor of 5 to 10 in relation to the structure volume [4]. The final step to achieve a component that can become commercial is the realization of the electrical injection structure for quantum wells. Moreover, even if papers related to the electrical injection of polaritons at low temperature in GaAs have just been published [5], no polariton laser effects have been yet demonstrated.

Therefore there are several problem to be solved. For example, the main issues to reach this goal come also from the work shown in this thesis and they are resumed in the following :

1) as already demonstrated in chapter 3, to achieve a good electrical injection scheme in a VCSEL, a small number of quantum wells in the active zone have to be used. This is especially true in GaN where the mobility of holes is low. In practice the number of quantum wells need to be less than five;

2) a polariton laser must contain a large number of quantum wells in order to maximize the coupling of the optical field. The polariton laser effect observed at 20 K in CdTe [6, 7] was for a structure with 16 wells. GaN structure showing the effect at 300 K contains 67 wells.

So there is a total contradiction between the condition 1 and condition 2. It seems therefore difficult or impossible to make a good GaN- based quantum wells polariton laser.

4.2 The patented design

The scheme we will discuss in the following has been the object of a patent made in collaboration with the LASMEA group. The patent concerns a scheme, shown in Fig. 4.3, where only a small portion of the wells (from 2 to 5) on 67 are electrically injected. In a normal laser, this scheme would be meaningless. Wells with no carrier injection are not efficient: they absorb light, and destroying the laser by increasing cavity losses.

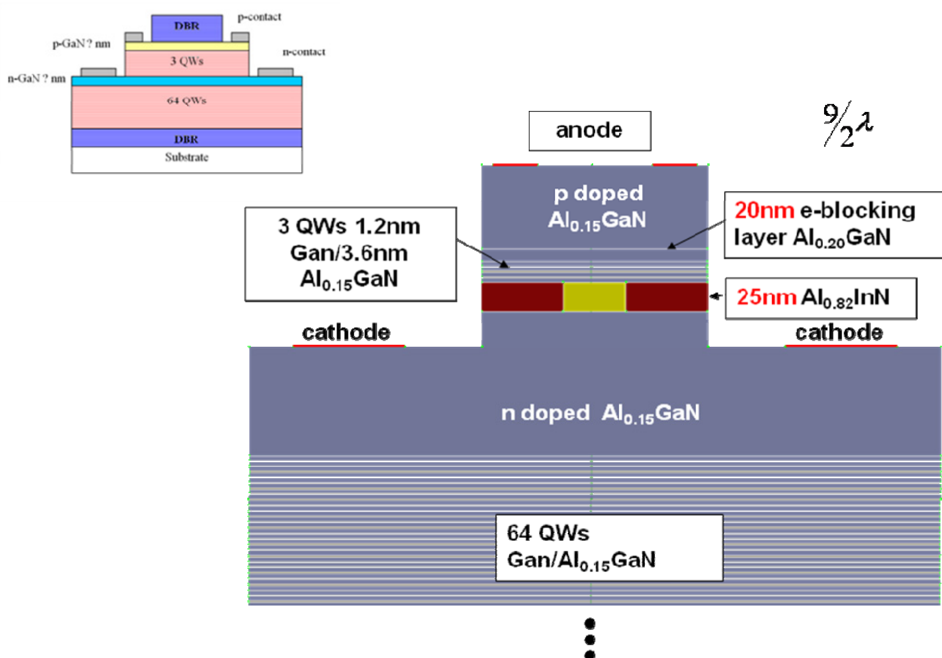

Fig. 4.3 - Optimized injected scheme for the polation laser.

In the polariton laser, the re-absorption of the light is what is sought. The light is absorbed by the non-pumped wells, and then re-emitted very quickly thanks to the strong coupling regime which reduces the photons emission-absorption time of two orders. Moreover, due to this strong coupling regime, the injected wells can emit photons very quickly, allowing the optimal transfer of energy from the pumped to the non-pumped part.

Simulations show that the injection of 1 to 4 wells would be sufficient to "illuminate" a laser that contains a total of 67 wells. The simulations also show that the electrical injection of 3 wells is achievable under good conditions and that the electrical injection does not affect the 64 “optical” quantum wells (Fig.4.4 and Fig 4.5).

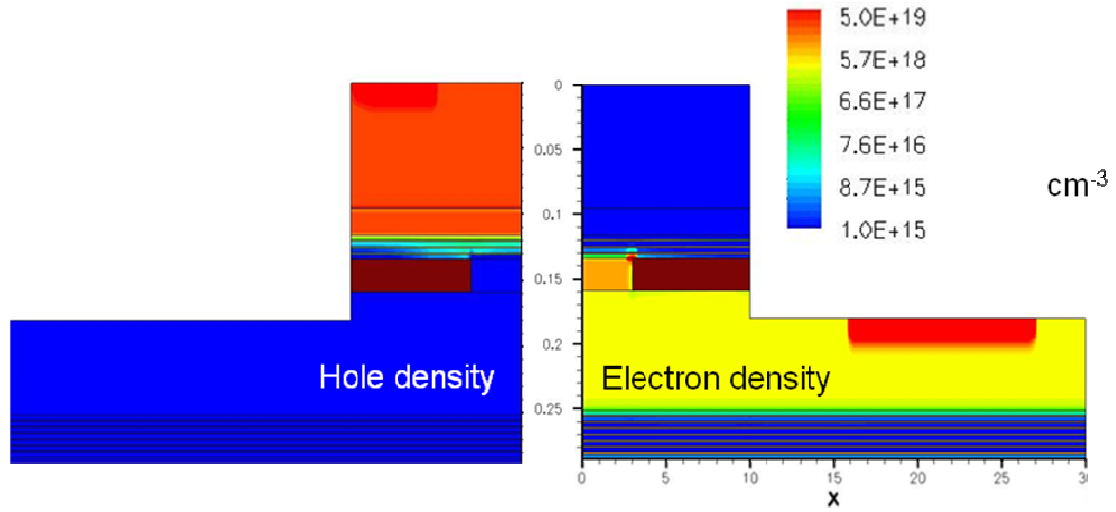

Fig. 4.4 – Map of Carrier Densities for 4V applied.

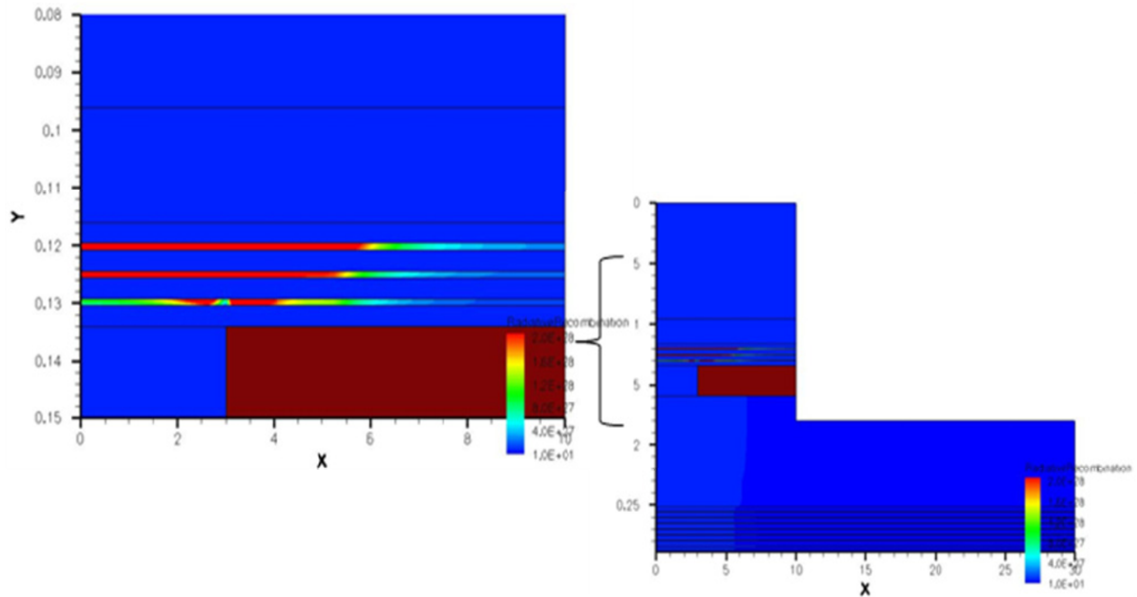

Fig. 4.5 – Map of Radiative Recombination inside the active region for 4V applied.

References

[1] S. Christopoulos, G. Baldassari, A. J. D. Grundy, P. Lagoudakis, A. V. Kavokin, J. J. Baumberg, G. Christmann, R. Butte, E. Feltin, J.-F. Carlin, and N. Grandjean, Phys. Rev. Lett. 98, 126405 (2007) and references therein.

[2] D. Solnyshkov, H. Ouerdane, and G. Malpuech, J. Appl. Phys. 103, 016101 (2008).

[3] G. Malpuech et al.,Appl. Phys. Lett. 81, 412 (2002).

[4] G. Cristmann et al, Phys Rev. B 2008; G. Cristmann et a, Lastis Symposium, Lausanne, Janvier 2008, et réunion du projet Stimscat, Cambridge, mars 2008.

[5] A.A. Khalifa et al, Appl. Phys. Letters 92, 061107 (2008); D. Bajoni et al, Phys. Rev. B 77, 113303 (2008); L. Sapienza et al, Phys. Rev. Letters 100, 136806 (2008).

[6] J. Kasprzak, et al., Nature 443, 409 (2006).

[7] M. Richard et al., Phys. Rev. B 72, 201301R (2005).

Chapter 5

Results of the StimScat Project (October 2008)

A further important feature of the consortium has been the close interaction between theory, modeling, device design and experimental observation.. Theory and modeling activity of the StimScat project was the main issue of this PhD thesis and have been described in the previous chapters. Now the whole activities and results of the StimScat project is being described to understand both the progress on the polariton laser realization and the influence of the work described in this thesis on the work of the other project's partners.

Stimscat has achieved a number of important successes including most notably: the first observation of a polariton laser and of Bose-Einstein condensation at room temperature, gallium nitride micro-resonators with record quality factors, vertical cavity electrical injection devices supporting current densities very close to lasing threshold, and electroluminescence emission from polariton states. The project has been underpinned by close interaction between crystal growth, device fabrication, advanced optical spectroscopy and theory and modelling. The results of the project have had an impact on both fundamental physics research and on device applications of GaN-based vertical cavity structures. The results of the project have received wide dissemination through 49 publications in the open literature, many in the highest profile international journals, and 33 invited presentations at international conferences.

Fig. 5.1 – StimScat project and its partners.

5.1 Microcavity properties and design

It was clear at the outset of the project that gallium nitride and related materials possessed the required properties of high exciton binding energy and large oscillator strength to achieve the goal of polariton laser operation at room temperature. The large exciton binding energy means that excitons are stable at room temperature, and the large oscillator strength leads to large splittings between the lower and upper polariton branches, greater than the thermal energy at 300K.

Nevertheless it was also clear at the outset of the project that GaN materials pose a number of technological challenges, particularly in the fabrication of vertical cavity device structures and in structures for efficient electrical injection. A schematic diagram of a generic microcavity structure is shown in Fig. 5.2. The microcavity is composed of a cavity an integer number of half wavelengths thick, surrounded by high reflectivity distributed Bragg reflector (DBR) mirrors.

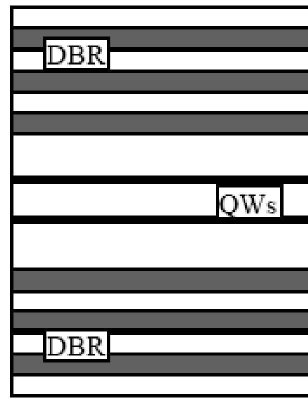

Fig. 5.2 - Schematic diagram of a semiconductor microcavity, showing quantum wells in the cavity region surrounded by high reflectivity distributed Bragg reflector (DBR) mirrors.

Particular issues which arise in the fabrication of such structures in GaN-materials are the lack of a suitably lattice matched substrate, build of strain in the Bragg mirrors, difficulties in achieving high doping levels, especially p-type, and mobility imbalance between electrons and holes, all of which were addressed during the project.

The first requirement to exploit the potentially favourable properties of GaN-microcavities was to achieve structures exhibiting well resolved polariton modes, with the splitting between the upper and lower polariton branches (the Rabi splitting) substantially greater than the linewidths of the modes. It is also important that to achieve strong coupling both narrow cavity and exciton modes are required. The requirement for narrow exciton lines requires fabrication of structures operating in the ultraviolet spectral region based either on GaN bulk layers or GaN/AlGaN quantum wells: the InGaN quantum wells which lead to blue/violet LEDs and lasers have too large linewidths due to alloy disorder to allow strong coupling to be attained. Narrow cavity modes require high quality factor cavities. Three overall approaches were adopted:

1. Epitaxially grown AlGaN/AlGaN lower Bragg mirrors and dielectric upper DBRs (‘half hybrid structures’), surrounding a bulk GaN cavity. In this case strain builds up during growth of the lower DBR leading to dislocation generation in the active region. [1][2]

2. Fully hybrid structures consisting of dielectric upper and lower DBRs surrounding a bulk GaN cavity. This technique involved development of advanced techniques for substrate removal before DBR deposition. [3]

3. 'Half-hybrid' structures consisting of a lattice matched (AlInN-AlGaN) lower DBR, either bulk cavities or cavities containing QWs, completed by the deposition of a dielectric top DBR. [4][5] A scanning electron micrograph of such a structure is shown in Fig 5.3.

Fig. 5.3 - 3λ/2 bulk GaN cavity surrounded by a bottom AlInN/AlGaN Bragg mirror and a top dielectric mirror

The goal of resolved polariton modes at room temperature was achieved by all three approaches, with best results being obtained using the lattice matched technology of approach 3. This technology has been developed at one of our partners (EPFL) [4][5], and allowed significant advances relative to the competition to be achieved.

The use of the epitaxial bottom-DBR avoids the processing complexities and device disadvantages (e.g. heat dissipation) associated with dielectric bottom DBRs, and has potential for commercial GaN vertical cavity laser (VCSEL) fabrication.

Using approach 3, ultra-violet DBRs with very high peak reflectivity of 99.5% at 340 nm and a stop band width of 20 nm were obtained. [4] Cavities of the type shown in Fig. 3 were fabricated. High quality factors exceeding several thousand on 10 to 20 micron length scales were obtained, with evidence for photonic disorder on larger length-scales. [5] Importantly the active regions exhibited excellent properties with photoluminescence linewidth of 30-35 meV, and dislocation densities of ~ $1x10^{9}$ cm^{-2}. A direct consequence of the relatively low dislocation density is a long free excitonic lifetime (30 ps), a critical parameter in achieving polariton lasing. Microcavities with similarly high quality have been obtained using multi-quantum well active regions and have also resulted in polariton lasing. Reflectivity spectra from optimised multi-quantum well cavities are shown in Fig. 5.4 exhibiting very well resolved strong coupling between lower and upper polariton branches. [6]

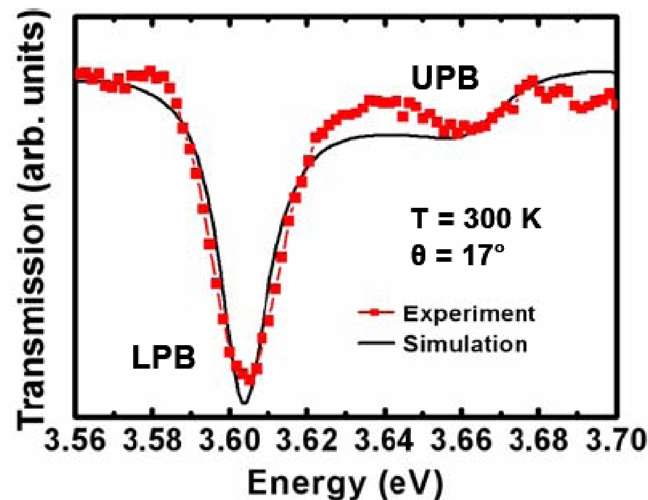

Fig. 5.4 - Transmission spectra from GaN/AlGaN multi-quantum well cavity with lattice matched epitaxial lower DBR and dielectric upper DBR.

It can be noticed that the fully hybrid structures of approach 2 also hold considerable promise for future developments of GaN-based vertical cavity devices, although they remain technologically demanding. [3] For example the Q-factor of the cavity can be increased by

increasing the number of dielectric mirror pair repeats, and high quality active regions can be obtained by optimizing further the substrate removal techniques.

5.2 Observation of Polariton lasing at room temperature: optical injection

Based on the advances in fabrication described above, half-hybrid cavities with lattice matched Al0.85In0.15N/Al0.2Ga0.8N 35 period lower DBR, 3λ/2 GaN cavity and 10 period upper dielectric DBR (similar to Fig 5.3) were studied under 100 femto-second non-resonant optical excitation at energies ~500meV above the lower polariton branch.

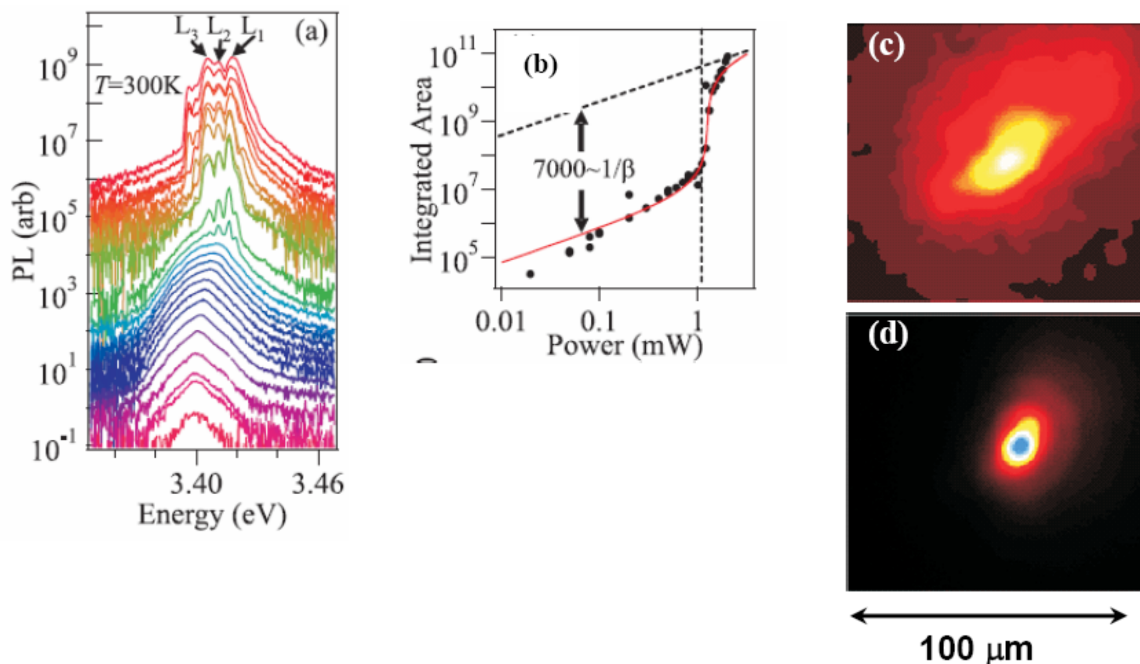

Fig. 5.5 - (a) Power-dependent coherent emission from a bulk GaN microcavity at T=300 K excited with 150 fs pulses at 300 nm incident at 20° and detected at 0°. (b) A clear threshold is observed at an average pump power of 1 mW. Spatial imaging of the emitting area (c) below, and (d) above

Evidence for polariton lasing was achieved at room temperature, as shown in Fig. 5.5a, an important first for the project. [7] At low pump powers, relatively broad spontaneous emission is

seen. With increasing power, and at a well defined threshold (Fig 5.5b), a very marked nonlinear increase of intensity is observed, accompanied by strong line-narrowing. Such nonlinear emission is obtained at a pumping threshold corresponding to a carrier density about one order of magnitude below the threshold density for exciton screening (Fig. 5.5b). A collapse of the emitting area is also observed above threshold (going from a diameter equal to the laser spot size (40-50 μm) to about 5 μm), a behaviour expected for such a coherent system operating in the strong coupling regime (Figs. 5.5c-d).

Subsequent to these observations related experiments were carried out on cavities containing GaN/AlGaN quantum wells. A very clear transition to the polariton lasing regime was observed with the non-linear emission more than 20meV in energy below that of the unperturbed cavity mode, as shown in Fig 5.6, again providing compelling evidence for the observation of polariton lasing. [8]

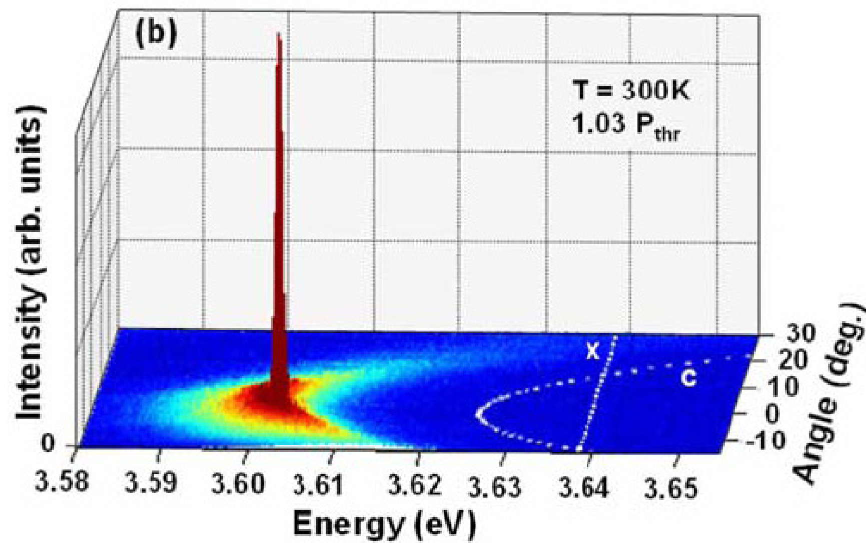

Fig. 5.6 - Far-field emission from a QW microcavity above threshold at room temperature, showing condensation of polaritons to states at zero wavevector and resulting polariton laser emission.

The realization of polariton lasing at room temperature, a major achievement of the Stimscat project, has been the subject of papers published in Physical Review Letters (54 citations so far) [7] and Applied Physics Letters.[8] It has created significant interest in the scientific press, and was highlighted in Nature, Nature Photonics, Laser Focus World, Physics World, and the SPIE Newsroom.

It is also noteworthy that the observation of polariton lasing, coherent emission from halfmatter/half-light states, corresponds to the observation of a non-equilibrium Bose-Einstein condensate at 300K from 'massive bosonic quasi-particles', a result which is equally significant from the fundamental point of view. In related work [9] the first measurements of the temporal coherence of polariton lasers were reported, thus revealing some of the fundamental differences between polariton and photon lasing. The difference between polariton lasing and the polariton BEC has been explained in [10].

5.3 Electrical injection structures

A further major goal of the project was to achieve efficient vertical cavity electrical injection devices. Major advances were achieved, particularly in the blue/violet weak coupling regime, with injection current densities close to lasing threshold being realized. New technologies were developed to overcome the challenges in the GaN-system including current apertures formed by lateral oxidation of AlInN, efficient intracavity p and n-contacts and conformal deposition of dielectric DBRs on small area mesas etc.

A schematic diagram of the device design adopted for the electrical injection structures is shown in Fig. 5.7. [11] The structures were grown on lattice matched DBRs of very similar design to those employed for optical injection structures. This avoids the processing complexities and device disadvantages (e.g. heat dissipation) associated with lower dielectric DBRs, and also has

strong potential as the foundation of an epitaxially-based GaN vertical cavity laser technology (VCSELs).

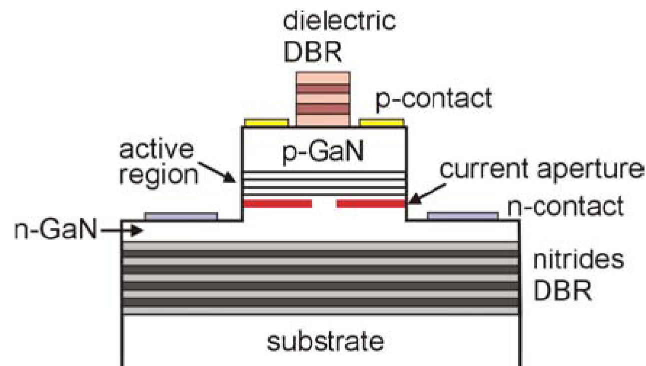

Fig. 5.7 - Schematic of electrically injected GaN-based vertical cavity device.

The structure in Fig. 5.7 also uses a novel current confinement layer using oxidised AlInN.

A full electrical blue-violet devices with top dielectric DBR according to the design of Fig. 5.7 have been successfully fabricated. Record Q-factors up to 1500 were measured under current injection conditions, with current densities up to 10 kA/cm^2, [11] close to the expected lasing threshold (see electroluminescence image in Fig. 5. 8).

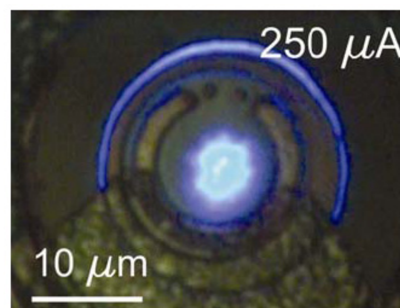

Fig. 5.8 - Electroluminescence image of vertical cavity device.

At the end of the project all the necessary technological steps to achieve a GaNbased VCSEL, using an epitaxial approach which has considerable potential for application, have been established. Issues still to be optimised include most efficient current spreading from the p-contact,

minimization of current spreading above the oxide aperture, and high doping levels of p-AlGaN contact regions.

Most effort on electrical injection was devoted to development of blue/violet vertical cavity structures. The challenges in electrical injection in ultraviolet devices in the strong coupling regime are considerably greater due to difficulties found in achieving high doping levels in the AlGaN p-contact. As a result main efforts were devoted to blue/violet devices. Nevertheless UV LEDs with and without epitaxial DBRs were successfully fabricated.

Finally electroluminescence emission was observed from polariton states in GaAs-based structures, a materials system where VCSEL technology is well-advanced. Clear signatures of electroluminescence emission from polariton states in the strong coupling regime were observed. [12] This result was a further important first for the project, and constitutes the realization of a polariton light emitting diode.

References

[1] I. R. Sellers, F. Semond, M. Leroux, J. Massies, M. Zamfirescu, F. Stokker-Cheregi, M. Gurioli, A. Vinattieri, M. Colocci, A. Tahraoui, and A.A. Khalifa Phys. Rev. B **74**, 193308 (2006)

[2] A. Alyamani, D. Sanvitto, A. A. Khalifa, M. S. Skolnick, T. Wang, F. Ranalli, P.J. Parbrook, A. Tahraoui,and R. Airey, J. Appl. Phys. **101**, 093110 (2007)

[3] K. Bejtka, F. Reveret, R. W. Martin, P. R. Edwards, A.Vasson, J. Leymarie, I.R. Sellers, J.Y. Duboz, M.Leroux, F. Semond, Appl Phys Lett, **92**, 241105, (2008)

[4] E. Feltin, J.-F. Carlin, J. Dorsaz, G Christmann, R Butté, M Laügt, M Ilegems and N Grandjean, Appl. Phys. Lett. **88**, 051108 (2006)

[5] G. Christmann, D. Simeonov, R. Butté, E. Feltin, J.-F. Carlin, and N. Grandjean, Appl. Phys. Lett. **89**, 261101 (2006)

[6] R. Butté, G. Christmann, E. Feltin, J.-F. Carlin, M. Mosca, M. Ilegems, and N. Grandjean, Phys. Rev. **B 73**, 033315 (2006)

[7] S. Christopoulos, G. Baldassarri Höger von Högersthal, A.J.D. Grundy, P.G. Lagoudakis, A.V. Kavokin, J.J. Baumberg, G. Christmann, R. Butté, E. Feltin, J.-F. Carlin, and N. Grandjean, Phys. Rev. Lett. **98**, 126405 (2007)

[8] G. Christmann, R. Butté, E. Feltin, J.-F. Carlin, and N. Grandjean, Appl. Phys. Lett. **93**, 051102 (2008)

[9] A P D Love, D N Krizhanovskii, D M Whittaker, R Bouchekioua, D Sanvitto, S Al Rizeiqi, R Bradley, M Skolnick, P R Eastham, R André, L S Dang, Phys Rev Lett 101, 067404, 2008

[10] J. Kasprzak, D. D. Solnyshkov, R. André, Le Si Dang, G. Malpuech, Phys. Rev. Lett. 101, 146404 (2008).

[11] A. Castiglia, D. Simeonov, H.J. Buehlmann, J.-F. Carlin, E. Feltin, J. Dorsaz, R. Butté, and N. Grandjean, Appl. Phys. Lett. **90**, 033514 (2007)

[12] A A Khalifa, A P D Love, D N Krizhanovskii, M S Skolnick, J S Roberts, Appl Phys Lett, 92, 061107, 2008

Appendix A

Dessis Input File - Example

In this appendix, an example of Dessis input file is shown. This file describes an hydrodynamic simulation of a GaN-based VCSEL structure with an applied voltage from 0 V to 10 V. The simulation is performed in cylindrical symmetry.

```
"INPUT.CMD"


Electrode {
        { Name="pcontact" Voltage=0  areafactor=1 }
        { Name="ncontact"  Voltage=0  areafactor= 1 }
}

File {
        Grid= "mesa_msh.grd"
        Doping= "mesa_msh.dat"
        Current= "curr_"
        Plot= "mesa.dat"
        Output= "MESA"
        Parameter= "pp_ok_des.par"
#  Load= "./result/device_cLF0_bur_3_des.sav"
}

Physics {
   Hydrodynamic

   Mobility (
        eHighfieldsaturation  (CarrierTempDrive)
        hHighfieldsaturation
        )
   EffectiveIntrinsicDensity (Nobandgapnarrowing)
   Recombination(SRH Auger
   eBarrierTunneling hBarrierTunneling Radiative)
   Fermi
   Thermionic

}
```

```
Physics (Material = "GaN") {
        IncompleteIonization
        Traps (Acceptor Level EnergyMid=0.3 fromCondBand
              Conc=1.0e15 #eXsection=1e-15 hXsection=1e-15
        )
}

Physics (Material="AlGaN") {
        IncompleteIonization
        MoleFraction(
                xFraction=0.15 Grading=0)
 }

Physics (Material="InGaN") {
        MoleFraction( xFraction=0.14 Grading=0)
 }

Physics (Material="AlInN") {
         MoleFraction(
         xFraction=0.36 Grading=0)
 }

Plot {
        Potential Electricfield/Vector
        eTemperature hTemperature
        eDensity hDensity
        eMobility hMobility
        eQuasiFermi hQuasiFermi
        eMobility hMobility
        eVelocity/Vector hVelocity/Vector
        eCurrent/Vector hCurrent/Vector TotalCurrent/Vector
        eGradQuasiFermi/Vector hGradQuasiFermi/Vector
        SRHRecombination Auger Radiative
        eBarrierTunneling hBarrierTunneling
        Avalanche
        eEparallel hEparallel
        DonorConcentration AcceptorConcentration
        Doping SpaceCharge
        ConductionBand ValenceBand
        BandGap Affinity
        xMoleFraction
        eTrappedCharge hTrappedCharge

}

Math {
        Extrapolate
        NotDamped=1000
        Iterations=20
        NewDiscretization
        Derivatives
        AvalDerivatives
        RelerrControl
        Digits=6
        ErrRef(electron) = 1E-2
        ErrRef(hole) = 1E-2
```

```
        Cylindrical
        ConstRefPotential
        DirectCurrentComputation

}

Solve {
        Coupled ( Iterations=500 )  { Poisson }
        Coupled ( Iterations=500 )  { Poisson Electron}
        Coupled ( Iterations=500 )  { Poisson Electron Hole
                                    eTemperature hTemperature
                                    }
        Quasistationary (InitialStep=0.01
        Minstep=1e-8 Maxstep=5e-1
        Goal {Name="ncontact" Voltage=0}
        Goal {Name="pcontact" Voltage=10}
        )
        {
        Coupled { Poisson Electron Hole
                   eTemperature hTemperature
                }

         Plot (FilePrefix="mesa"
               Time = (0.001; 0.1; 0.2; 0.3; 0.4; 0.5;
                       0.6; 0.7; 0.8; 0.9; 1) NoOverwrite)
        }

        Quasistationary (InitialStep=1e-2
        Minstep=1e-8
        Goal {Name="pcontact" Voltage=10}
        Goal {Name="ncontact" Voltage= 0}
        )
        {
        Coupled { Poisson Electron Hole
                   eTemperature hTemperature
                }

        Plot (FilePrefix="mesa"
             Time = (0.001; 0.1; 0.2; 0.3; 0.4; 0.5;
                       0.6; 0.7; 0.8; 0.9; 1) NoOverwrite)

        }
}
```

Appendix B

Dessis material parameter file

In this appendix, the Dessis material parameter file is shown. This is called in the “file section” of the input file .cmd by using the command:

```
Parameter= "pp_ok_des.par"
```

The original material file (set by Dessis developers) has been modified and upgraded following the new information on GaN based material coming from literature and from the work of StimScat partners.

```
"PP_OK_DES.PAR"
________________________________________________________________________________

Material = "GaN" {

**** Dielectric Constant: ****
******************************
Epsilon
{ *  Ratio of the permittivities of material and vacuum
  * epsilon() = epsilon
   epsilon    = 9.5                         # [1]
}

**** Lattice Heat Capacity: ****
********************************
LatticeHeatCapacity
{ *  lumped electron-hole-lattice heat capacity
  * cv() = cv + cv_b * T + cv_c * T^2 + cv_d * T^3
   cv    = 3.0                         # [J/(K cm^3)]
   cv_b  = 0.0000e+00                       # [J/(K^2 cm^3)]
   cv_c  = 0.0000e+00                       # [J/(K^3 cm^3)]
   cv_d  = 0.0000e+00                       # [J/(K^4 cm^3)]
}
```

```
**** Thermal Conductivity: ****
*******************************
Kappa
{ *  Lattice thermal conductivity

  Formula = 1
  * Formula = 1:
  * kappa() = kappa + kappa_b * T + kappa_c * T^2
   kappa= 1.3 # [W/(K cm)]
   kappa_b    = 0.0000e+00                  # [W/(K^2 cm)]
   kappa_c    = 0.0000e+00                  # [W/(K^3 cm)]
}


****  Hydro Parameters  ****
****************************


EnergyRelaxationTime


{ *  Energy relaxation times in picoseconds
   (tau_w)_ele     = 0.2               # [ps]
   (tau_w)_hol     = 0.2               # [ps]

  * Below is the example of energy relaxation time approximation
  * by the ratio of two irrational polynomials.
  * If Wmax(interval-1) < Wc < Wmax(interval), then:
  * tau_w = (tau_w)*(Numerator^Gn)/(Denominator^Gd),
  * where (Numerator or Denominator)=SIGMA[A(i)(Wc^P(i))],
  * Wc=(k*Tcar)/q (in eV).
  * By default: Wmin(0)=Wmax(-1)=0; Wmax(0)=infinity.
  *  The  option  can  be  activated  by  specifying  appropriate
Formula equal to 2.
  *      Formula(tau_w)_ele = 2
  *      Formula(tau_w)_hol = 2
  *      Wmax(interval)_ele =
  *      (tau_w)_ele(interval)     =
  *      Numerator(interval)_ele{
  *        A(0)  =
  *        P(0)  =
  *        A(1)  =
  *        P(1)  =
  *        G     =
  *      }
  *      Denominator(interval)_ele{
  *        A(0)  =
  *        P(0)  =
  *        G     =
  *      }

  *      Wmax(interval)_hol =
  *      (tau_w)_hol(interval)     =
}

AvalancheFactors
```

```
   { *  Coefficientss for avalanche generation with hydro
     *   Factors n_l_f, p_l_f for energy relaxation length in the
expressions
     *  for effective electric field for avalanche generation
     *  eEeff = eEeff / n_l_f  ( or b = b*n_l_f )
     *  hEeff = hEeff / p_l_f  ( or b = b*p_l_f )
     *  Additional coefficients n_gamma, p_gamma, n_delta, p_delta
      n_l_f = 0.8                     # [1]
      p_l_f = 0.8                     # [1]
      n_gamma    = 0.0000e+00                     # [1]
      p_gamma    = 0.0000e+00                     # [1]
      n_delta    = 0.0000e+00                     # [1]
      p_delta    = 0.0000e+00                     # [1]
   }

   ****Bandgap  ****
   *****************

   Bandgap
   { * Eg = Eg0 + alpha Tpar2 / (beta + Tpar) - alpha T2 / (beta +
T)
     * Parameter 'Tpar' specifies the value of lattice
     * temperature, at which parameters below are defined
     * Chi0 is electron affinity.
      Chi0  = 3.1                     # [eV]
      Bgn2Chi    = 0.5                     # [1]
      Eg0   = 3.4                     # [eV]
      alpha = 0.909e-3 #7.40e-04                    # [eV K^-1]
      beta  = 830 #6.00e+02                # [K]
      Tpar  = 300e00 #0.0000e+00                    # [K]
   }


   eDOSMass
   {
     *   For   effective   mass   specificatition   Formula1   (me
approximation):
     * or Formula2 (Nc300) can be used :
      Formula    = 2   # [1]
     * Formula2:
     * me/m0 = (Nc300/2.540e19)2/3
     * Nc(T) = Nc300 * (T/300)3/2
      Nc300 = 2.23e18                 # [cm-3]
     * mass=0.222*mo
   }

   hDOSMass
   {
     *   For   effective   mass   specificatition   Formula1   (mh
approximation):
     * or Formula2 (Nv300) can be used :
      Formula    = 2   # [1]
     * Formula2:
     * mh/m0 = (Nv300/2.540e19)2/3
     * Nv(T) = Nv300 * (T/300)3/2
      Nv300 = 4.62e19                 # [cm-3]
```

```
    *mass=1.0*mo
   }

   ****  Mobility Models: ****
   ***************************

   *  mu_lowfield^(-1)  =  mu_dop(mu_max)^(-1)  +  mu_Enorm^(-1)  +
mu_cc^(-1)
   * Variable = electron value ,   hole value         # [units]

   ConstantMobility:
   { * mu_const = mumax (T/T0)^(-Exponent)
     mumax= 1.1e3 ,  2.0000e+01 #1.7e3     # [cm2/(Vs)]
     Exponent   = 1 ,2.1             # [1]
   }

   DopingDependence:
   {
     * For doping dependent mobility model three formulas
     *  can  be  used.  Formula1  is  based  on  Masetti  et  al.
approximation.
     * Formula2 uses approximation, suggested by Arora.
      formula    = 1 ,1                    # [1]
     * If formula=1, model suggested by Masetti et al. is used:
     *    mu_dop    =    mumin1    exp(-Pc/N)    +    (mu_const    -
mumin2)/(1+(N/Cr)^alpha)
     *                           - mu1/(1+(Cs/N)^beta)
     * with mu_const from ConstantMobility
      mumin1     = 85, 33                  # [cm2/Vs]
      mumin2     = 75, 0.00E+00            # [cm2/Vs]
      mu1   = 50, 20                 # [cm2/Vs]
      Pc    = 6.50E+15,     5.00E+15        # [cm3]
      Cr    = 9.50E+16,     8.00E+16        # [cm3]
      Cs    = 7.20E+19,     8.00E+20        # [cm3]
      alpha= 0.55,              0.55            # [1]
      beta  = 0.75,         0.7             # [1]


     * If formula=2, model suggested by Arora is used:
     ***** Not Callibrated  *****
     ***** Parameters Below are for InN  *****
     * mu_dop = muminA + mudA/(1.+(N/N00)^AA),
     *     where     muminA=Ar_mumin*(T/T0)^Ar_alm;     mudA     =
Ar_mud*(T/T0)^Ar_ald
     * N is net doping
     * N00=Ar_N0*(T/T0)^Ar_alN; AA = Ar_a*(T/T0)^Ar_ala

   }

   HighFieldDependence:
   { * Caughey-Thomas model:
     *  mu_highfield  =  mu_lowfield  /  (  1  +  (mu_lowfield  E  /
vsat)^beta )1/beta
     * beta = beta0 (T/T0)^betaexp.
      beta0= 1.7 ,   1.7                   # [1]
      betaexp    = 0.0000e+00 ,  0.0000e+00      # [1]
```

```
     *  Smoothing  parameter  for  HydroHighField  Caughey-Thomas
model:
     * if Tl < Tc < (1+K_dT)*Tl, then smoothing between low field
mobility
     * and HydroHighField mobility is used.
      K_dT = 0.2 ,    0.2                   # [1]
     * Transferred-Electron Effect:
     *mu_highfield=
(mu_lowfield+(vsat/E)*(E/E0_TrEf)4)/(1+(E/E0_TrEf)4)
      E0_TrEf    = 1.5000e+05 ,  1.5000e+05      # [1]
      Ksmooth_TrEf    = 1 ,1                # [1]

    * For vsat either Formula1 or Formula2 can be used.
      Vsat_Formula    = 2 ,2                # [1]
    * Formula2 for saturation velocity:
    *           vsat = A_vsat - B_vsat*(T/T0)
    * (Parameter Vsat_Formula has to be equal to 2):
      A_vsat     = 1.9e+07 ,     1.5000e+07      #  2.1e7[1]
      B_vsat     = 0 ,  0                   # [1]
      vsat_min   = 1.000e+07 ,   1.000e+07  # [1]1.5e7
   }


   **** Recombination/Generation Models: ****
   ********************************
   * Variable = electron value ,   hole value         # [unit]
   ****************************************************************
   Scharfetter * relation and trap level for SRH recombination:
   { * tau = taumin + ( taumax - taumin ) / ( 1 + ( N/Nref )^gamma
     * tau(T) = tau * ( (T/300)^Talpha )            (TempDep)
     * tau(T) = tau * exp( Tcoeff * ((T/300)-1) ) (ExpTempDep)
      taumin     = 0.0000e+00 ,  0.0000e+00      # [s]
      taumax     = 1.0000e-9 ,   1.0000e-9       # [s]
      Nref  = 1.0000e+16 ,  1.0000e+16      # [cm^(-3)]
      gamma = 1 ,1                     # [1]
      Talpha     = -1.5000e+00 , -1.5000e+00           # [1]
      Tcoeff     = 2.55 ,   2.55            # [1]
      Etrap = 0.0000e+00                    # [eV]
   }


   vanOverstraetendeMan * Impact Ionization:
   { * G_impact = alpha_n n v_drift_n  +  alpha_p p v_drift_p
     * with alpha = gamma a  exp(-b gamma/E) for E<E0 (low) and
E>E0 (high)
     *      with    gamma    =    tanh(hbarOmega/(2kT0))    /
tanh(hbarOmega/(2kT))
      a(low)     = 0.0000e+06 ,  0.000e+06  # [1/cm]
      a(high)    = 2.9000e+08 ,  2.9000e+08 # [1/cm]30
      b(low)     = 0.0000e06  ,  0.0000e+06 # [V/cm]
      b(high)    = 3.400e+07  ,  3.4000e+07 # [V/cm]2e9
      E0    = 0.00e+06 ,    0.00e+06   # [V/cm]E0 =   3.2000e+06   ,
      3.0000e+06
      hbarOmega  = 0.035 ,  0.035 # [eV]
   }
```

```
*************************************************************
*  Parameters for the recombination models below were taken
*  from GaAs and require calibration for accurate simulations
*************************************************************
Auger * coefficients:
{ * R_Auger = ( C_n n + C_p p ) ( n p - ni_eff^2)
  * with C_n,p = (A + B (T/T0) + C (T/T0)^2) (1 + H exp(-
{n,p}/N0))
   A     = 1.0000e-34 ,  1.0000e-34 # [cm^6/s]
   B     = 0.0000e+00 ,  0.0000e+00 # [cm^6/s]
   C     = 0.0000e+00 ,  0.0000e+00 # [cm^6/s]
   H     = 0.0000e+00 ,  0.0000e+00 # [1]
   N0    = 1.0000e+18 ,  1.0000e+18 # [cm^(-3)]
}

RadiativeRecombination * coefficients:
{ * R_Radiative = C (n p - ni_eff^2)
   C     = 0.470000e-10  # [cm^3/s]
}

Ionization
{
   E_P_0       = 0.025    # [eV]
   alpha_P     = 3.1000e-08    # [eV cm]
   g_P         = 2   # [1]
   Xsec_P           = 1.0000e-12    # [cm^2/sec]


   E_B_0       = 0.170    # [eV]
   alpha_B     = 3.1000e-08    # [eV cm]
   g_B         = 4   # [1]
   Xsec_B           = 1.0000e-12    # [cm^2/sec]

}

TableBGN
{ * In the band-gap narrowing table, a list of concentrations
  * and the bandgap narrowing for them can be specified.
  * The first possibility is to specify total concentrations
(the sum
  * of acceptor and donor concentration) and the band gap
narrowing,
  * and then the table entries have the form:
  *   Total       Nt, deltaEg   # [ cm-3, eV ]
  * The second possibility is to specify the band gap narrowing
for
  * acceptors and donors separately (This must not be combined
with
  * specification of total concentrations).  The bandgap
narrowing
  * then will be the sum of both contributions; if no acceptor
or donor
  * entry exists, the respective bandgap narrowing contribution
is 0.
  * The entries take the form:
```

```
     *   Donor       Nd, deltaEg   # [ cm-3, eV ]
     *   Acceptor    Na, deltaEg   # [ cm-3, eV ]
     * For each of the two possibilities, any number of table
entries might
     * be given in any order.  For concentrations which are below
(above)
     * the smallest (largest) concentration specified in the
appropriate
     * table, the bandgap narrowing associated to the smallest
(largest)
     * entry is assumed.  For concentration which fall in between
table
     * entries, the bandgap narrowing is assumed to be linear in
the
     * logarithm of the respective concentration and is
interpolated
     * accordingly.
     Donor     1.0000e+17,   0.0000e+00   # [ cm-3, eV ]
     Donor     2.0000e+18    0.0
     Donor     1.0000e+19,   0.0000e+00   # [ cm-3, eV ]
     Donor     1.0000e+22,   0.0000e+00  # [ cm-3, eV ]
   }

   Traps:
   { * XsecFormula=1: Xsec(F) = Xsec
   * XsecFormula=2: Xsec(F) = Xsec*(1+a1*(F/1)^p1+a2*(F/1)^p2)^p0
   XsecFormula = 2 , 2 # [1]
   Xsec = 1.0000e-15 , 1.0000e-15 # [cm^2]
   a1 = 0.0000e+00 , 0.0000e+00 # [1]
   p1 = 1 , 1 # [1]
   a2 = 0.0000e+00 , 0.0000e+00 # [1]
   p2 = 1 , 1 # [1]
   p0 = 1 , 1 # [1]
   Jcoef = 0.0000e+00 , 0.0000e+00 # [1]
   }


   }
```

```
   Material = "AlN" {

   ***** Dielectric Constant: ****
   *******************************

   Epsilon
   { *  Ratio of the permittivities of material and vacuum

     * epsilon() = epsilon
      epsilon    = 8.5                     # [1]
   }

   ***** Lattice Heat Capacity: ****
```

```
*******************************

LatticeHeatCapacity
{ *  lumped electron-hole-lattice heat capacity
  * cv() = cv + cv_b * T + cv_c * T^2 + cv_d * T^3
   cv   = 1.94                          # [J/(K cm^3)]
   cv_b  = 0.0000e+00                   # [J/(K^2 cm^3)]
   cv_c  = 0.0000e+00                   # [J/(K^3 cm^3)]
   cv_d  = 0.0000e+00                   # [J/(K^4 cm^3)]
}

**** Thermal Conductivity: ****
******************************

Kappa
{ *  Lattice thermal conductivity

  Formula = 1
  * Formula = 1:
  * kappa() = kappa + kappa_b * T + kappa_c * T^2
   kappa= 2.85                          # [W/(K cm)]
   kappa_b    = 0.0000e+00                   # [W/(K^2 cm)]
   kappa_c    = 0.0000e+00                   # [W/(K^3 cm)]
}


****  Hydro Parameters  ****
***************************

EnergyRelaxationTime
{ *  Energy relaxation times in picoseconds
   (tau_w)_ele     = 0.1                # [ps]
   (tau_w)_hol     = 0.1                # [ps]

 * Below is the example of energy relaxation time approximation
 * by the ratio of two irrational polynomials.
 * If Wmax(interval-1) < Wc < Wmax(interval), then:
 * tau_w = (tau_w)*(Numerator^Gn)/(Denominator^Gd),
 * where (Numerator or Denominator)=SIGMA[A(i)(Wc^P(i))],
 * Wc=(k*Tcar)/q (in eV).
 * By default: Wmin(0)=Wmax(-1)=0; Wmax(0)=infinity.
 *  The  option  can  be  activated  by  specifying  appropriate
Formula equal to 2.
 *      Formula(tau_w)_ele = 2
 *      Formula(tau_w)_hol = 2
 *      Wmax(interval)_ele =
 *      (tau_w)_ele(interval)     =
 *      Numerator(interval)_ele{
 *        A(0)  =
 *        P(0)  =
 *        A(1)  =
 *        P(1)  =
 *        G     =
 *      }
 *      Denominator(interval)_ele{
```

```
    *        A(0)  =
    *        P(0)  =
    *        G     =
    *      }

    *      Wmax(interval)_hol =
    *      (tau_w)_hol(interval)     =
   }

   AvalancheFactors
   { *  Coefficientss for avalanche generation with hydro
     *  Factors n_l_f, p_l_f for energy relaxation length in the
expressions
     *  for effective electric field for avalanche generation
     *  eEeff = eEeff / n_l_f  ( or b = b*n_l_f )
     *  hEeff = hEeff / p_l_f  ( or b = b*p_l_f )
     *  Additional coefficients n_gamma, p_gamma, n_delta, p_delta
      n_l_f = 0.8                      # [1]
      p_l_f = 0.8                      # [1]
      n_gamma    = 0.0000e+00                    # [1]
      p_gamma    = 0.0000e+00                    # [1]
      n_delta    = 0.0000e+00                    # [1]
      p_delta    = 0.0000e+00                    # [1]
   }

   **** Bandgap  ****
   ******************

   Bandgap
   { * Eg = Eg0 + alpha Tpar2 / (beta + Tpar) - alpha T2 / (beta +
T)
     * Parameter 'Tpar' specifies the value of lattice
     * temperature, at which parameters below are defined
     * Chi0 is electron affinity.
      Chi0  = 1.25    #0.25              # [eV]
      Eg0   = 6.2                    # [eV]
      alpha = 0 #1.7900e-03              # [eV K^-1]
      beta  = 0 #1.4620e+03              # [K]
      Tpar  = 300.0000e+02               # [K]
   }



   eDOSMass
   {
     *   For   effective   mass   specificatition   Formula1   (me
approximation):
     * or Formula2 (Nc300) can be used :
      Formula    = 2                     # [1]
     * Formula2:
     * me/m0 = (Nc300/2.540e19)2/3  = 0.3
     * Nc(T) = Nc300 * (T/300)3/2
      a     = 0.1905                 # [1]
      ml    = 0.9163                 # [1]
      mm    = 0.0000e+00                 # [1]
      Nc300 = 6.23e18 #4.10e18                # [cm-3]
```

```
   }

   hDOSMass
   {
     * For effective mass specificatition Formula1 (mh
approximation):
     * or Formula2 (Nv300) can be used :
      Formula    = 2   # [1]
     * Formula2:
     * mh/m0 = (Nv300/2.540e19)2/3  ~= 5.0
     * Nv(T) = Nv300 * (T/300)3/2
      a     = 0.443587                # [1]
      b     = 3.6095e-03                   # [K^-1]
      c     = 1.1735e-04                   # [K^-2]
      d     = 1.2632e-06                   # [K^-3]
      e     = 3.0256e-09                   # [K^-4]
      f     = 4.6834e-03                   # [K^-1]
      g     = 2.2869e-04                   # [K^-2]
      h     = 7.4693e-07                   # [K^-3]
      i     = 1.7275e-09                   # [K^-4]
      mm    = 0.0000e+00                   # [1]
      Nv300 = 4.88e20   #  2.8400e+20                # [cm-3]
   }


   ****  Mobility Models: ****
   ***************************

   *  mu_lowfield^(-1)  =  mu_dop(mu_max)^(-1)  +  mu_Enorm^(-1)  +
mu_cc^(-1)          *
   * Variable = electron value ,    hole value        # [units]
*
   ConstantMobility:
   { * mu_const = mumax (T/T0)^(-Exponent)
      Exponent   = 1,  2.1            #[1]
      mumax = 300,     14                  #[cm2/(Vs)]
   }

   DopingDependence:
   {
     * For doping dependent mobility model three formulas
     *  can  be  used.  Formula1  is  based  on  Masetti  et  al.
approximation.
     * Formula2 uses approximation, suggested by Arora.
      formula    = 1 ,1    # [1]
     * If formula=1, model suggested by Masetti et al. is used:
     *    mu_dop    =    mumin1    exp(-Pc/N)    +    (mu_const    -
mumin2)/(1+(N/Cr)^alpha)
     *                        - mu1/(1+(Cs/N)^beta)
     * with mu_const from ConstantMobility
      mumin1     = 20,      11                 # [cm2/Vs]
      mumin2     = 65,      0.00E+00           # [cm2/Vs]
      mu1   = 20,      10                # [cm2/Vs]
      Pc    = 8.00E+17,     5.00E+18         # [cm3]
      Cr    = 7.00E+16,     8.00E+17         # [cm3]
      Cs    = 5.20E+17,     8.00E+18         # [cm3]
```

```
      alpha = 0.88,         1.05                # [1]
      beta  = 0.75,         0.75           # [1]


     * If formula=2, model suggested by Arora is used:
     ***** Not Callibrated  *****
     ***** Parameters Below are for InN  *****
     * mu_dop = muminA + mudA/(1.+(N/N00)^AA),
     *     where     muminA=Ar_mumin*(T/T0)^Ar_alm;     mudA     =
Ar_mud*(T/T0)^Ar_ald
     * N is net doping
     * N00=Ar_N0*(T/T0)^Ar_alN; AA = Ar_a*(T/T0)^Ar_ala

   }


   HighFieldDependence:
   { * Caughey-Thomas model:
     *  mu_highfield  =  mu_lowfield  /  (  1  +  (mu_lowfield  E  /
vsat)^beta )1/beta
     * beta = beta0 (T/T0)^betaexp.
      beta0 = 2, 2                    #[1]
      betaexp    = 0.0000e+00,   0.0000e+00      #[1]

     *  Smoothing  parameter  for  HydroHighField  Caughey-Thomas
model:
     * if Tl < Tc < (1+K_dT)*Tl, then smoothing between low field
mobility
     * and HydroHighField mobility is used.
      K_dT  = 0.2 ,    0.2                 # [1]
     * Transferred-Electron Effect:
     *                        mu_highfield                        =
(mu_lowfield+(vsat/E)*(E/E0_TrEf)4)/(1+(E/E0_TrEf)4)
      E0_TrEf    = 2.7000e+05 ,  2.7000e+05      # [1]
      Ksmooth_TrEf    = 1 , 1              # [1]

    * For vsat either Formula1 or Formula2 can be used.
      Vsat_Formula    = 2 , 2              # [1]
    * Formula2 for saturation velocity:
    *           vsat = A_vsat - B_vsat*(T/T0)
    * (Parameter Vsat_Formula has to be equal to 2):
      A_vsat     = 1.5000e+07,   1.5000e+07      #[cm/s]
      B_vsat     = 0, 0    #[cm/s]
      vsat_min   = 5.0000e+06,   5.0000e+06 #[cm/s]


   }

   ****  Recombination/Generation Models: *****
   **************************************************************
   * Variable = electron value ,   hole value      # [units]
   ***************************************************************
   Scharfetter * relation and trap level for SRH recombination:
   { * tau = taumin + ( taumax - taumin ) / ( 1 + ( N/Nref )^gamma
     * tau(T) = tau * ( (T/300)^Talpha )          (TempDep)
     * tau(T) = tau * exp( Tcoeff * ((T/300)-1) ) (ExpTempDep)
```

```
      taumin     = 0.0000e+00 ,  0.0000e+00      # [s]
      taumax     = 1.0000e-9 ,   1.0000e-9       # [s]
      Nref = 1.0000e+16 ,  1.0000e+16      # [cm^(-3)]
      gamma = 1 ,1                     # [1]
      Talpha     = -1.5000e+00 , -1.5000e+00          # [1]
      Tcoeff     = 2.55 ,   2.55            # [1]
      Etrap = 0.0000e+00                    # [eV]
   }

   vanOverstraetendeMan * Impact Ionization:
   { * G_impact = alpha_n n v_drift_n  +  alpha_p p v_drift_p
     * with alpha = gamma a  exp(-b gamma/E) for E<E0 (low) and
E>E0 (high)
     *       with     gamma     =     tanh(hbarOmega/(2kT0))     /
tanh(hbarOmega/(2kT))
      a(low)     = 2.9e8 ,  1.3400e+07      # [1/cm]
      a(high)    = 2.9e8 ,  1.3400e+07      # [1/cm]
      b(low)     = 3.4e8 ,  2.0300e+08      # [V/cm]
      b(high)    = 3.4e8 ,  2.0300e+08      # [V/cm]
      E0   = 4.0000e+05,   4.0000e+05      #[V/cm]
      hbarOmega  = 0.035,   0.035      #[V/cm]
   }

   RadiativeRecombination * coefficients:
   { * R_Radiative = C (n p - ni_eff^2)
      C     = 0.180000e-10  # [cm^3/s]
   }


   TableBGN
   { * In the band-gap narrowing table, a list of concentrations
     * and the bandgap narrowing for them can be specified.
     * The first possibility is to specify total concentrations
(the sum
     * of acceptor and donor concentration) and the band gap
narrowing,
     * and then the table entries have the form:
     *   Total       Nt, deltaEg   # [ cm-3, eV ]
     * The second possibility is to specify the band gap narrowing
for
     * acceptors and donors separately (This must not be combined
with
     * specification of total concentrations).   The bandgap
narrowing
     * then will be the sum of both contributions; if no acceptor
or donor
     * entry exists, the respective bandgap narrowing contribution
is 0.
     * The entries take the form:
     *   Donor       Nd, deltaEg   # [ cm-3, eV ]
     *   Acceptor    Na, deltaEg   # [ cm-3, eV ]
     * For each of the two possibilities, any number of table
entries might
     * be given in any order.  For concentrations which are below
(above)
```

```
     * the smallest (largest) concentration specified in the
appropriate
     * table, the bandgap narrowing associated to the smallest
(largest)
     * entry is assumed.  For concentration which fall in between
table
     * entries, the bandgap narrowing is assumed to be linear in
the
     * logarithm of the respective concentration and is
interpolated
     * accordingly.
     Donor     1.0000e+17,   0.0000e+00   # [ cm-3, eV ]
     Donor     1.0000e+18    0.75
     Donor     1.0000e+19,   0.0000e+00   # [ cm-3, eV ]
     Donor     1.0000e+20,   0.0000e+00   # [ cm-3, eV ]
     Donor     1.0100e+20,   0.7500e+00  # [ cm-3, eV ]
     Donor     1.0000e+22,   0.0000e+00  # [ cm-3, eV ]
   }

   }
```

```
   Material = "AlGaN" {
   *  Mole dependent material: AlGaN(x = 0) = GaN
   *  Mole dependent material: AlGaN(x = 1) = AlN


   vanOverstraetendeMan * Impact Ionization:
   { * G_impact = alpha_n n v_drift_n  +  alpha_p p v_drift_p
     * with alpha = gamma a  exp(-b gamma/E) for E<E0 (low) and
E>E0 (high)
     *       with     gamma     =     tanh(hbarOmega/(2kT0))     /
tanh(hbarOmega/(2kT))
      a(low)     = 0.0000e+06 ,  0.000e+06  # [1/cm]
      a(high)    = 2.9000e+08 ,  2.9000e+08 # [1/cm]30
      b(low)     = 0.0000e06  ,  0.0000e+06 # [V/cm]
      b(high)    = 3.400e+07  ,  3.4000e+07 # [V/cm]2e9
      E0   = 0.00e+06 ,    0.00e+06   # [V/cm]E0 =   3.2000e+06   ,
      3.0000e+06
      hbarOmega  = 0.035 ,  0.035 # [eV]
   }

   Ionization
   {
      E_P_0      = 0.025    # [eV]
      alpha_P    = 3.1000e-08    # [eV cm]
      g_P        = 2  # [1]
      Xsec_P          = 1.0000e-12    # [cm^2/sec]


      E_B_0      = 0.170    # [eV]
      alpha_B    = 3.1000e-08    # [eV cm]
      g_B        = 4  # [1]
```

```
    Xsec_B          = 1.0000e-12    # [cm^2/sec]

   }

   Scharfetter * relation and trap level for SRH recombination:
   { * tau = taumin + ( taumax - taumin ) / ( 1 + ( N/Nref )^gamma
     * tau(T) = tau * ( (T/300)^Talpha )          (TempDep)
     * tau(T) = tau * exp( Tcoeff * ((T/300)-1) ) (ExpTempDep)
    taumin     = 0.0000e+00 ,  0.0000e+00      # [s]
    taumax     = 1.0000e-9 ,   1.0000e-9       # [s]
    Nref  = 1.0000e+18 ,  1.0000e+18      # [cm^(-3)]
    gamma= 1 ,1                      # [1]
    Talpha     = -1.5000e+00 , -1.5000e+00          # [1]
    Tcoeff     = 2.55 ,   2.55            # [1]
    Etrap= 0.0000e+00                     # [eV]
   }


   Auger * coefficients:
   { * R_Auger = ( C_n n + C_p p ) ( n p - ni_eff^2)
     * with C_n,p = (A + B (T/T0) + C (T/T0)^2) (1 + H exp(-
{n,p}/N0))
    A     = 1.0000e-34 ,  1.0000e-34 # [cm^6/s]
    B     = 0.0000e+00 ,  0.0000e+00 # [cm^6/s]
    C     = 0.0000e+00 ,  0.0000e+00 # [cm^6/s]
    H     = 0.0000e+00 ,  0.0000e+00 # [1]
    N0    = 1.0000e+18 ,  1.0000e+18 # [cm^(-3)]
   }


   RadiativeRecombination * coefficients:
   { * R_Radiative = C (n p - ni_eff^2)
    C     = 0.310000e-10  # [cm^3/s]
   }

     BarrierTunneling {
      mt  = 0.24 ,   1    # [1]
     }


   TableBGN
   { * In the band-gap narrowing table, a list of concentrations
     * and the bandgap narrowing for them can be specified.
     * The first possibility is to specify total concentrations
(the sum
     * of acceptor and donor concentration) and the band gap
narrowing,
     * and then the table entries have the form:
     *   Total       Nt, deltaEg   # [ cm-3, eV ]
     * The second possibility is to specify the band gap narrowing
for
     * acceptors and donors separately (This must not be combined
with
     * specification of total concentrations).  The bandgap
narrowing
```

```
     * then will be the sum of both contributions; if no acceptor
or donor
     * entry exists, the respective bandgap narrowing contribution
is 0.
     * The entries take the form:
     *   Donor       Nd, deltaEg   # [ cm-3, eV ]
     *   Acceptor    Na, deltaEg   # [ cm-3, eV ]
     * For each of the two possibilities, any number of table
entries might
     * be given in any order.  For concentrations which are below
(above)
     * the smallest (largest) concentration specified in the
appropriate
     * table, the bandgap narrowing associated to the smallest
(largest)
     * entry is assumed.  For concentration which fall in between
table
     * entries, the bandgap narrowing is assumed to be linear in
the
     * logarithm of the respective concentration and is
interpolated
     * accordingly.
     Donor     1.0000e+17,   0.0000e+00   # [ cm-3, eV ]
     Donor     1.0000e+18    0.75
     Donor     1.0000e+19,   0.0000e+00   # [ cm-3, eV ]
     Donor     1.0000e+20,   0.0000e+00   # [ cm-3, eV ]
     Donor     1.0100e+20,   0.7500e+00  # [ cm-3, eV ]
     Donor     1.0000e+22,   0.0000e+00  # [ cm-3, eV ]
   }

   }
```

```
   Material = "InN" {


   **** Dielectric Constant: ****
   ******************************

   Epsilon
   { *  Ratio of the permittivities of material and vacuum
     epsilon    = 15.3                          # [1]
   }

   **** Lattice Heat Capacity: ****
   ********************************

   LatticeHeatCapacity
   { *  lumped electron-hole-lattice heat capacity

     * cv() = cv + cv_b * T + cv_c * T^2 + cv_d * T^3
     cv    = 2.2                     # [J/(K cm^3)]
     cv_b  = 0.0000e+00                    # [J/(K^2 cm^3)]
     cv_c  = 0.0000e+00                    # [J/(K^3 cm^3)]
```

```
    cv_d = 0.0000e+00                      # [J/(K^4 cm^3)]
  }

  **** Thermal Conductivity: ****
  *******************************

  Kappa
  { *  Lattice thermal conductivity
    kappa= 0.45                            # [W/(K cm)]
  }

  ****  Hydro Parameters  ****
  *******************************

  EnergyRelaxationTime
  { *  Energy relaxation times in picoseconds
    (tau_w)_ele     = 0.3                  # [ps]
    (tau_w)_hol     = 0.3                  # [ps]

   * Below is the example of energy relaxation time approximation
   * by the ratio of two irrational polynomials.
   * If Wmax(interval-1) < Wc < Wmax(interval), then:
   * tau_w = (tau_w)*(Numerator^Gn)/(Denominator^Gd),
   * where (Numerator or Denominator)=SIGMA[A(i)(Wc^P(i))],
   * Wc=(k*Tcar)/q (in eV).
   * By default: Wmin(0)=Wmax(-1)=0; Wmax(0)=infinity.
   *  The  option  can  be  activated  by  specifying  appropriate
Formula equal to 2.
   *      Formula(tau_w)_ele = 2
   *      Formula(tau_w)_hol = 2
   *      Wmax(interval)_ele =
   *      (tau_w)_ele(interval)     =
   *      Numerator(interval)_ele{
   *        A(0)  =
   *        P(0)  =
   *        A(1)  =
   *        P(1)  =
   *        G     =
   *      }
   *      Denominator(interval)_ele{
   *        A(0)  =
   *        P(0)  =
   *        G     =
   *      }

   *      Wmax(interval)_hol =
   *      (tau_w)_hol(interval)     =
  }

  AvalancheFactors
  { *  Coefficientss for avalanche generation with hydro
    *  Factors n_l_f, p_l_f for energy relaxation length in the
expressions
    *  for effective electric field for avalanche generation
    *  eEeff = eEeff / n_l_f  ( or b = b*n_l_f )
    *  hEeff = hEeff / p_l_f  ( or b = b*p_l_f )
```

```
     *  Additional coefficients n_gamma, p_gamma, n_delta, p_delta
      n_l_f= 0.8                      # [1]
      p_l_f= 0.8                      # [1]
      n_gamma    = 0.0000e+00                    # [1]
      p_gamma    = 0.0000e+00                    # [1]
      n_delta    = 0.0000e+00                    # [1]
      p_delta    = 0.0000e+00                    # [1]
   }

   **** Bandgap  ****
   *****************

   Bandgap
   { * Eg = Eg0 + dEg0 + alpha Tpar2 / (beta + Tpar) - alpha T2 /
(beta + T)
     * dEg0(<bgn_model_name>) is a band gap correction term.  It
is used together with
     * an appropriate BGN model, if this BGN model is chosen in
Physics section
     * Parameter 'Tpar' specifies the value of lattice
     * temperature, at which parameters below are defined
     * Chi0 is electron affinity.
      Chi0  = 5.7                     # [eV]
      Bgn2Chi    = 0.5                        # [1]
           Eg0     = 0.8                             # [eV]
      alpha= 2.45e-4                  # [eV K^-1]
      beta  = 6.2400e+02                      # [K]
      Tpar  = 300.0000e+00                    # [K]
   }

   eDOSMass
   {
     *   For   effective   mass   specificatition   Formula1   (me
approximation):
     * or Formula2 (Nc300) can be used :
      Formula    = 2                          # [1]
     * Formula2:
     * me/m0 = (Nc300/2.540x1019 )^(2/3)
     * Nc(Te) = Nc300 x((T/300))^(3/2)   cm^-3

      Nc300 = 1.3000e+18                      # cm^-3
   }

   hDOSMass
   {
     *   For   effective   mass   specificatition   Formula1   (mh
approximation):
     * or Formula2 (Nv300) can be used :
      Formula    = 2                          # [1]
     * Formula2:
     * mh/m0 = (Nv300/2.540x1019 )^(2/3)
     * Nv(Te) = Nv300 x((T/300))^(3/2)   cm^-3

      Nv300 = 5.3000e+19                      # cm^-3
   }
```

```
**** Mobility Models: ****
**************************

* mu_lowfield^(-1) = mu_dop(mu_max)^(-1) + mu_Enorm^(-1) +
mu_cc^(-1)
* Variable = electron value , hole value # [units]

ConstantMobility:
{ * mu_const = mumax (T/T0)^(-Exponent)
  mumax= 2.400e+03 , 2.400e+03 # [cm2/(Vs)]
  Exponent = 1.9 , 1.9 # [1]
}

DopingDependence:
{
  * For doping dependent mobility model three formulas
  * can be used. Formula1 is based on Masetti et al.
approximation.
  * Formula2 uses approximation, suggested by Arora.
  formula = 1 ,1 # [1]
  * If formula=1, model suggested by Masetti et al. is used:
  * mu_dop = mumin1 exp(-Pc/N) + (mu_const -
mumin2)/(1+(N/Cr)^alpha)
  * - mu1/(1+(Cs/N)^beta)
  * with mu_const from ConstantMobility
  mumin1 = 120 , 44.9 # [cm2/Vs]
  mumin2 = 115 , 0.0000e+00 # [cm2/Vs]
  mu1 = 130 , 50 # [cm2/Vs]
  Pc = 6.50E+17 , 6.50e+17 # [cm3]
  Cr = 9.6800e+16 , 9.6800e+16 # [cm3]
  Cs = 7.20E+20 , 7.20e+20 # [cm3]
  alpha= 1.45 , 1.45 # [1]
  beta = 1.85 , 1.85 # [1]
  * If formula=2, model suggested by Arora is used:
  * mu_dop = muminA + mudA/(1.+(N/N00)^AA),
  * where muminA=Ar_mumin*(T/T0)^Ar_alm; mudA =
Ar_mud*(T/T0)^Ar_ald
  * N is net doping
  * N00=Ar_N0*(T/T0)^Ar_alN; AA = Ar_a*(T/T0)^Ar_ala
  Ar_mumin = 88, 54.3 # [cm2/Vs]
  Ar_alm = -6.70E-01, -5.70E-01 # [1]
  Ar_mud = 2.20E+03, 4.07E+02 # [cm2/Vs]
  Ar_ald = -4.00E+00, -2.23E+00 # [1]
  Ar_N0 = 1.25E+17, 2.35E+17 # [cm^(-3)]
  Ar_alN = 1.9, 2.4 # [1]
  Ar_a = 0.98, 0.88 # [1]
  Ar_ala = -1.50E-01, -1.46E-01 # [1]

}

HighFieldDependence:
{ * Caughey-Thomas model:
  * mu_highfield = mu_lowfield / ( 1 + (mu_lowfield E /
vsat)^beta )1/beta
  * beta = beta0 (T/T0)^betaexp.
  beta0= 2.2 , 2.2 # [1]
```

```
      betaexp    = 0.0000e+00 ,  0.0000e+00      # [1]

     *  Smoothing  parameter  for  HydroHighField  Caughey-Thomas
model:
     * if Tl < Tc < (1+K_dT)*Tl, then smoothing between low field
mobility
     * and HydroHighField mobility is used.
      K_dT = 0.2 ,   0.2                   # [1]
     * Transferred-Electron Effect:
     *                       mu_highfield                        =
(mu_lowfield+(vsat/E)*(E/E0_TrEf)4)/(1+(E/E0_TrEf)4)
      E0_TrEf    = 7.1000e+04 ,  7.1000e+04      # [1]
      Ksmooth_TrEf    = 1 ,1               # [1]

    * For vsat either Formula1 or Formula2 can be used.
      Vsat_Formula    = 2 ,2               # [1]
    * Formula2 for saturation velocity:
    *            vsat = A_vsat - B_vsat*(T/T0)
    * (Parameter Vsat_Formula has to be equal to 2):
      A_vsat     = 2.600e+07 ,   2.60e+07        # [1]
      B_vsat     = 0 , 0   # [1]
      vsat_min   = 2.2000e+07 ,  2.2000e+07 # [1]
   }


   ****  Recombination/Generation Models ****
   ****************************************************************
   * Variable = electron value ,   hole value  # [units]
   ****************************************************************
   Scharfetter * relation and trap level for SRH recombination:
   {  *  tau  =  taumin  +  (  taumax  -  taumin  )  /  (  1  +  (  N/Nref
)^gamma)
     * tau(T) = tau * ( (T/300)^Talpha )          (TempDep)
     * tau(T) = tau * exp( Tcoeff * ((T/300)-1) ) (ExpTempDep)
      taumin     = 0.0000e+00 ,  0.0000e+00      # [s]
      taumax     = 1.0000e-9 ,   1.0000e-9       # [s]
      Nref  = 1.0000e+18 ,  1.0000e+18      # [cm^(-3)]
      gamma = 1 ,1                    # [1]
      Talpha     = -1.5000e+00 , -1.5000e+00          # [1]
      Tcoeff     = 2.55 ,  2.55            # [1]
      Etrap = 0.0000e+00                   # [eV]
   }

   vanOverstraetendeMan * Impact Ionization:
   { * G_impact = alpha_n n v_drift_n  +  alpha_p p v_drift_p
     * with alpha = gamma a   exp(-b gamma/E) for E<E0 (low) and
E>E0 (high)
     *         with     gamma     =     tanh(hbarOmega/(2kT0))     /
tanh(hbarOmega/(2kT))
      a(low)     = 2.9e+08 ,     1.3400e+08      # [1/cm]
      a(high)    = 2.9e+08 ,     1.3400e+08      # [1/cm]
      b(low)     = 3.4e+07 ,     2.0300e+07      # [V/cm]
      b(high)    = 3.4e+07 ,     2.0300e+07      # [V/cm]
      E0   = 4.0000e+05 ,  4.0000e+05      # [V/cm]
      hbarOmega  = 0.035 ,  0.035     # [eV]
   }
```

```
****************************************************************
*  Parameters for the recombination models below were taken
*  from GaAs and require calibration for accurate simulations
****************************************************************
Auger * coefficients:
{ * R_Auger = ( C_n n + C_p p ) ( n p - ni_eff^2)
  * with C_n,p = (A + B (T/T0) + C (T/T0)^2) (1 + H exp(-
{n,p}/N0))
    A     = 1.0000e-34 ,  1.0000e-34 # [cm^6/s]
    B     = 0.0000e+00 ,  0.0000e+00 # [cm^6/s]
    C     = 0.0000e+00 ,  0.0000e+00 # [cm^6/s]
    H     = 0.0000e+00 ,  0.0000e+00 # [1]
    N0    = 1.0000e+18 ,  1.0000e+18 # [cm^(-3)]
}

RadiativeRecombination * coefficients:
{ * R_Radiative = C (n p - ni_eff^2)
    C     = 0.520000e-10  # [cm^3/s]
}

}
```

```
Material = "AlInN" {

****************************************************************
*  Parameters for the recombination models below were taken
*  from GaAs and require calibration for accurate simulations
****************************************************************
Scharfetter * relation and trap level for SRH recombination:
{  * tau = taumin + ( taumax - taumin ) / ( 1 + ( N/Nref
)^gamma)
   * tau(T) = tau * ( (T/300)^Talpha )           (TempDep)
   * tau(T) = tau * exp( Tcoeff * ((T/300)-1) ) (ExpTempDep)
    taumin     = 0.0000e+00 ,  0.0000e+00 # [s]
    taumax     = 1.0000e-09 ,  1.0000e-09 # [s]
    Nref  = 1.0000e+16 ,  1.0000e+16 # [cm^(-3)]
    gamma = 1 , 1    # [1]
    Talpha     = 0.0000e+00 ,  0.0000e+00 # [1]
    Tcoeff     = 0.0000e+00 ,  0.0000e+00 # [1]
    Etrap = 0.0000e+00    # [eV]
}

Ionization
{
    E_P_0      = 0.025    # [eV]
    alpha_P    = 3.1000e-08    # [eV cm]
    g_P        = 2   # [1]
    Xsec_P          = 1.0000e-12    # [cm^2/sec]

}
```

```
Auger * coefficients:
{ * R_Auger = ( C_n n + C_p p ) ( n p - ni_eff^2)
  * with C_n,p = (A + B (T/T0) + C (T/T0)^2) (1 + H exp(-
{n,p}/N0))
    A    = 1.0000e-30 ,  1.0000e-30 # [cm^6/s]
    B    = 0.0000e+00 ,  0.0000e+00 # [cm^6/s]
    C    = 0.0000e+00 ,  0.0000e+00 # [cm^6/s]
    H    = 0.0000e+00 ,  0.0000e+00 # [1]
    N0   = 1.0000e+18 ,  1.0000e+18 # [cm^(-3)]
}

RadiativeRecombination * coefficients:
{ * R_Radiative = C (n p - ni_eff^2)
    C    = 2.0000e-10    # [cm^3/s]
}

Bandgap
{ * Eg = Eg0 + dEg0 + alpha Tpar2 / (beta + Tpar) - alpha T2 /
(beta + T)
   * dEg0(<bgn_model_name>) is a band gap correction term.  It
is used together with
   * an appropriate BGN model, if this BGN model is chosen in
Physics section
   * Parameter 'Tpar' specifies the value of lattice
   * temperature, at which parameters below are defined
   * Chi0 is electron affinity.

        Eg0     = 4.2                        # [eV]

}

}

_____________________________________________________________

Material = "InGaN" {

***************************************************************
*  Parameters for the recombination models below were taken
*  from GaAs and require calibration for accurate simulations
***************************************************************
Scharfetter * relation and trap level for SRH recombination:
{  *  tau  =  taumin  +  (  taumax  -  taumin  )  /  (  1  +  (  N/Nref
)^gamma)
   * tau(T) = tau * ( (T/300)^Talpha )          (TempDep)
   * tau(T) = tau * exp( Tcoeff * ((T/300)-1) ) (ExpTempDep)
    taumin     = 0.0000e+00 ,  0.0000e+00 # [s]
    taumax     = 1.0000e-09 ,  1.0000e-09 # [s]
    Nref  = 1.0000e+18 ,  1.0000e+18 # [cm^(-3)]
    gamma = 1 , 1     # [1]
    Talpha     = 0.0000e+00 ,  0.0000e+00 # [1]
    Tcoeff     = 0.0000e+00 ,  0.0000e+00 # [1]
    Etrap = 0.0000e+00    # [eV]
}
```

```
   Auger * coefficients:
   { * R_Auger = ( C_n n + C_p p ) ( n p - ni_eff^2)
     * with C_n,p = (A + B (T/T0) + C (T/T0)^2) (1 + H exp(-
{n,p}/N0))
      A     = 1.0000e-34 ,  1.0000e-34 # [cm^6/s]
      B     = 0.0000e+00 ,  0.0000e+00 # [cm^6/s]
      C     = 0.0000e+00 ,  0.0000e+00 # [cm^6/s]
      H     = 0.0000e+00 ,  0.0000e+00 # [1]
      N0    = 1.0000e+18 ,  1.0000e+18 # [cm^(-3)]
   }

   RadiativeRecombination * coefficients:
   { * R_Radiative = C (n p - ni_eff^2)
      C     = 0.50000e-10   # [cm^3/s]
   }

   }
```

Appendix C

List of publications and activities

Papers

E. Petrolati and A. Di Carlo, Enhancement of carrier focusing GaN based vertical cavity surface emitting lasers and polariton lasers, Appl. Phys. Lett. vol 94 (2009) - pages 091105

D. Solnyshkov, **E. Petrolati**, A. Di Carlo, and G. Malpuech, Theory of an electrically injected bulk polariton laser, Applied Physics Letters, vol. 94 (2009) - pages 011110

E. Petrolati and A. Di Carlo, The influence of mobility unbalance on GaN based vertical cavity surface emitting lasers, Appl. Phys. Lett. 92 (2008) - pages 151116

E. Petrolati, M. Auf Der Maur, M. Povolotskyi, A. Di Carlo, Simulation of exciton formation and transport in electrically driven polariton laser structures, Superlattices and microstructures, 41 (2007) - pages 364-367

Patents

"Schéma d'injection electrique d'un laser à polaritons à puits quantiques » - CNRS, Univ. Blaise Pascal, Univ. Tor Vergata - Patent number 08/06323, deposited with Institut National de la Propriété Industrielle, France.

"High frequency triode-type field emission device and process for manufacturing the same " - *Univ. Tor Vergata* - PCT/IT2007/000931

Proceedings

R. Riccitelli, F. Brunetti, **E. Petrolati**, C. Paoloni, A. Di Carlo, F. Toschi, M. Terranova, M. Cirillo, Innovative design of nano-vacuum triode**.** Proceeding In: IEEE International Vacuum Electronics Conference (2007)

F. Brunetti, P. Lugli, A. Fiori, S. Orlanducci, V. Sessa, E. Tamburri, F. Toschi, M. Terranova, R. Riccitelli, **E. Petrolati**, L. Von Neumann, C. Paoloni, A. Reale, A. Di Carlo, A. Ciorba, M. Cirillo, V. Merlo, Realization of a carbon nanotube-based triode, Proceeding In: Sixth IEEE Conference on Nanotechnology (2006)

E. Petrolati, C. Paoloni A. Di Carlo, Simulation of a THz vacuum triode using carbon-nanotube emitter, 2006 IEEE International Vacuum Electronics Conference held jointly with 2006 IEEE International Vacuum Electron Sources (IEEE Cat. No.06EX1278), (2006)

A. Di Carlo, A. Pecchia, **E. Petrolati**, C. Paoloni, Modelling of carbon nano tube-based devices: From nanoFETs to THz emitters - Proceedings of SPIE - The International Society for Optical Engineering, 6328 (2006)

Posters

E. Petrolati et al., *Experimental and theoretical study of test GaN-based light-emitting structures as a step toward the electrically driven polariton laser,* 15th International Conference on Nonequilibrium Carrier Dynamics in Semiconductors *(HCIS15),* Japan, 2008

E. Petrolati, A. Di Carlo, *The influence of mobility unbalance on GaN based VCSEL and Polariton LASER*, GE2008, Otranto (Le), Giugno 2008

E. Petrolati et al., *Experimental and theoretical study of test GaN-based light-emitting structures as a step toward the electrically driven polariton laser*, GE2007, Lerici, 20-22 Giugno 2007

A. Di Carlo, F. Brunetti, R. Riccitelli, E.Petrolati, et al., *Nano Vacuum amplifiers for THz security applications, Ricerca e tecnologia per la sicurezza: la collaborazione tra Finmeccanica e il sistema universitario,* 10 november 2005 Auditorium di Finmeccanica (Roma)

PhD Schools and Conferences

“International School of Nanophotonics” - Maratea (Italy) – September 2005

“IWCE11 - International Workshop on Computational Electronics” – Wien – May 2006

“Summerschool on Wide-bandgap Semiconductor Quantum Structures” - MonteVerità, Ascona (Switzerland) - August 2006

“PLMCN6”, 6th International Conference on Physics of Light-Matter Coupling in Nanostructures” 25.-29. September 2006, Magdeburg, Germany

“GE2007 – Gruppo elettronica”, Lerici (Sp) 20-22/06/2007

“GE2008 - Gruppo elettronica”, Otranto (Le) 18-20/06/2008

“ISOPHOS 2007 - International School on Organic Photovoltaic” – Ventotene (Lt) 23-27/09/2007 – Member of organizing committee

“ISOPHOS 2008 - International School on Organic Photovoltaic” – Ventotene (Lt) – 22-26/09/2008 - Member of organizing committee

StimScat Meetings

1. London (UK), September 2005
2. Nice (France), March 2006
3. Oxford (UK), October 2006
4. Lausanne (Switzerland), March 2007
5. Rome (Italy), October 2007
6. Cambridge (UK), April 2008
7. Sheffield (UK), November 2008

Acknowledgements

E anche l'avventura del dottorato è giunta al termine. Il primo ringraziamento non può non andare al Prof. Aldo Di Carlo, che, senza retorica, si è dimostrato essere guida, supporto e incoraggiamento durante questo percorso. Ringrazio poi il Dr. Andrea Reale che in questi anni è sempre stato presente e pronto a consigliarmi. Grazie a loro questi tre anni sono stati di vera crescita e formazione.

Tengo inoltre a ringraziare il Prof. Riccardo Marino e il Prof. Corrado Di Natale, coordinatori attenti, disponibili e puntuali e tutti i partner del progetto StimScat, con i quali mi sono confrontata in questi tre anni e che mi hanno permesso di apprendere tantissimo, citando fra tutti Guillaume, Dmitry e Alexey con i quali ho condiviso la dura vita del teorico in un gruppo di sperimentali.

Un grazie particolare va a tutto il gruppo TiberCad ai quali auguro anche un grande in bocca al lupo per la loro avventura.

Se ho raggiunto questo traguardo lo devo anche e soprattutto a mia madre che mi ha sostenuto (moralmente, materialmente ed incondizionatamente!) e a mio marito che per me è stato esempio e forza. Grazie!!!

A questo punto voglio ringraziare nuovamente Aldo: le parole non bastano per spiegare come per me sia stato un amico e un compagno di viaggio perfetto. Grazie per aver creduto in me e per continuare a farlo. Inoltre il mio grazie va ad Andrea e Thomas che negli ultimi tempi mi hanno saputo coinvolgere, incoraggiare e guidare verso il nuovo mondo lavorativo che mi aspetta.

I tre anni di dottorato si sono dimostrati veramente intensi. Se il mio bagaglio scientifico ne esce arricchito, altrettanto posso dire di quello affettivo. E per questo devo ringraziare Riccardo e Stefano, che con me hanno condiviso fin dall'inizio come una squadra non solo l'esperienza del dottorato, ma tutte le "avventure" nelle quali ci siamo imbarcati in questi anni . In loro ho trovato i colleghi migliori che potessi sperare. Ma soprattutto Riccardo e Stefano si sono rivelati essere due amici, due fratelli e infine… due soci (nel senso più ricco ed esteso della parola "socio"). I "tretre" per eccellenza sono solo all'inizio!

Il mio grazie va anche Francesca, amica ed esempio: un bellissimo regalo ricevuto grazie a questa esperienza.

Grazie inoltre a Giuseppe, Gabriele, Luigi ed Enrico, per essere stati prima che colleghi, amici e a tutto l'Olab, passato e presente, per essere stato un gruppo invidiabile, fonte di ispirazione, arricchimento: una seconda famiglia.

Più che un grazie, va fatto un applauso ai "miei tesisti" per essere sopravvissuti sotto le mie grinfie. E soprattutto ai "miei dottorandi"… e va bene… colleghi… Fabrizio e Simone per la pazienza che hanno avuto in queste ultime settimane nel sopportare il continuo "Oddio… devo scrivere la tesi!" del loro "TT-di-riferimento" (ormai un'unica parola). Ma dopotutto cosa potevo aspettarmi dal gruppo più fashion di Chose? Grazie, ragazzuoli… ora siete pronti a entrare nella legenda?